NUMERICAL MODELING OF WATER CIRCULATION AND SEDIMENT TRANSPORT FOR POLLUTION CONTROL IN FETHIYE BAY: A COMPOUND ANALYSIS

A THESIS SUBMITTED TO
THE GRADUATE SCHOOL OF NATURAL AND APPLIED SCIENCES
OF
MIDDLE EAST TECHNICAL UNIVERSITY

BY

BİLGE KARAKÜTÜK

IN PARTIAL FULFILLMENT OF THE REQUIREMENTS
FOR
THE DEGREE OF MASTER OF SCIENCE
IN
CIVIL ENGINEERING

SEPTEMBER 2024

Approval of the thesis:

NUMERICAL MODELING OF WATER CIRCULATION AND SEDIMENT TRANSPORT FOR POLLUTION CONTROL IN FETHIYE BAY: A COMPOUND ANALYSIS

submitted by **BİLGE KARAKÜTÜK** in partial fulfillment of the requirements for the degree of **Master of Science** i**n Civil Engineering, Middle East Technical University** by,

Prof. Dr. Naci Emre Altun
Dean, **Graduate School of Natural and Applied Sciences** _____

Prof. Dr. Erdem Canbay
Head of the Department, **Civil Engineering** _____

Prof. Dr. Ahmet Cevdet Yalçıner
Supervisor, **Civil Engineering, METU** _____

Examining Committee Members:

Assist. Prof. Dr. Cüneyt Baykal
Civil Engineering, METU _____

Prof. Dr. Ahmet Cevdet Yalçıner
Civil Engineering, METU _____

Assist. Prof. Dr. Gülizar Özyurt Tarakcıoğlu
Civil Engineering, METU _____

Assoc. Prof. Dr. Emre Alp
Environmental Engineering, METU _____

Assist. Prof. Dr. Doğan Kısacık
Civil Engineering, IZTECH _____

Date: 03.09.2024

I hereby declare that all information in this document has been obtained and presented in accordance with academic rules and ethical conduct. I also declare that, as required by these rules and conduct, I have fully cited and referenced all material and results that are not original to this work.

Name Last name : Bilge Karakütük

Signature :

ABSTRACT

NUMERICAL MODELING OF WATER CIRCULATION AND SEDIMENT TRANSPORT FOR POLLUTION CONTROL IN FETHIYE BAY: A COMPOUND ANALYSIS

Karakütük, Bilge
Master of Science, Civil Engineering
Supervisor: Prof. Dr. Ahmet Cevdet Yalçıner

September 2024, 120 pages

This study focuses on the changing water circulation and sediment transport patterns in Fethiye Bay, a semi-enclosed basin located in southwestern Türkiye under the dredging activities considered for pollution control. The bay suffers from heavy pollution and sedimentation as a consequence of low circulation, inadequate waste management and waste discharge. Through the study, the water circulation driven by oceanographic (winds, tides and waves) and fluvial (river discharges) sources is assessed and the optimum dredging scenarios (area and depth) are identified by evaluating current patterns and sediment deposition within the bay. Bathymetric variations (erosion and deposition zones) over a fifteen-year period are analyzed and shallowing zones are identified. Then, a numerical modeling approach is taken by using Delft3D, incorporating the tide, wind, wave and river characteristics of the region. Available bathymetric, hydrographic, meteorological, and sea level data are utilized to set the model, and current velocity measurements are used for model calibration. The study results provide insights for dredging operations by evaluating different scenarios based on changes in water circulation and sediment transport. It

finds a relation between the amount of water entering and leaving the bay and sediment deposition rates, primarily influenced by site characteristics, and evaluates the effects of dredging operations on water circulation and sediment transport with a multi-dimensional analysis, considering different dredging depths and wind directions. Recommendations are presented to serve as a roadmap for the planning of costly dredging operations.

Keywords: Water Circulation Modeling, Sediment Transport, Dredging Operations, Delft3D, Fethiye Bay

ÖZ

FETHİYE KÖRFEZİ'NDE KİRLİLİK KONTROLÜ İÇİN SU ÇEVRİM VE SEDİMAN TAŞINIMI MODELLEMESİ: BÜTÜNLEŞİK BİR ANALİZ

Karakütük, Bilge
Yüksek Lisans, İnşaat Mühendisliği
Tez Yöneticisi: Prof. Dr. Ahmet Cevdet Yalçıner

Eylül 2024, 120 sayfa

Bu çalışma, Türkiye'nin güneybatısında yer alan ve yarı kapalı bir havza olan Fethiye Körfezi'nde kirlilik kontrolü için düşünülen tarama faaliyetleri kapsamında değişen su çevrimi ve sediman taşınımı modellerine odaklanmaktadır. Körfez, düşük su çevrimi ve yetersiz atık yönetiminin bir sonucu olarak körfez içi ağır kirlilik ve sedimantasyondan etkilenmektedir. Bu çalışmada oşinografik (rüzgarlar, gelgitler ve dalgalar) ve flüvyal (nehir deşarjları) kaynakların etkisiyle Fethiye Körfezi'nde oluşan su çevrimi değerlendirilmiş ve körfezdeki akıntı değişimleri ve sediman birikimi davranışları göz önünde bulundurularak optimum tarama senaryoları (alan ve derinlik) belirlenmiştir. On beş yıllık bir sürede körfezde meydana gelen batimetrik değişimler (erozyon ve birikim bölgeleri) analiz edilmiş ve sığlaşma bölgeleri belirlenmiştir. Ardından, Delft3D modeli kullanılarak bölgenin gelgit, rüzgar, dalga ve nehir özelliklerini içeren bir sayısal modelleme yaklaşımı benimsenmiştir. Modelin oluşturulması için mevcut batimetrik, hidrografik, meteorolojik ve deniz seviyesi verileri, model kalibrasyonu için de akıntı hızı ölçümleri kullanılmıştır. Çalışma sonuçları, su çevrimi ve sediman taşınımındaki değişikliklere dayalı farklı senaryoların değerlendirilmesi ile tarama operasyonları

için bilgi sağlamaktadır. Körfeze giren ve çıkan su miktarı ile sediman birikim oranları arasında büyük ölçüde saha özelliklerine bağlı bir ilişki bulunmuş ve tarama operasyonlarının su çevrimi ve sediman taşınımı üzerindeki etkileri farklı tarama derinlikleri ve rüzgar yönü açısından çok boyutlu bir analizle değerlendirilmiştir. Çalışma bulguları temel alınarak, maliyetli tarama operasyonlarının planlanması için yol gösterici nitelikte öneriler sunulmuştur.

Anahtar Kelimeler: Su Çevrimi, Sediman Taşınımı, Tarama Operasyonları,
Delft3D, Fethiye Körfezi

To myself…

ACKNOWLEDGMENTS

First of all, I would like to express my gratitude to my dear supervisor, Prof. Dr. Ahmet Cevdet Yalçıner, who has shared with me not only his academic mindset but also his views and feelings about life, especially in this thesis, as well as in the other projects, conferences and field trips we have been involved in together. I am proud and thankful to work with him, to share the same team and for all the advice he has provided to me.

Whatever I wish to describe the mentoring and sincere friendship that Dr. Gözde Güney Doğan Bingöl has put forward for me will not be enough. She has both guided me academically and listened to my life concerns and worries about the future without questioning or ignoring them. Working, talking and producing new things with her has been one of the things that made me excited about each and every project. I would like to thank her for the academic and personal guidance she has provided for me and for being my co-advisor even though I could not write it on the cover of my thesis.

I would also like to express my thanks to my beloved advisor, Prof. Dr. Ayşen Ergin, who cheerfully drew me to coastal and ocean engineering, whom I enjoyed working with and who taught me so much about people and relations. I am very glad that she shared her most sincere views on life journey with me by saying, “The best is to laugh” in the difficult and perhaps depressing situations we went through.

My dear Dr. Işıkhan Güler taught me a lot about research and learning, both in engineering and social relations through the courses and the field trips we have been on together, during my graduate studies. I am very thankful to him for sharing his knowledge with me.

I also want to extend my thanks to the laboratory director, Assist. Prof. Dr. Cüneyt Baykal. From the moment I joined the laboratory team, I have gained a lot of insights

about engineering and looking through different perspectives from him both in the lectures and in the different projects we have worked on.

Before coming to the laboratory, I have learned a lot about coastal design and management in coastal engineering from Assist. Prof. Dr. Gülizar Özyurt Tarakcıoğlu, and this learning has created a curiosity and an impact for me to start my graduate studies in this division. I am thankful to have shared many academic discussions and various perspectives with her.

I would also like to thank dear Dr. Gökhan Güler, with whom I had the opportunity to have many conversations during lunch and coffee breaks. He has listened to us, shared his own life experiences, and always tried to be there not only for me but also for the other assistants in the laboratory.

I am also sure that this journey would not have been fulfilling without my dear Nuray Emre, with whom I have shared so much about life, and Yusuf Korkut, with whom I am so pleased to say good morning every day. I would like to thank them and my coastal engineering family.

I also owe a special thanks to my dear friends Akdeniz İnce, Alperen Korkmaz, Arif Çağatay Uysal, Aslıhan Devran, Ayşenur Gökdağ, Barış Ufuk Şentürk, Berkay Akyol, Berkay Erler, Cem Sevindik, Elif Ayşe Öztürk, Furkan Demir, Görkem Kılıç, Günay Gazaloğlu, İrem Naz Kösem, Işım Ergülen, Mert Yaman, Serim Doğaç Sayar, Setenay Pakize Özaslan, Utku Uzun and Yağız Arda Çiçek, with whom I had fun in the laboratory, complained and learned together. It has been a great joy for me to share my graduate studies with you.

To my lovely friends Baran Şimşek, Cem Maraşlıoğlu, Erhan Öz, Satuk Buğrahan Sari, Vera Can, my dear best friend, Irmak Özdemir and my beloved Samed Cemal Kılıç, whom I met during my undergraduate studies, I extend my heartfelt thanks. I would not be sharing these lines without the beautiful friendships they have offered me, and the many fun memories and the fulfilling stories we have overcome together. I have learned a lot from you all, and I would deeply like to thank you all separately.

Finally, I would like to thank my dear family: my mother, Meliha Karakütük, my father, Kasım Karakütük, my sister, Özge Oytun, my brother, Özgür Oytun and my lovely niece İdil Oytun, for their unconditional love, care and advice. I would not be the person I am today without the generous opportunities they gave me, their meaningful perspectives on life and their teachings. I am truly lucky to have such a family, and I am grateful for their endless support and trust.

Part of the bathymetric metadata used in this thesis study has been derived from the METU TRANSFER Project (2007). In addition, this thesis study has been supported with data of bathymetry, current, and wind, which has been provided by Muğla Metropolitan Municipality (MMM) and the Environment Protection and Control Department of Muğla Metropolitan Municipality.

TABLE OF CONTENTS

LIST OF TABLES

TABLES

LIST OF FIGURES

FIGURES

LIST OF ABBREVIATIONS

ABBREVIATIONS

ASTER	Advanced Space borne Thermal Emission and Reflection Radiometer
CFSR	Climate Forecast System Reanalysis
ECMWF	European Centre for Medium-Range Weather Forecasts
ERA5	ECMWF Climate Reanalysis Dataset v5
FVCOM	Finite Volume Community Ocean Model
GEBCO	General Bathymetric Chart of the Oceans
GUI	Graphical User Interface
MEVBIS	Turkish State Meteorological Service
MMM	Muğla Metropolitan Municipality
NCEP	National Centers for Environmental Information
RMSE	Root Mean Square Error
ROMS	Regional Ocean Modeling System
SWAN	Simulating Waves in the Nearshore
TUDES	Turkish National Sea Level Monitoring System
1D	One Dimensional
2D	Two Dimensional
3D	Three Dimensional

LIST OF SYMBOLS

SYMBOLS

B_k	Buoyancy production or destruction of k
B_ε	Buoyancy production or destruction of ε
$c_{2\varepsilon}$	Emprical constant based on ε
c_g	Group velocity vector
c_{kmx}	Mass concentration of the sediment
c_{vol}^{l}	Volumetric concentration of sediment fraction
c_θ	Propagation velocity of direction
c_σ	Propagation velocity of frequency
C_D	Wind drag coefficient
C_{Dmax}	Maximum magnitude of wind drag coefficient
c	Sediment concentration
c_a	The sediment concentration at a different reference height or layer in the water column
D_H	Horizontal diffusivity term
D_V	Vertical diffusivity term
D_v	Vertical sediment diffusion coefficient
D_{N50}	Nominal diameter of median sediment size
d_{50}	Median sediment diameter
ϵ_x	Diffusion coefficient in the x direction
ϵ_y	Diffusion coefficient in the y direction
ϵ_z	Diffusion coefficient in the z direction
$E(f,\theta)$	Energy density spectrum
$E(\sigma,\theta)$	Wave energy density
ε	Dissipation
η	Relative availability of sediment fraction through the mixing layer
F_x	Horizontal Reynold's stresses in the x direction

F_x	Horizontal Reynold's stresses in the y direction
f_{MOR}	Morphological acceleration factor
f_w	Wave frequency
f	Coriolis parameter
g	Acceleration of gravity
h	Total water depth
k	Turbulent energy
l	Sediment fraction
$LSED$	Total number of sediment fractions
M	Mixing layer
M_e	Excess sediment mobility number
M_x	External source effect due to discharge effects in the x direction
M_y	External source effect due to discharge effects in the y direction
N	Total number of the data points in RMSE
$N(\sigma, \theta)$	Action density spectrum
P	Probability in Gumbel old fit
ω_s	Settling velocity of the sediment
ω	Vertical velocity
P_k	Production of turbulence kinetic energy due to mean velocity gradients
P_x	Horizontal pressure term in the x direction
P_y	Horizontal pressure term in the y direction
P_ε	Production of turbulence dissipation rate due to mean velocity gradients
Q	River discharge
ρ	Effective density of the fluid-sediment mixture
ρ_0	Ambient density of water
ρ_s^l	Density of the solid particles
ρ_w	Density of water

S_{diss}	Dissipation source term
S_{ij}	Radiation stress tensor
$\overline{S_{ij}}$	Time-averaged radiation stress
S_{in}	Wind input source term
S_{nl}	Non-linear wave-wave interactions source term
$\|S_b\|$	Magnitude of bed load transport
$\Delta S_{sus}^{(m,n)}$	Net sediment changes due to suspended transport
S	Effects of the water discharge per unit area
σ'	Vertical coordinate of the specified time step
σ	Vertical coordinate in general
σ	Relative angular frequency of waves
t	Time
T	Total simulation duration
θ	Wave direction
U	Generalized Lagrangian Mean velocity component in *x* direction
U_{10}	Wind speed at 10 m above mean sea level
U_{on}	High-frequency near-bed orbital velocity
u	Eulerian velocity components in the x direction
Ω	Angular speed
V	Generalized Lagrangian Mean velocity component in *y* direction
v	Eulerian velocity components in the y direction
v_R	Magnitude of the depth-averaged Eulerian velocity in the bottom
v_H	Horizontal velocity
v_V	Vertical velocity
v_{cr}	Critical depth-averaged velocity based on Shields curve
$v_{measured}$	Measured velocity data of horizontal velocity
$v_{predicted}$	Model result of horizontal velocity
w_{Δ_s}	Settling velocity of the sediment particles with relative density
Δz	Vertical distance from the specified level

Δ_s	Relative sediment density
ζ	Free surface elevation
∇	Divergence Operator

CHAPTER 1

INTRODUCTION

1.1 Background and problem statement

Preserving coastal zones is essential for sustainable development as these areas are vital for human prosperity, considering the economic, cultural, and natural resources they offer to humanity (Clark, 1997). However, many of the coastal cities face challenges due to overpopulation and consequent human caused problems like overfishing, pollution, and misuse. Pollution in those areas could be linked to inadequate water circulation, consequently lower current velocities and possible transport of cohesive substances with their settlement and deposition on the seabed. Hence, understanding the morphological characteristics of a coastal area facing pollution is a key step before developing appropriate design strategies for the prosperity of local communities.

Semi-enclosed basins have been one of the most important coastal areas throughout human history as they are naturally preserved in coastal zones (Raicevich et al., 2018). The sheltering nature of such areas also brings about low circulation and accumulation of various materials. The Mediterranean region features numerous semi-enclosed basins due to its geography. Fethiye Bay is a good example of such areas, which suffers from excessive sedimentation and shoaling as well as heavy pollution in its inner bay. Hence, in this thesis, it is selected as the case study for semi-enclosed bays, considering the Aegean-Mediterranean region. The issues in Fethiye Bay arise from inadequate water circulation and transport of cohesive materials from rivers, compounded by insufficient freshwater inflow. Pollution from cruise boats, the wastewater treatment plant in Fethiye, poorly planned river and channel rehabilitation works, fish farms, and small industrial sites along the coast

also cause additional problems. Consequently, costly dredging operations are often necessary. Effective dredging operations in the inner bay area of Fethiye offer a potential solution; however, they require detailed investigation and validation through modeling studies to ensure optimal performance. Hence, these operations must be guided by comprehensive modeling studies that consider the oceanographic and fluvial drivers in the study area.

The models used in three previous studies by Akbasoglu (2011), Dzabic (2012) and Akdeniz (2018) on water circulation and sediment transport in Fethiye Bay are also evaluated in terms of both applicability and model limitations. The model results are analyzed, and the problem in the region appears to be not fully reflected. Sediment deposition zones observed in real life are not captured in their model results of the sediment distribution due to the low-resolution, having horizontal grid sizes of 900 m and no vertical layers are taken into consideration (Akbasoglu, 2011). The similar model set-up is also used for the water circulation patterns are evaluated under only wind input, and the problem in the bay is investigated focusing on the yacht carrying capacity (Dzabic, 2012). In addition, the obtained water circulation behaviors are limited in examining the areal current distribution in the bay since it is not performed with a high-resolution model, having horizontal grid sizes of 100 m and 5 vertical layers (Akdeniz, 2018). At this point, it is important to note that no field research or field measurements were available in the region at the time of these studies, meaning that calibration and validation could not be performed.

In the literature, studies on dredging operations mostly focus on suspended sediment motion modeling during these operations (Bai et al., 2003; Je et al., 2007; Beercroft, 2019), responses of rivers under dredging (Jeong et al., 2016; Lagasse, 1986), possible damages of dredging to various species on the seabed such as posidonias, and water quality measurements (Torres et al., 2009; Chen et al., 2016). Although there are several studies on the optimization of dredging operations and the appropriate methodologies to be applied, they usually cover dredging operations planned for the creation of navigation channels in harbor mouths or investigate the

dynamic response for different dredging types (Alvarez et al., 2007; Silveira et al., 2017; Campmans et al., 2021). The studies on dredging operations based on the water circulation and sediment transport modeling in semi-enclosed basins that evaluate the characteristics of the area by incorporating both oceanographic and fluvial effects such as tidal, wind, wave and river discharge are very limited. In addition, the presented optimization of dredging operations is generally examined in terms of boat sizes related to cost and port capacity in the available studies, where their analysis of dredging operations does not consider parameter variances that may reflect the characteristics of the region.

All these summarized above indicate the need for a study on the analysis of optimal conditions for dredging operations, including water circulation and sediment transport modeling, before the planned costly operations in Fethiye Bay, an example of a semi-enclosed basin that faces pollution related to sedimentation.

1.2 Objective and research questions

The aim of this thesis is to conduct a comprehensive analysis of water circulation and sediment transport dynamics during dredging operations for pollution control in a semi-enclosed bay: Fethiye Bay. This research intends to demonstrate the relationship between water circulation and sediment transport in the bay through modeling that incorporates the characteristics of the region. It seeks to examine the relationship between these two dynamics and to illustrate the effect of dredging operations on water inflow and outflow and sediment deposition. Additionally, the study discusses the effects of different dredging depths and area variations on water circulation and sediment transport patterns. This thesis study is structured to address the following key questions:

i. How do the tide, wind, wave, and river discharge interactions affect water circulation and sediment transport dynamics in semi-enclosed basins, particularly in Fethiye Bay?

ii. To what extent do water circulation behaviors correlate with sediment transport dynamics in semi-enclosed basins, especially in Fethiye Bay?
iii. Do dredging operations increase water exchange behavior and current velocities in semi-enclosed basins and decrease cumulative deposition rates in the region, Fethiye Bay?
iv. How do circulation patterns and sediment transport patterns vary with different dredging depths and areas?

The relationship between water circulation and sediment transport behavior under the current input parameters and the dredging operations, specifically examining whether a correlation between them exists in Fethiye Bay. This analysis is conducted through areal distributions of maximum horizontal velocity, total sediment transport and cumulative sediment deposition from the model results. These relations are also analyzed through water exchange and cumulative sediment deposition rates under the changing effect of wind direction and dredging depths.

1.3 Methodology and structure of the thesis

The thesis consists of six chapters, where the second chapter of the thesis presents a literature review of the thesis topic. In this chapter, the numerical models used for water circulation and sediment transport are summarized through similar studies and the studies on dredging operations and pollution from these models are reviewed. The characteristics of semi-enclosed basins and the characteristics of the selected case study area are presented.

The third chapter describes the methodology of the compound analysis. It gives the properties of the numerical model used as well as the significant equations, presents the available data coverage examined for the model, and shares the details of the model built within the scope of the study. It describes the effect of the input parameter change given within the scope of the study on the calibration process and how much the determined inputs change the model results.

In the fourth chapter, the analysis of available data conditions is presented, with the details behind the performed analyses, followed by an explanation of the scenarios developed for the study and the methodology behind their creation.

The fifth chapter contains the results of the numerical experiments, containing the investigation of the relation between the water circulation and sediment transport dynamics under the scenarios specified in the fourth chapter. It shows the effects of various dredging scenarios on these two dynamics, and also explores the link between water exchange and cumulative deposition volumes over the study region.

The sixth chapter is the conclusion that evaluates the results of the study conducted within the scope of the thesis. It summarizes the findings of the study and outlines the planned future work.

CHAPTER 2

LITERATURE REVIEW

Understanding and evaluating the available tools and methods, e.g., numerical models within the scope of this thesis, from the literature is essential to comprehend the changing water circulation and sediment transportation dynamics due to dredging operations in semi-enclosed basins. This chapter provides an overview of the numerical models and approaches commonly used in the literature to study various problems in coastal environments related to the water circulation and sediment transport characteristics along with the dredging operations. It also covers the characteristics of the model selected for this study and its formulations of hydrodynamic and sediment transport, citing examples in semi-enclosed basins and the current condition of the selected case study area.

2.1 Numerical models used for circulation and sediment transport

Numerical models are useful tools and time-efficient research methods for understanding complex real-life behaviors of coastal engineering problems, such as water circulation and sediment transport in coastal areas. These models address complex real-life circulation and sediment transport dynamics in various environmental conditions, helping to solve numerous problems in coastal areas. Papanicolaou et al. (2008) evaluated these models in terms of their solution capacity and source code dynamics, intended use, flow characteristics and sediment transport conditions and model characteristics of sediment exchange processes. Five hydrodynamic-sediment models are selected for evaluation both among the models with three-dimensional (3D) solution capacities shown in this paper and among the models studied in the literature in the field of Fethiye: FVCOM, MIKE3, ROMS, TELEMAC and DELFT3D.

The finite-volume community ocean model (FVCOM), one of the most widely used open-source hydrodynamic-sediment models, was developed by Chen et al. (2003). Since the model simulates only currents, temperature and salinity, Yang (2011) introduced the Simulating Waves in the Nearshore (SWAN) model and FVCOM wave-current model to add wave characteristics. This model is used by Qi et al. (2023) to model suspended sediment concentrations in Weifang Port under tidal, wind and wave conditions, and a sediment-settling-velocity formula is proposed. In which, the study revealed that the coupled model gives better results than the results given by FVCOM alone.

The Regional Ocean Modeling System (ROMS) model developed by Warner et al. (2008) is also another open source hydrodynamic-sediment model, which is available for coupling with SWAN. Cheng et al. (2017) used the ROMS model to study wind- and tidal-induced water circulation and sediment transport in Beibu Bay, but since ROMS is only a hydrodynamic-sediment model, wave effect is not included in such studies. Huang et al. (2008) compared the FVCOM and ROMS model in various idealized scenarios, and emphasized that FVCOM may give better results for cases with higher horizontal resolution than ROMS in the wind-driven scenario.

Although not open source, the MIKE 3 model developed by DHI (DHI, 2012) has been used in many studies in the literature and Liu et al. (2024) compared the model with observation data after a post-reclamation in the Bohai Sea and demonstrated its reliability. Srše et al. (2023) used the MIKE 3 model to perform hydrodynamic and sediment transport modeling to investigate the dynamics of sediment resuspension on the bottom caused by large ships at Port of Koper, Slovenia, demonstrating the versatility of the model to study different dynamics.

TELEMAC (Villaret et al., 2013), also one of the open source models, has been widely used in estuary and coastal scenarios, primarily developed for tide and current-induced hydrodynamic transport. Brown & Davies (2009) ran TELEMAC with SISPHYE and TOMAWAC modules together in order to investigate the flow-

wave effect together and examined the sediment transport effect caused by wave and tidal effects together in Dyfi Estuary. Tassi et al. (2023) presented the GAIA module that can be implemented on the TELEMAC model, in which the module efficiently manages hydrodynamic analysis and sediment transport problems on unstructured networks proposed within the TELEMAC system. In addition, Samaras et al. (2016) showed that the TELEMAC model suite produced similar results to MIKE 21/3 in a multi-parametric analysis in their modeling study on the Italian coast.

The Delft3D model (Deltares, 2020) is another widely used model in the literature as it is open-source, offering both a source-code and a Graphical User Interface (GUI) based interface, which provides a user friendly modeling environment for water circulation and sediment transport. Elias et al. (2000) demonstrated the validation of the model in hydrodynamic terms with field measurements of water level, current and wave in Egmond, the Netherlands, which is part of the Dutch coastal systems.

Lesser et al. (2004), on the other hand, examined sediment transport under 3D flow in three different experiments of trench mitigation, curved flume, and wave-current flume experiments and validated the model in the IJmuiden harbor through the bathymetry and near-bed flow field changes, by following the model's response to entrainment, transport and settling of sediment, varying levels of uniform bed shear stress and the effects of wave orbital motion on suspended sediment concentration. This study contains the morphological developments of Delft3D by giving a new perspective to the morphological models working in one-dimensional (1D) and two-dimensional (2D) which were generally used at that time.

Delft3D mainly focuses on hydrodynamic conditions and sediment transport under tide and river discharge as well as wind inputs, especially in delta-type formations, considering the need in the Netherlands. Yu et al. (2024) studied the development of tidal-flats in the context of de-reclamation in Jiangsu, China, whereas Brakenhoff et al. (2020) studied the effect of bottom roughness under wave and tide on the

hydrodynamics and sediment transport in the Ameland ebb-tidal delta in the area of Vaklodingen, the Netherlands.

In addition, Delft3D has many applications in coastal areas such as gulfs, straits and bays where the dynamics of water circulation and sediment transport are relatively different than the tidal-flats. Through similar examples from Türkiye, Koşucu et al. (2019) and Erdik et al. (2019) modeled the water circulation in the Bosphorus via Delft3D model and studied the flow based on salinity and temperature. The occurrence of significant vertical mixing flows, especially in the "hydraulic control" sections are highlighted and discussed over salinity profiles over seasonal changes and exchange flows and corresponding drivers.

Song et al. (2020) investigated the hydrodynamic and morphological physics of Bohai Bay with a wave and current coupled model for extreme weather conditions by taking into account tide, wind, and wave effects, where the depth-averaged current velocity in southwestern Bohai Bay is significantly reduced during extreme weather conditions due to enhanced bottom roughness from wave-current interactions, particularly in areas with severe wave breaking near jetties, which in turn affects sediment transport dynamics.

2.1.1 Approaches and models used for dredging operations and pollution control

Although water circulation and sediment transport dynamics under the dredging operations are limited in the literature, here, similar studies available for each of the selected models and their general scope are presented.

Wang et al. (2014) modeled the stability and sediment transport in the channel after dredging operations in Tieshan Bay using FVCOM. The model that is implemented under wind and tidal-driven scenarios, simulates the hydrodynamics and the sediment transport patterns in the region in general terms, but does not include river and wave characteristics in the domain. Land reclamation and the background causes

responsible for siltation in the channel to be dredged and the optimization of maintenance for this operation have been studied, where the combined effects of bottom friction and advective sediment transport are found to be crucial in promoting the erosion of channels and the accretion of shoals, thereby maintaining the system's stability, but no analysis of dredging depth has been carried out.

Liu et al. (2020) evaluated the effects of dredging operations in the Ship Shoal area on the Louisiana Shelf for coastal restoration using the ROMS model. The impressive aspect of this study is that both non-cohesive and cohesive material transport modeling was examined in the study. In this context, the results of salinity and suspended mud transport behavior were evaluated by calibrating daily average significant wave height values. The study concluded that the Caminada and Raccoon Island pits are not suitable as renewable borrow areas for future dredging activities, and coastal restoration due to significant sediment infilling.

Truong et al. (2021) investigated the impact of dredging operations on the suspended sediment transport dynamics through the outputs of water quality using MIKE 21/3 under wind and wave conditions to study sediment transport patterns in Vung Ang Harbor, Vietnam. WAVEWATCH-III was used to obtain wave characteristics. Although the study provides a very comprehensive case study for the dredging operations planned in front of the port, it does not take into account the river discharge effect of the estuary located about 4.5km away from the port.

Maerker & Malcherek (2011) presented a software package called DredgeSim that can be coupled with the TELEMAC and SISPHYE by putting the effects of dredging operations on waterways on the Rhine River. At this point, this coupling process transfers velocities and water levels from the hydrodynamic TELEMAC model to SISPHYE, which in turn transfers depths and sediment distribution from the model without dredging to the DredgeSim module. DredgeSim then transfers the active suspended sediment movement behavior in the dredged scenario back to Sisphye, which in turn transfers the changed depths in the model domain to Telemac and this coupling process is completed. This study demonstrates the high adaptive capacity

of the TELEMAC model with different packages that can be experimented with in different cases, but also shows that the model is quite complicated for the user. Within the scope of the study, different dredging scenarios were tested on the Rhine River under river discharge only and the filling capacity and volume of disposal of these dredging areas were analyzed.

Fernandez-Fernandez et al. (2019) studied the wave conditions in the Mondego estuary-inlet, Portugal, and performed a modeling using Delft3D to observe the effects of high-energy waves in this system. Long-term dredging operation decisions are investigated under tide, wind and extreme wave conditions by coupling FLOW and WAVE modules. The study evaluated the sediment accumulation and erosion zones in tidal inlets, paying attention to the navigation channel depths in ports and marinas at the mouth of the Mondego River, and revealed that dredging operations prevent a rapid sedimentation behavior at the entrance of the system that can be problematic. This study demonstrates the convenience of examining the changes in tidal inlets under dredging operations with the Delft3D model depending on various parameters and the diversity and reliability of results in the Delft3D model.

2.1.2 Model selection – Delft3D model

Considering the numerical models discussed in this study, the first priority of the model selection is determined as the numerical infrastructure to be open-source. Ease of use of the model is also another priority in order to make the model easily adaptable to the characteristics of the region. Comparing the three most used models, ROMS, TELEMAC and Delft3D, it is concluded that all three models solve similar equations in terms of hydrodynamics and are equivalent in terms of computational capacity. At this point, modeling with ROMS revealed that to accurately reflect the wave effects in the model, it was necessary to couple it with the SWAN model, possibly through an offline-coupling process. On the contrary, it was thought that online coupling would give more accurate results with the FLOW and WAVE

modules in Delft3D, as this method is preferred to reflect both tidal, wind, wave and river discharge effects in the model at the same time.

Since TELEMAC is an open-source model with a high computational capacity in terms of numerical modeling, it is one of the most widely used models in the literature and appeals to a wide range of users. However, when the ease of use is discussed, due to the lack of an interactive interface and the fact that it defines a very raw process for the user, it was considered whether the real-life effects could be fully reflected in a limited time, concluding a preference for Delft3D. Considering all these conditions, Delft3D was chosen as the numerical model infrastructure to be used in this study due to its ease of use in the model, applicability to a wide range of problems, online coupling process, and appeal to a relatively diverse audience.

2.2 Characteristics of semi-enclosed basins

Semi-enclosed basins, which are formed due to tectonic movements, have different dynamics in terms of water circulation compared to regular bays with their characteristic bowl-shape formations (Aleman et al., 2013). Due to their topography, water inflow and outflow are limited in these basins and water circulation and in-bay water velocities are generally low. In addition, these basins suffer from various problems such as poor in-bay water and sediment quality and eutrophication due to human utilization in densely populated and developed areas (Nishima et al., 2019).

Semi-enclosed basins have hosted different cultures and civilizations (Scovazzi, 2024) in terms of fishing and tourism throughout history due to their sheltered natures and are among the important coastal structures in this respect. When the semi-enclosed basins in Europe are analyzed (Raicevich et al., 2018), compared to the North Sea, Finnish Arcipelago Sea, Northeast Atlantic, Azores and Black Sea, the Mediterranean Sea covers a larger proportion of semi-enclosed basins due to tectonic formations.

2.2.1 Dredging operation studies in semi-enclosed basins

To understand whether these basins have similar characteristics in terms of water circulation and sediment transport, the case studies of semi-enclosed basins on the European coasts through numerical modeling are examined. Given the large area of the Mediterranean Sea, the area to be selected as a case study within the scope of this thesis is considered to be one of the semi-enclosed basins along the Turkish coasts. In that regard, the Gulf of Riga case study for the North Sea, examples of Boka Kotorska Bay, and Izmir Bay for the Mediterranean Sea are reviewed.

Lips et al. (2016) developed a regional model to study the circulation in the Gulf of Riga in the Baltic Sea. The circulation status in the study area was assessed through areal salinity distributions and revealed that the variability of the results is mostly dependent on wind stress. This is an additional study that shows that the wind effect is significant, which has been demonstrated for other semi-enclosed basins.

The 1979 UNESCO World Heritage Site Boka Kotorska Bay is one of the examples of a semi-enclosed basin in the Mediterranean, which is evaluated in terms of pollution (Mikac et al., 2022). The study analyzed sediment samples from the site and investigated the sources and patterns of metal contamination in the bay. The causes of in-bay water pollution in semi-enclosed basins, in topographies with possible river discharges, have been investigated, and although it does not focus on numerical modeling of water circulation and sediment transport, it has shed light on the general problems that may occur in such bays located in Mediterranean.

Although Izmir Inner Bay in the Gulf of Izmir is not exactly a semi-enclosed basin, considering the low water circulation pattern, low amount of water entering and leaving the gulf, and pollution patterns in the gulf, it may be important in terms of intensive capacity in Türkiye and providing insights within the scope of studies in the literature. Karahan (2002) evaluated the water exchange volumes entering and leaving the inner bay of Izmir Bay with a simple 3D hydrodynamic model according to different wind directions. The study focuses on the low water circulation in the

inner bay and the accumulation of sediment transported by the Gediz river, resulting in insights into the conditions of water circulation behaviors in semi-enclosed basins.

All these studies confirmed the general understanding of semi-enclosed basins and provided valuable insights for the scope of this study. They indicate that, due to the geographical structure of these areas, various problems such as wind- dependent changes in water circulation, eutrophication and pollution have been shown to commonly occur.

2.2.2 Fethiye case study: a semi-enclosed basin

Fethiye Bay is selected as the case study area because it is a semi-enclosed basin located on the Mediterranean coast of Türkiye, significant for tourism and economy. The region offers various insights into the problem due to existing studies, and there is a need for up-to-date research because of increased pollution in the area. The bay is located in the Gulf of Fethiye in the Mediterranean Sea, between Dalaman and Fethiye in Muğla city, in southwestern Turkiye (Figure 2.1).

It provides water in and out of the bay through two entrances to the left and right of Şövalye Island. The left side entrance is deeper and exposed to more water inflow and outflow, while the right side opening has less water interaction due to bathymetric conditions and shallowness. This geographical condition has a direct impact on the water circulation within the bay.

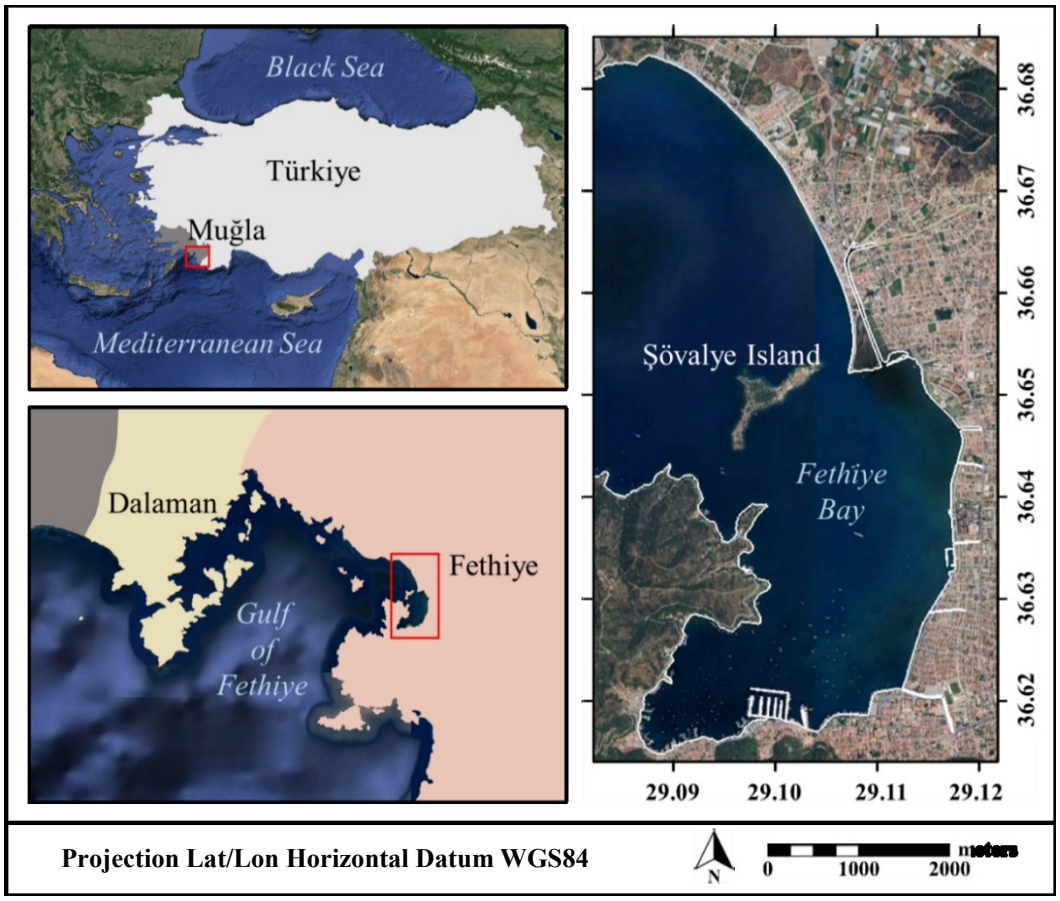

Figure 2.1. General view of the study area and location of Fethiye Bay (base images retrieved from Google Earth, 2024)

The low water circulation in the region also affects the pollution in the bay. The insufficient amount of water entering and leaving the bay negatively affects the water quality inside. Previous studies (Akbasoglu, 2011; METU OERC, 2011; Akdeniz, 2018) reveal that this situation is caused by both the geographical location and structure of the bay as well as the inflow of mud-type substances from rivers entering the bay. In addition, the wastewater treatment plant connected to Fethiye, the high touristic demand of the region, the large number of boats and marinas and the chemical and solid wastes of these boats are other sources of pollution in the region and cause an increase in pollution either directly or indirectly (Figure 2.2).

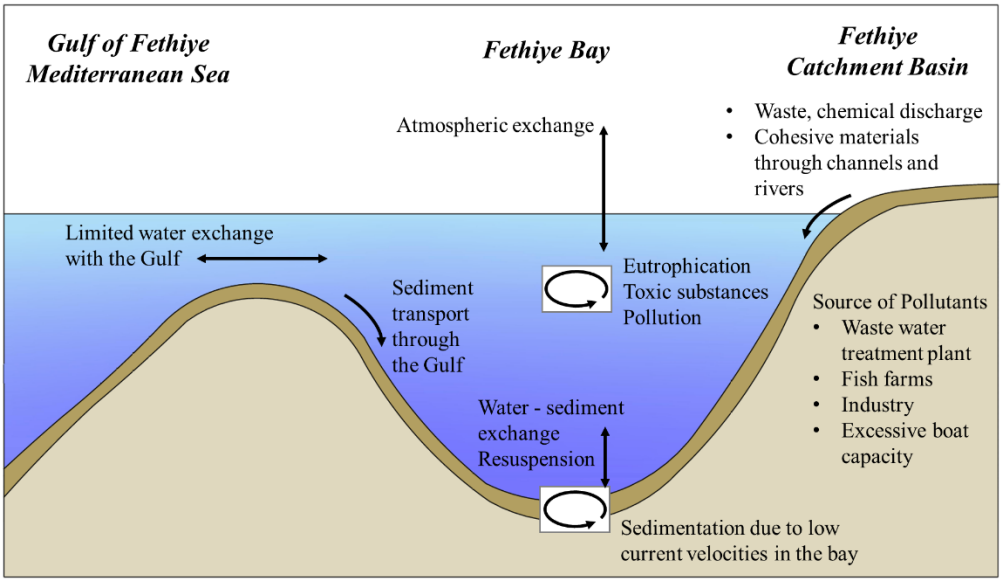

Figure 2.2. Schematic view of the problems involved in the pollution inside the Fethiye Bay

2.2.3 Site visit to Fethiye Bay

Understanding the dynamic interactions of hydrodynamic parameters is essential for effective environmental management and conservation in coastal regions. To have an understanding of the real-life conditions of the study area and to accurately reflect them in the numerical model, a site visit to Fethiye Bay is conducted on 14 (via survey by sea) and 15 (via survey by land) June. The general water condition in the bay, including the hydrodynamic characteristics, water quality, and areas of erosion and deposition, were observed during a boat trip. Considering the significant role that rivers and channels play in water discharge within the bay, these features were also examined during the investigations at site in the boat and at land. Several views taken at different locations inside the bay to understand the present conditions. The locations of the points and the pictures at these location are given in Figure 2.3.

The observed sea water conditions reveal that at points a, b, c, and d, the water appears blurry, with a greener color tone and noticeable sand movement on the

bottom due to boat activity, indicating shallower depths. Conversely, at points e, f, and g, despite a higher density of boats, the water exhibits a bluer and clearer appearance with no significant sediment movement observed from boat activity. Near the entrance of the bay, close to Şövalye Island, flow measurements are taken at points h and i. Observations indicate that the water in these areas aligns with known general problems and problematic deposition zones, highlighting the rivers and channels along the bay as contributing factors. The investigated river and channel areas and their current conditions are given in Figure 2.4.

The Murt river (points a, b, and c in Figure 2.4) and the T2-discharge channel of General Directorate of State Water Works (DSİ) (h and i) are the primary water discharge systems into the bay. These channels, along with others (d, e, f and g) have been rehabilitated to address previous issues of odor and pollution. As a result of the rehabilitation, these systems transport cohesive materials into the bay, contributing to problematic deposition areas.

The site visit to Fethiye Bay provided invaluable insights into the real-life behaviors and conditions that are crucial for validating the numerical model setup. Observations of hydrodynamic characteristics, water quality, and sediment movement at various points within the bay highlighted the complex relation between environmental processes and human activities. The detailed examination of rivers and channels further underscored their significant impact on water discharge and sediment deposition. This study demonstrates that site visits are essential in case studies to bridge the gap between theoretical models and practical, on-ground realities. Such comprehensive field investigations ensure that numerical models are reflective of actual environmental conditions, particularly in vulnerable coastal areas.

Figure 2.3. Current water conditions of the bay at different points

Figure 2.4. Current conditions of the rivers and the channels in the bay

CHAPTER 3

METHODOLOGY

The methodology followed in this thesis study covers the following steps, which are explained in detail below in this chapter: i) overall approach, ii) numerical model background, iii) analysis of available data, iv) model setup, v) sensitivity analysis and calibration, vi) and model validation. Following those steps, the scenario simulations are performed using the Delft3D numerical model based on the determined input data.

3.1 Overall Approach

This study is conducted in six phases (Figure 3.1). First, the general basics of numerical model is reviewed, and the corresponding mathematical background of the model and the coupling process details are investigated. Then, the current regional conditions are examined, up-to-date data are checked and available field measurements in the region are analyzed. Within the scope of these data, a numerical setup is built for a compound analysis via experiments, following the calibration and validation steps. In the next phase, tide, wind, wave and river discharge patterns are examined and corresponding modeling inputs are determined through long-term and extreme conditions to reflect the characteristics of the region, and dredging scenarios in terms of depth and areas are developed. Finally, these scenarios are simulated and the model results are analyzed following different conditions based on the research questions. The outputs are presented in terms of the relation between the water circulation and sediment transport patterns in areal distributions over the study region under the determined input scenarios and both for the non-dredged and dredged scenarios in the bay, and a two-dimensional analysis approach is conducted

for understanding the relation between water exchange volume and cumulative deposition inside the bay over wind directions and dredging depths.

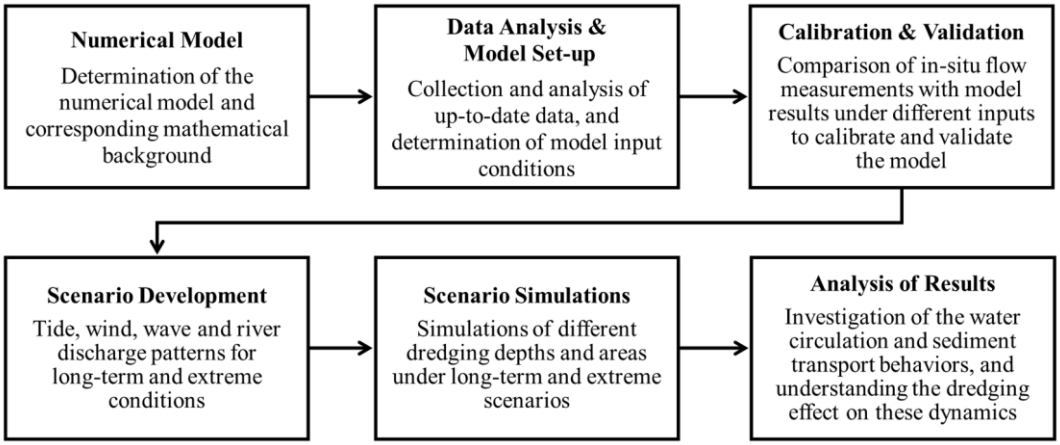

Figure 3.1. Flowchart of the modeling approach followed in this thesis

3.2 Numerical Model Background

The Delft3D model suit is an open-source comprehensive numerical modeling tool developed by Deltares for simulating various hydrodynamic, sediment transport, and water quality processes in coastal, estuarine, and riverine environments (Deltares, 2020). It contains several modules interacting consistently to provide an integrated modeling environment (Lesser et al., 2004). Among these modules, Delft3D-FLOW module is used for hydrodynamic modeling to cover tidal, wind and river effects and Delft3D-WAVE module is used to reflect wave effects. Briefly, the FLOW module considers the dynamics of flow and transport phenomena, while the WAVE module takes into account the wave propagation effect (Elias et al., 2000). In modeling complex coastal structures such as semi-enclosed basins, and especially for the integrated analysis performed in this study, it becomes essential to consider all effects on the characteristics of the region. The dynamics of both FLOW and WAVE modules provide a more detailed modeling approach and more accurate results, which is also important for the detailed assessment of water circulation and sediment transport dynamics (Gerritsen et al., 2008).

3.2.1 Hydrodynamic model equations

The hydrodynamic component of the Delft3D-FLOW module solves the unsteady shallow-water equations in both two and three dimensions, which include the horizontal momentum equations, the continuity equation, and transport equations for various scalar quantities (Lesser et al., 2004). The fundamental assumptions of the model involve the hydrostatic pressure approximation, where vertical accelerations are considered negligible compared to gravitational forces (Gerritsen et al., 2008). This assumption simplifies the vertical momentum equation into a hydrostatic pressure relation.

The horizontal momentum equations, based on the Reynolds-averaged Navier-Stokes framework for non-hydrostatic conditions, are adapted to account for the effects of turbulence through a closure model (Equations 3.1 and 3.2). These equations are typically solved on a Cartesian grid, but the model also supports curvilinear and spherical grids, providing flexibility in representing complex geometries and boundaries (Lesser et al., 2004). It assumes that the sum of the rate of velocity change with time and change in velocity due to the motion of fluid in the respective directions, the vertical advection and the Coriolis effects, is in balance with the sum of pressure gradient forces, the external including wind stress applied to the water body, the momentum sources or sinks and the vertical diffusion of momentum effects.

$$\frac{\partial U}{\partial t} + U\frac{\partial U}{\partial x} + v\frac{\partial U}{\partial y} + \frac{\omega}{h}\frac{\partial U}{\partial \sigma} - fV = -\frac{1}{\rho_0}P_x + F_x + M_x + \frac{1}{h^2}\frac{\partial U}{\partial \sigma}\left(v_V\frac{\partial U}{\partial \sigma}\right) \quad (3.1)$$

$$\frac{\partial V}{\partial t} + U\frac{\partial V}{\partial x} + V\frac{\partial U}{\partial y} + \frac{\omega}{h}\frac{\partial V}{\partial \sigma} - fU = -\frac{1}{\rho_0}P_y + F_y + M_y + \frac{1}{h^2}\frac{\partial U}{\partial \sigma}\left(v_V\frac{\partial v}{\partial \sigma}\right) \quad (3.2)$$

Where U and V are Generalized Lagrangian Mean velocity components, that are generally used for the models with wave effect, u and v are the Eulerian velocity components in the x and y directions respectively, ω is the vertical velocity, ρ_0 is the ambient density of water, P_x and P_y are the gradients of pressure in the respective

directions and v_V is the vertical velocity. f is the Coriolis parameter which is caused by Earth's rotation and geographic latitude and the angular speed Ω (Equation 3.3) (Lesser et al., 2004).

$$f = 2\Omega sin\phi \tag{3.3}$$

M_x and M_y are external source effects due to the discharge effects. P_x and P_y are the horizontal pressure terms, expressed by Boussinesq approximations (Equation 3.4 and 3.5).

$$\frac{1}{\rho_0}P_x = g\frac{\partial\zeta}{\partial x} + g\frac{h}{\rho_0}\int_\sigma^0\left(\frac{\partial\rho}{\partial x} + \frac{\partial\sigma'}{\partial x}\frac{\partial\rho}{\partial\sigma'}\right)d\sigma' \tag{3.4}$$

$$\frac{1}{\rho_0}P_y = g\frac{\partial\zeta}{\partial y} + g\frac{h}{\rho_0}\int_\sigma^0\left(\frac{\partial\rho}{\partial y} + \frac{\partial\sigma'}{\partial y}\frac{\partial\rho}{\partial\sigma'}\right)d\sigma' \tag{3.5}$$

F_x and F_y are the horizontal Reynold's stresses given with the eddy viscosity (Equation 3.6 and 3.7).

$$F_x = v_H\left(\frac{\partial^2 U}{\partial x^2} + \frac{\partial^2 U}{\partial y^2}\right) \tag{3.6}$$

$$F_y = v_H\left(\frac{\partial^2 V}{\partial x^2} + \frac{\partial^2 V}{\partial y^2}\right) \tag{3.7}$$

These vertical velocities are based on the continuity equation, where the equation for the incompressible flow is given in Equation 3.8.

$$\frac{\partial\zeta}{\partial t} + \frac{\partial hU}{\partial x} + \frac{\partial hV}{\partial y} = S \tag{3.8}$$

Where ζ is the free surface elevation, and h is the total water depth and S is the effects of the water discharge per unit area (van Rijn & Walstra, 2003). The general transport equation based on advection-diffusion dynamics is given in Equation 3.9.

$$\frac{\partial[hc]}{\partial t}+\frac{\partial[hUc]}{\partial x}+\frac{\partial[hVc]}{\partial y}+\frac{\partial[\omega c]}{\partial \sigma}$$
$$=h\left[\frac{\partial}{\partial x}\left(D_H\frac{\partial c}{\partial x}\right)+\frac{\partial}{\partial y}\left(D_H\frac{\partial c}{\partial y}\right)\right]+\frac{1}{h}\frac{\partial}{\partial \sigma}\left[D_V\frac{\partial c}{\partial \sigma}\right]+hS \tag{3.9}$$

Where D_H and D_V are the corresponding horizontal and vertical diffusivity terms that are specified along with the region characteristics. Sum of the change of concentration with the water depth with respect to time, and the advection flux of concentration in corresponding directions of x, y and σ is assumed to be in balance with the sum of horizontal and vertical diffusions of the concentration and the additional source and sink terms within the water column.

For the turbulence dynamics there are three models that can be selected: constant, *k–ε* and algebraic. Through the overall scenarios *k–ε* turbulence model is used by considering the effects of the shear stresses through the bed, surface and flow, where the turbulent energy *k* and dissipation *ε* is calculated with Equation 3.10 and 3.11.

$$\frac{\partial k}{\partial t}+u\frac{\partial k}{\partial x}+v\frac{\partial k}{\partial y}+\frac{\omega}{h}\frac{\partial k}{\partial \sigma}=\frac{1}{h^2}\frac{\partial}{\partial \sigma}\left[D_V\frac{\partial k}{\partial \sigma}\right]+P_k+B_k-\varepsilon \tag{3.10}$$

$$\frac{\partial \varepsilon}{\partial t}+u\frac{\partial \varepsilon}{\partial x}+v\frac{\partial \varepsilon}{\partial y}+\frac{\omega}{h}\frac{\partial \varepsilon}{\partial \sigma}=\frac{1}{h^2}\frac{\partial}{\partial \sigma}\left[D_V\frac{\partial \varepsilon}{\partial \sigma}\right]+P_\varepsilon+B_\varepsilon-c_{2\varepsilon}\frac{\varepsilon^2}{k} \tag{3.11}$$

Where, the temporal change of *k* and *ε,* and the advection of these in the x, y and σ directions is assumed to be in balance with the diffusion of *k* and *ε* in the vertical direction, with the addition of production of turbulence, buoyancy and dissipation.

The wave-current interactions are taken through the coupling procedure of FLOW module with the WAVE module. The wave effects are taken into consideration by the wave radiation stress that can be solved according to the selected coupling method with WAVE module. In the online coupling formulation, the energy density spectrum changes every time step (Equation 3.12), whereas in the offline coupling a time-averaged version is followed (Equation 3.13).

$$S_{ij} = \int_0^{\infty} \int_0^{2\pi} E(f_w, \theta)(\cos^2\theta - \frac{1}{2}\delta_{ij}) d\theta df_w \quad (3.12)$$

$$\overline{S_{ij}} = \frac{1}{T}\int_0^T S_{ij}(t)dt \quad (3.13)$$

Where S_{ij} is the radiation stress tensor, $E(f, \theta)$ is the energy density spectrum, θ is the wave direction, f_w is the wave frequency and $\overline{S_{ij}}$ is the time-averaged radiation stress used as steady forcing in FLOW module.

The primarily used equation is the action balance equation solved in Simulating Waves Nearshore (SWAN) model, that is integrated in the WAVE module, in which the equation governs the evolution of wave energy density through space and time (Equation 3.14).

$$\frac{\partial N}{\partial t} + \nabla \cdot \left(c_g N\right) + \frac{\partial (c_\sigma N)}{\partial \sigma} + \frac{\partial (c_\theta N)}{\partial \theta} = \frac{S_{in} + S_{nl} + S_{diss}}{\sigma} \quad (3.14)$$

Where $N(\sigma, \theta)$ is the action density spectrum, and $N = E(\sigma, \theta)/\sigma$, with $E(\sigma, \theta)$ being the wave energy density, c_g is the group velocity vector, σ is the relative angular frequency of the waves, θ is the wave direction, c_σ and c_θ are the propagation velocities respectively in frequency and direction, and S_{in}, S_{nl}, S_{diss} are the source terms representing energy input by wind, non-linear wave-wave interactions and dissipation due to the key physical processes of white-capping, bottom friction and depth-induced breaking respectively. The local rate of change of the wave action density through time, with the addition of the propagation of wave action in physical space, the changes in the action density due to the wave frequency and direction is assumed to be in balance with the source and sink terms affecting the wave action.

3.2.2 Sediment transport model equations

For sediment transport, parameters that also affect water circulation should be taken into account. The overall density of the fluid-sediment mixture is determined by accounting the contribution of multiple sediment fractions and water density, which varies depending on salinity and temperature in the model (Equation 3.15).

$$\rho = \rho_w + \sum_{l=1}^{LSED} c_{vol}^{l}(\rho_s^l - \rho_w)l \tag{3.15}$$

Where the ρ_w is the density of water, c_{vol}^{l} is the volumetric concentration of sediment fraction l, ρ_s^l is the density of the solid particles and $LSED$ is the total number of sediment fractions. This formulation is essential for accurately modeling sediment transport, buoyancy effects and other processes in the model where sediments are present in the water column.

The sediment transport model in Delft3D consists of separate formulations for bed load and suspended load transport (Deltares, 2020). Bed load transport is computed using empirical formulas that account for the shear stress exerted by water flow and waves on the sediment bed. For the models including the hydrodynamic and wave effect together, van Rijn (2001) methodology, including the effect of wave orbital velocity asymmetry, is being used (Equation 3.16).

$$|S_b| = \eta 0.006 \rho_{\Delta_s} w_{\Delta_s} M^{0.5} M_e^{0.7} \tag{3.16}$$

The equation considers various parameters such as the relative sediment density, settling velocity and Shield's parameter, which together describe how sediment particles are mobilized and transported along the bed of a water body under the influence of flowing water. In which, $|S_b|$ is the magnitude of bed load transport (kg/m/s), η is the relative availability of sediment fraction through the mixing layer, M is the sediment mobility number due to waves and currents and M_e is the excess

sediment mobility number depending on the relative sediment density ($\Delta_s = \rho_s/\rho$) and the median sediment diameter (d_{50}) (Equation 3.17, Equation 3.18)

$$M = \frac{v_R^2 + U_{on}^2}{(\Delta_s - 1) g d_{50}} \tag{3.17}$$

$$M_e = \frac{(\sqrt{v_R^2 + U_{on}^2} - v_{cr})^2}{(\Delta_s - 1) g d_{50}} \tag{3.18}$$

Where the v_R is the magnitude of the depth-averaged Eulerian velocity in the bottom later, assuming a logarithmic velocity profile, v_{cr} is the critical depth-averaged velocity based on Shields curve and U_{on} is the high-frequency near-bed orbital velocity in the direction on wave propagation based on the significant wave height due to short waves (Isobe & Horikawa, 1982). This methodology is based on the fifth-order Stokes wave theory and third-order cnodial wave theory.

Suspended load transport is governed by the advection-diffusion equation for sediment concentration (Equation 3.19).

$$\begin{aligned} &\frac{\partial c}{\partial t} + u\frac{\partial c}{\partial x} + \vartheta\frac{\partial c}{\partial y} + w\frac{\partial c}{\partial z} \\ &= \frac{\partial}{\partial x}\left(\epsilon_x \frac{\partial c}{\partial x}\right) + \frac{\partial}{\partial y}\left(\epsilon_y \frac{\partial c}{\partial y}\right) + \frac{\partial}{\partial z}\left(\epsilon_z \frac{\partial c}{\partial z}\right) - \omega_s \frac{\partial c}{\partial z} \end{aligned} \tag{3.19}$$

Where c is the sediment concentration, ϵ_x, ϵ_y, ϵ_z are the diffusion coefficients in the respective directions, and ω_s is the settling velocity of the sediment (van Rijn et al., 2003). The equation models the combined effects of advection, diffusion, and settling on the concentration of the fluid, and used in modeling the distribution of pollutants, nutrients or sediments in water bodies. The advection terms accounts for the transport by the flow, while the diffusion terms represent the spreading of the substance due to concentration.

The net sediment changes due to suspended sediment transport is calculated considering the effects of vertical diffusion, sediment settling, and differences in

sediment concentration at various heights within the water column through Equation 3.20.

$$\Delta S_{sus}^{(m,n)} = f_{MOR}\left(c_{kmx}\left(\frac{D_v}{\Delta z} + w_s\right) - c_a\left(\frac{D_v}{\Delta z}\right)\right)\Delta t \tag{3.20}$$

Where f_{MOR} is the morphological acceleration factor, D_v is the vertical sediment diffusion coefficient, Δz is the vertical distance from the specified level, and c_{kmx} is the mass concentration of the sediment.

The model includes various formulations to account for different sediment types and sizes, ensuring an accurate representation of sediment dynamics under varying hydrodynamic conditions. The exchange of sediment between the bed and the water column is also modeled, allowing for the simulation of sediment deposition and erosion processes (van Rijn et al., 2003; Luijendijk, 2001).

3.2.3 Coupling of Delft3D-FLOW and Delft3D-WAVE modules

Running Delft3D-FLOW and Delft3D-WAVE modules together to include current and wave effects together in the hydrodynamic simulation increases the capacity to examine real-life effects (Deltares, 2020). There are two different coupling options given in the model: offline (one-way) or online (two-way) coupling. In the offline coupling process, the sequential execution is performed where output from WAVE module, such as wave radiation stresses, are averaged over time and then used as steady forcing in FLOW in a separate run, with no real-time feedback. It is generally preferred in cases where the wave effects are not critical, since it is potentially less accurate for dynamic interactions. On the other hand, in the online coupling process, a real-time data exchange between FLOW and WAVE modules is performed during the simulation, at every time step, ensuring dynamic feedback between the models, such as wave-induced current changes, with a higher accuracy capturing the wave-current interactions. It is generally preferred when wave-current interactions are strong, such as in nearshore environments where wave action directly influences

currents like in this case. Therefore, the online coupling of these two modules is adopted for a compound analysis, to consider the effects of tide, wind, wave and flow discharges of the rivers carrying water to Fethiye Bay and their non-linear interactions (Figure 3.2).

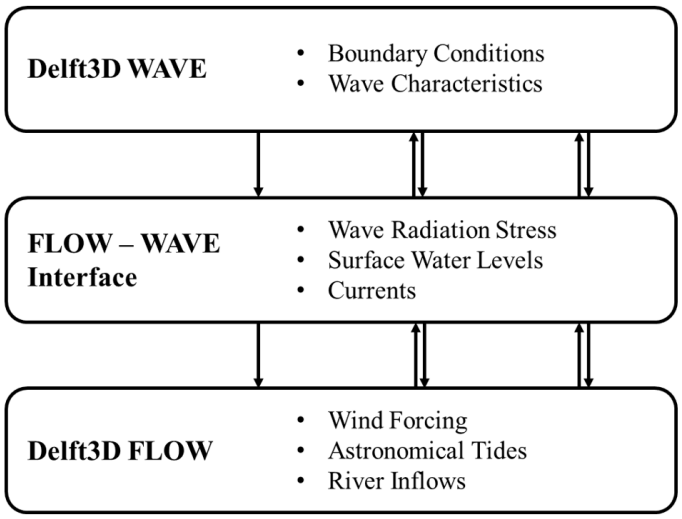

Figure 3.2. Coupling structure of the FLOW and WAVE modules

The FLOW module links with the WAVE module through wave radiation stress, surface water levels and current velocities under wind forcing, astronomical tides and river discharges. In addition, the WAVE module dynamically adapts to changes in wave characteristics on these parameters under specified boundary conditions (Lesser et al., 2004). By running these two models in multi-directional interaction, the combined effect of wind, tides and sea waves will be taken into account when modeling the water circulation in Fethiye Bay.

3.3 Available Data

Since Fethiye is an economic and touristic hub in the Aegean Sea, it has gained significant importance for the region. Consequently, the available data is more comprehensive than that for other study areas located in the Mediterranean. Through the initial data preparation phase, an up-to-date bathymetry dataset has been

prepared. In addition, the effect of tidal conditions, wind and wave characteristics and the possible discharge effects to the inner bay have been determined through the collected and analyzed data, which have been detailed as follows.

3.3.1 Bathymetry measurements

The changes in the bathymetry of a bay, provide insights for an initial understanding of the water circulation and the sediment transport inside the bay. Hence, high-resolution bathymetric measurements at certain time intervals are important data sources for such studies and monitoring the changes. The available bathymetry data of Fethiye Bay was taken by field measurements only for the two years of 2007 (METU TRANSFER Project, 2007) and 2022 (MMM, 2022). The bathymetry map of 2007 is considered as the modeling base (Figure 3.3), and the following 2022 map is constructed considering the same area.

For the current bathymetry preparation, point elevation data is taken from the field measurements (MMM, 2022) and combined with the current shoreline (Google Earth, 2022) and the land topography (ASTER, 2022), and all together projected in UTM-WGS84 (Figure 3.4). Since the bathymetry measurements are limited to the inner bay area, the outer bay bathymetry is used from the bathymetry of 2007.

Comparing the 1 m, 3 m and 5 m contour lines in these two bathymetric datasets, particularly in the area in front of the rivers, the extent of shallowing and potential sediment deposition over 15 years becomes evident. This transformation in bathymetry is discussed in more detail in Chapter 4.

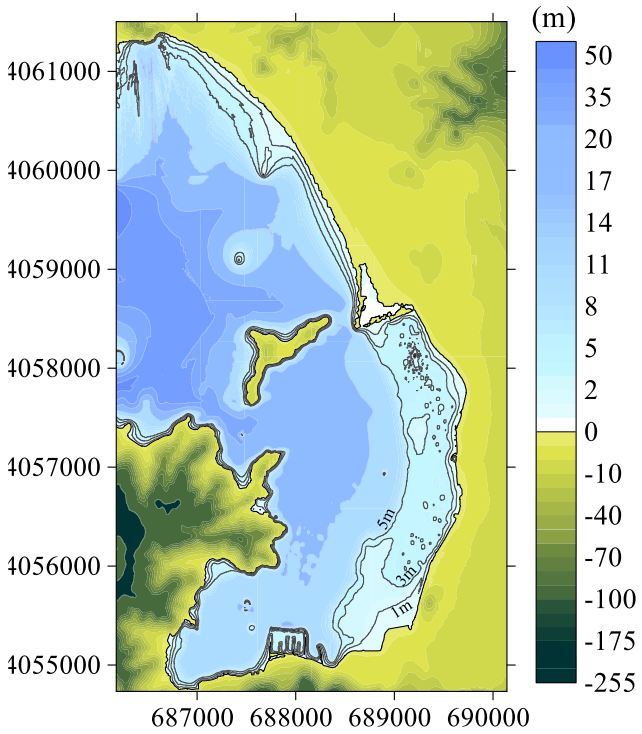

Figure 3.3. Bathymetry of Fethiye Bay in 2007

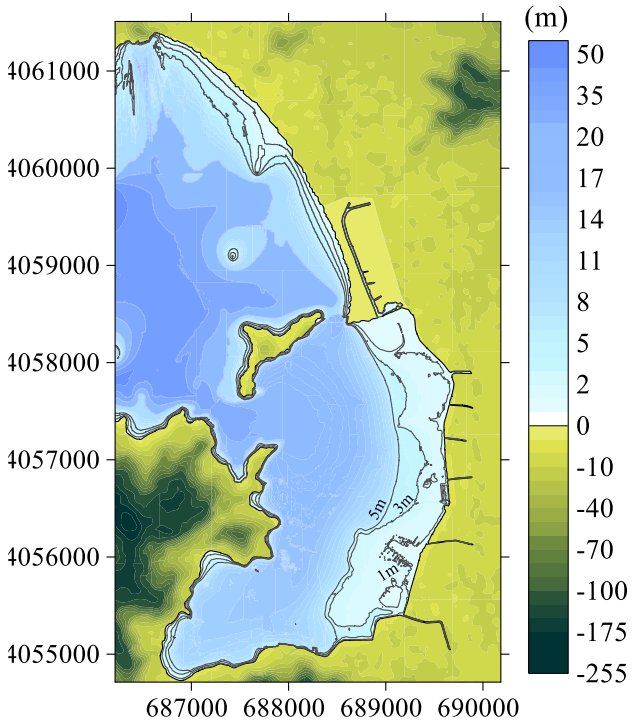

Figure 3.4. Bathymetry of Fethiye Bay in 2022

3.3.2 Current velocity measurements

The most important part of this research is to provide real life effects to enhance better results for the study area. Current velocity profile measurements at two locations near Şövalye Island (RDCP01 & RDCP02) are performed for three months, April, May, and June in 2023 by the Environment Protection and Control Department of Muğla Metropolitan Municipality. The locations of the current measurements are shown in Figure 3.5. The measurements are taken at RDCP01 (36.644703° N, 29.095361° E) located at a depth of 23 m, with 11 velocity measurement layers, and at RDCP02 (36.653200° N, 29.108089° E) located at a depth of 17 m, with 8 velocity measurement layers in all water-column for one point. This dataset for three-months duration is used for the model calibration and validation process.

Figure 3.5. The location of field measurement points near Şövalye Island (base image retrieved from Google Earth, 2024)

Horizontal current velocity values and directions obtained from these two points are evaluated in each layer as well as their behavior along the water column. In order to perform a proper time-series analysis, three different layers are selected near the surface, in the middle and near the seafloor, and the model results are evaluated at these levels. The velocities on the surface layer are not used during the calibration step as they are more prone to instantaneous misleading effects and the other layers

under the surface layer are considered as more representative of the flow conditions in the area.

The calibration layers are specified for RDCP01 as 3-5 m, 11-13 m, and 17-19 m and for RDCP02 as 3-5 m, 7-9 m, and 11-13 m and the current speeds and directions in these layers are compared to understand the general behavior along these layers. Compared time-series for April 2023 is given for RDCP01 and RDCP02 in Figure 3.6 and Figure 3.7, respectively. The details of the overall comparison for the three-month duration and comparison for May and June 2023 are given in Appendix A.

Analyzing the horizontal current velocity values from both measurement points reveals that these values generally decrease from the surface to the depth, but at times, the current speed increases at deeper levels with different current patterns. This behavior primarily indicates the influence of wind, commonly observed in semi-enclosed basins. However, it also suggests that wind input alone may not fully account for the observed variations in capturing different current patterns.

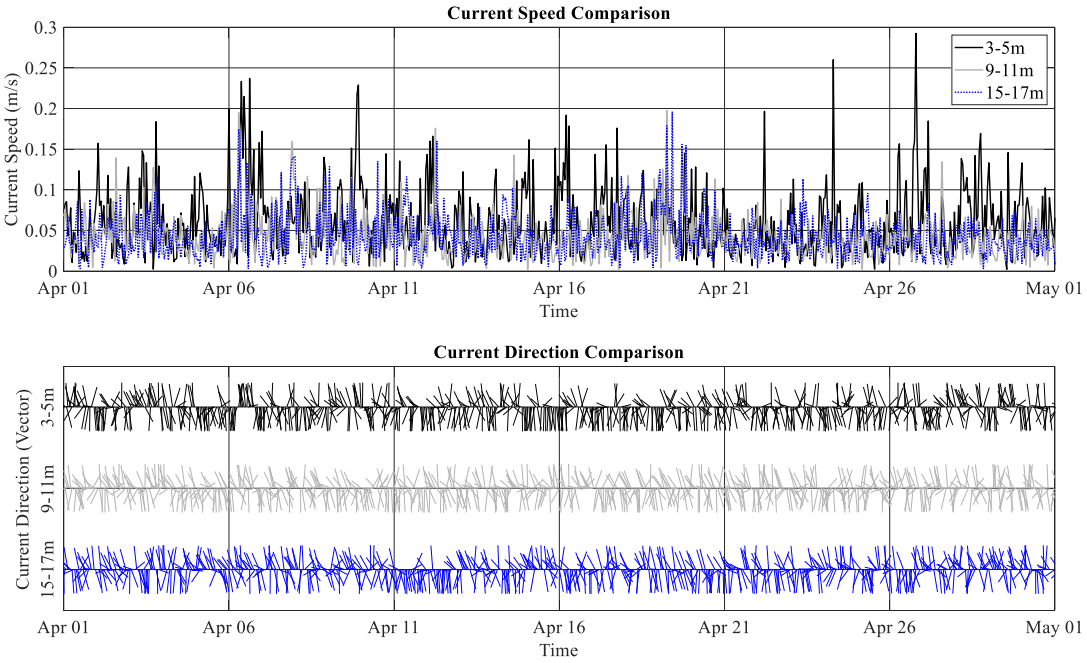

Figure 3.6. Comparison of current speeds and directions in three different measurement layers for RDCP01

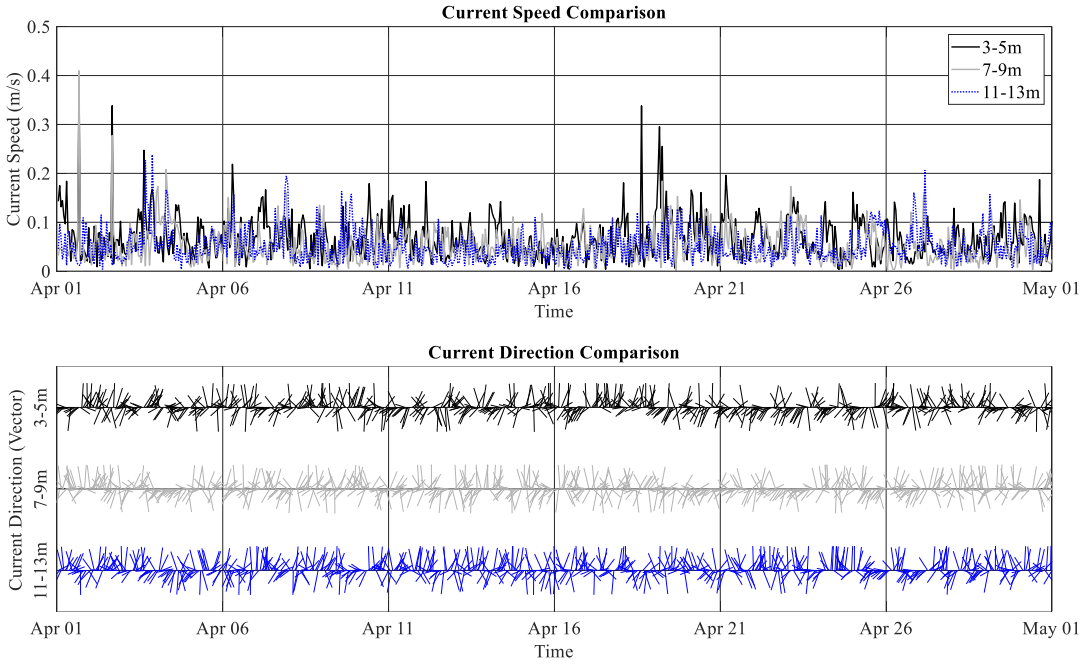

Figure 3.7. Comparison of current speeds and directions in three different measurement layers for RDCP02

3.3.3 Tidal characteristics and water level measurements

The tidal amplitudes in the Mediterranean are relatively low compared to the Aegean Sea and Black Sea (Ozturk & Yalçın, 2023). Since no field measurements are taken during the current velocity measurements in Fethiye, several databases have been investigated, and the water level elevations are taken as time series at fifteen-minutely temporal resolution from the nearest station available in Marmaris (36.838111° N, 28.385013° E) through Turkish National Sea Level Monitoring System – TUDES (2023) for the same time duration of April, May, and June in 2023. The time series of tidal data in Marmaris station has undergone quality control for potential gaps, spikes, and shifts, and a tide prediction is performed using TIDALFIT on MATLAB, where the results for the duration of April 2023 are given (Figure 3.8) respectively. The tide prediction for the three-month duration is also given in Appendix A.

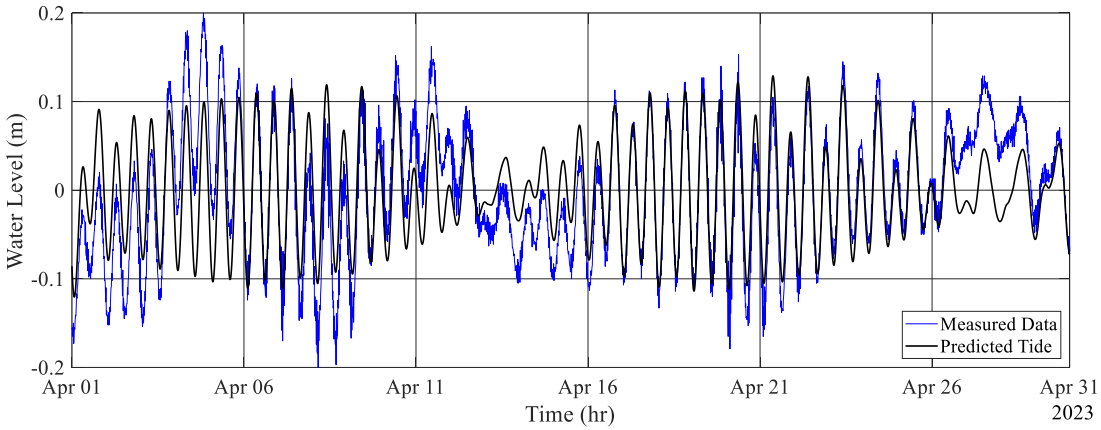

Figure 3.8. Time series of water level measurements at Marmaris station and predicted tide

The measurements in Figure 3.8 and predicted tidal signal confirm the low tidal range in the region, where tidal amplitude is observed as approximately 20-30 cm, in which it is taken as 30 cm in the model.

3.3.4 Wind conditions

Three different datasets were analyzed to understand the wind characteristics in the region: European Centre for Medium-Range Weather Forecasts (ECMWF) Climate Reanalysis Dataset v5 (ERA5), the National Centers for Environmental Information (NCEP) Climate Forecast System Reanalysis (CFSR), and the Turkish State Meteorological Service (MEVBIS) datasets. The wind data obtained from ERA5 as time series for the u and v components of wind at 10 m above sea level at hourly temporal resolution by combining the analysis of one- through three-hour forecasts with a spatial resolution of 0.25° (≈ 25 km) for the time duration of 1979 – 2023. On the other hand, the wind data is taken from CFSR as time series for the u and v components of wind at 10 m above sea level at hourly temporal resolution, by combining the analysis of one- through six-hour forecasts with a spatial resolution of 0.312° (≈ 35 km) for the time duration of 1976 – 2023. In addition, specifically, three-month data of 2023 April, May and June with hourly temporal resolution, by

combining the minutely taken wind-measurements directly at the project site, are collected from MEVBIS. Using these datasets, both long-term and three-month data were analyzed at the points in each dataset that are identified as closest to the study area (Figure 3.9).

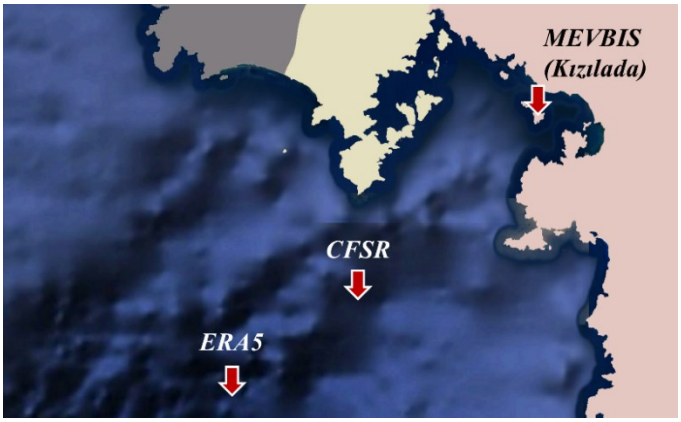

Figure 3.9. Locations of the three datasets compared (base image retrieved from Google Earth, 2024)

The spatial resolution of the ERA5 and CFSR data are low, where the nearest data points are located respectively 45 km and 30 km away to the study region. Using the ERA5 and CFSR data, long-term wind analyses were carried out and the results of the analyses are detailed in Chapter 4. Before the calibration process, time series of three-month duration from these data sources are compared to address appropriate input conditions for wind. For simplicity, the wind speed and direction comparison for the 2023 April is given in (Figure 3.10). The details of the overall comparison for three-month duration (April, May and June) and other comparison for each month separately are given in Appendix A.

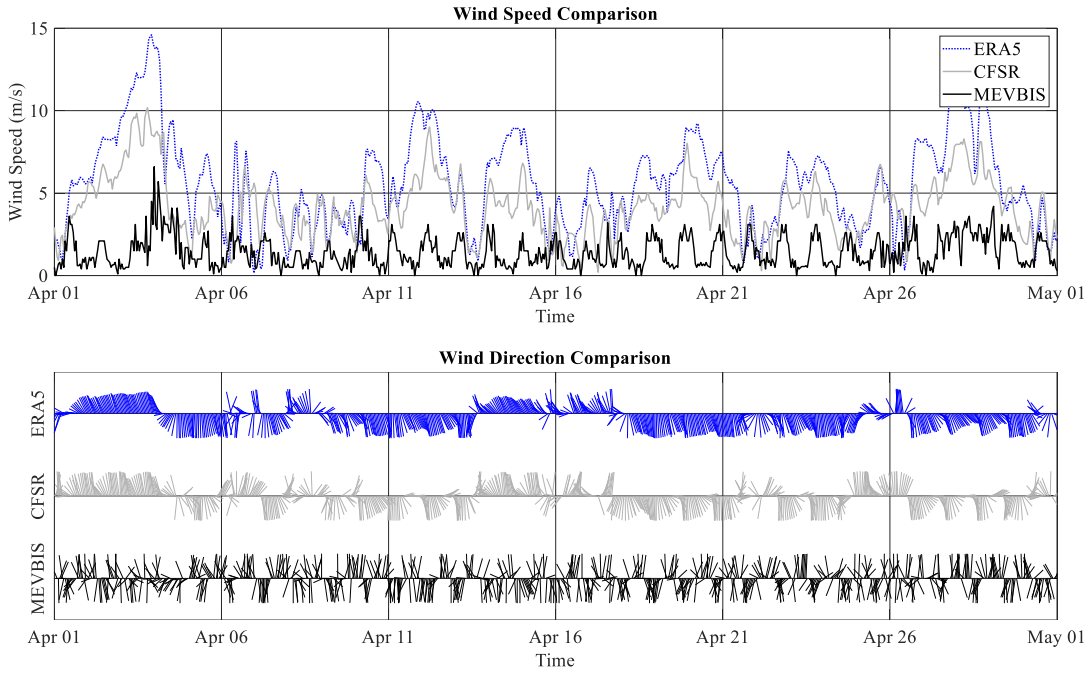

Figure 3.10. Wind speed and direction comparison for April 2023

When the data from the three data sources are compared, considering their distance to the study area, it is observed that the wind speeds in the ERA5 dataset, show larger values in the order of 2-3 times of those measured in MEVBIS Kızılada station. This difference can be attributed to the location of the ERA5 data point, which is at a distant point offshore, and the temporal resolution of ERA5 and CFSR are created by combining forecasts with long time intervals in global, resulting in low-resolution. The wind speeds relatively decrease in the CFSR and MEVBIS datasets as they approach the bay. In addition, the wind directions are similar for ERA5 and CFSR, where for some periods, parallel directions are observed, whereas a completely different direction pattern is observed through the MEVBIS station, which could be ideal to better observe the change of currents under winds coming from different directions. Hence, to ensure that the model is not forced with unrealistic extreme conditions during the calibration phase, it is preferred to use data from MEVBIS, Kızılada station, considering the temporal and spatial resolutions of the investigated datasets, to better reflect the characteristics of the region.

3.3.5 Wave characteristics

The most recent data available for understanding the general wave characteristics in the region include significant wave height, corresponding significant wave period and direction for the years 1976 – 2023 in the ERA5 reanalysis dataset (ERA5, 2023) with a spatial resolution of 0.5° (≈ 50 km). Similar to the wind analysis, the wave characteristics obtained from ERA5 dataset have been investigated through long-term and extreme analysis. For the model calibration, three-month data for April, May and June 2023 is utilized. For simplicity, the wave characteristics obtained for April 2023 are presented in Figure 3.11. A detailed comparison for the entire three-month period, and for the other two months is given in Appendix A.

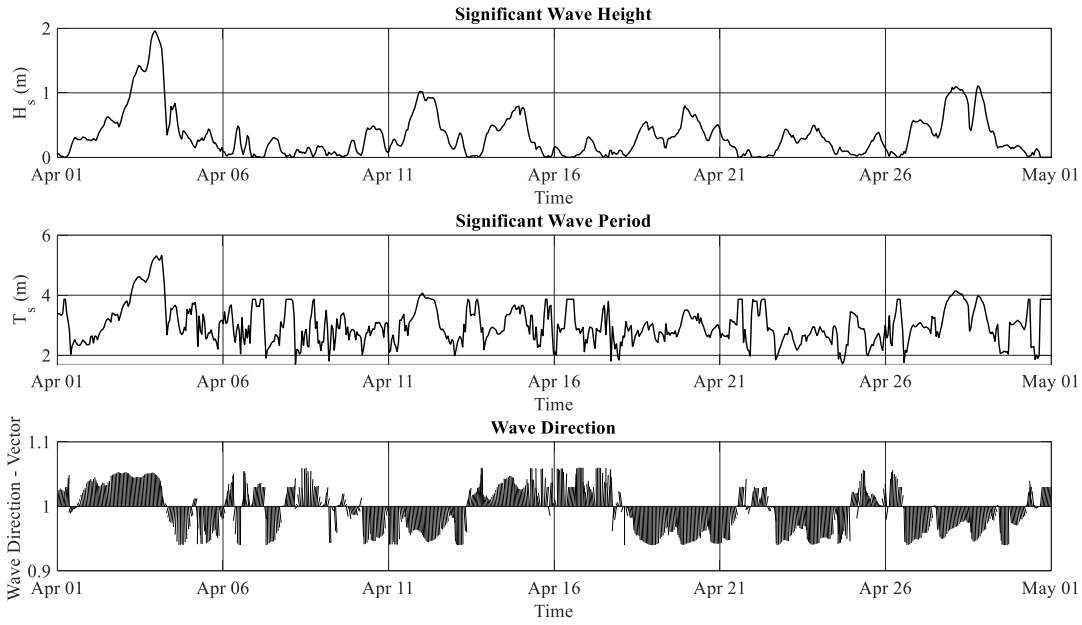

Figure 3.11. Time series obtained for the significant wave height, period and direction for April 2023

The point where the wave data is extracted is the same offshore ERA5 point given in Figure 3.9 (same with the wind data). Although it is located at a considerable distance from Fethiye Bay, the available data shows that the values of significant wave height reach up maximum to 2 m for the selected time duration but the rest are

generally low. The periods are generally in between 2-4 sec, and the wave directions changes over time, but in general southern waves are more frequent.

3.3.6 River discharge and sediment concentration measurements

River discharge and suspended solids measurements were taken at 22 different points along the rivers draining into Fethiye Bay as instantaneous measurements taken on four different days to represent a period of four months by Environment Protection and Control Department of Muğla Metropolitan Municipality. These values are then averaged to obtain an approximate estimate for the river discharge and suspended solid amount and they were used as the model input. Among the measurement points, the ones (FBD01, FBD02, FBD03, FBD04, FBD05 and FBD06) close to the river mouths where the flow discharges into the bay were selected to be used in the model (Figure 3.12).

Figure 3.12. River discharge measurement points near the bay (original image retrieved from Google Earth, 2024)

The instantaneous measurements of river discharge and total suspended sediment concentrations taken at the selected points are given in Figure 3.13, where the detailed version is given in Appendix A.

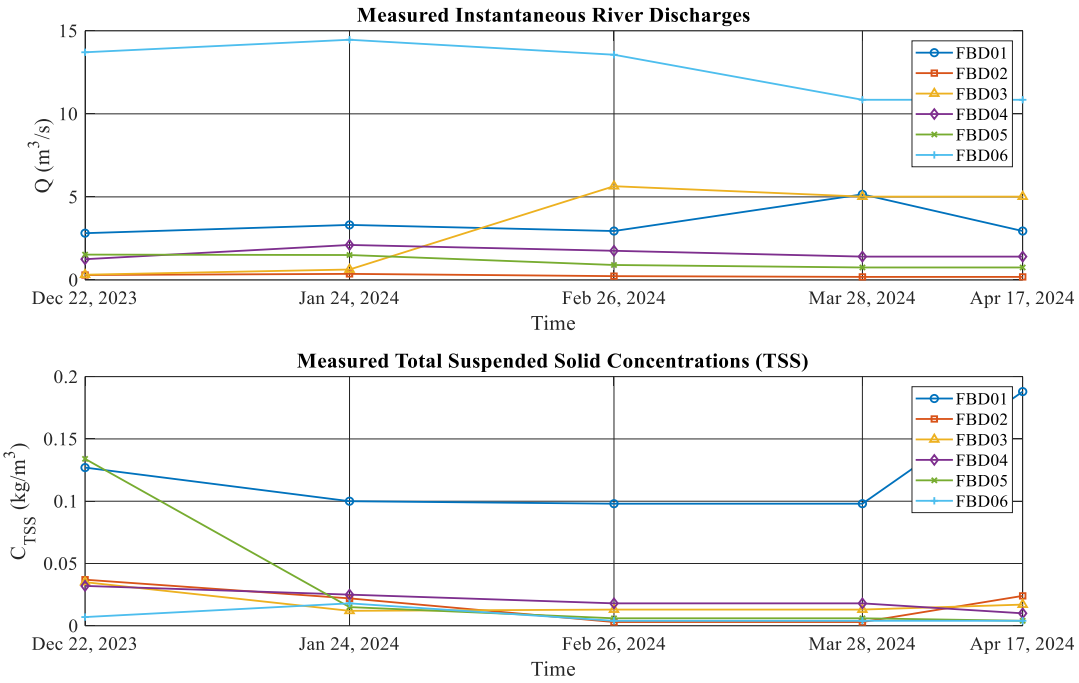

Figure 3.13. Measurements of instantaneous river discharges and corresponding total suspended sediment concentrations for the specified points

Figure 3.13 indicates that the discharge from the T2 channel (FBD06) can be sufficiently large to affect the water movement within the bay. Additionally, the discharges from the Murt river (FBD01) and the river at FBD03 are expected to significantly contribute to the water circulation patterns, and thus the current velocities. Although the measured total suspended solid concentration values do not directly represent sediment content, they clearly demonstrate the presence of pollution elements transported to the bay through the rivers. These values are assumed as initial sediment concentrations transported to the bay at the river discharge points at the point of examining the effects of sediment transport and applied in the model.

3.3.7 Sediment characteristics

Sediment characteristics should also be well represented in the numerical model, significantly affecting the sediment transport model results. Hence, available data

should be collected before the modeling stage, to represent the current condition in the region. Understanding the overall sediment grain diameter distribution within the bay is one of the important parameters for an initial understanding of the patterns of sediment transport within the bay. In that regard, the sediment grain diameter data were collected from sediment core samples taken from a large number of points distributed over the inner bay area. These sampling locations are shown in Figure 3.14.

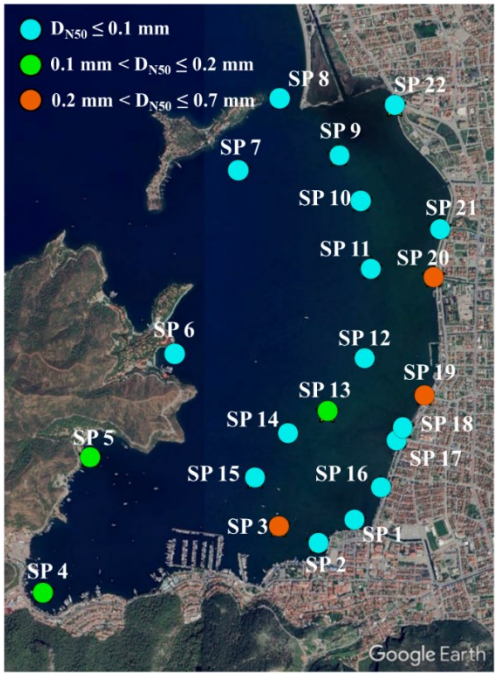

Figure 3.14. Sediment sampling points (original image retrieved from Google Earth, 2024)

The grain size distribution in the inner bay area is obtained through the sediment samples collected via sieve analysis. The results of the median grain size (D_{N50}) show that most of the sediment samples have fine-grained structure ($D_{N50} \leq 0.2$ mm), and this small grain size characteristic is generally dominant in the area. The blue points especially in front of the rivers, such as SP1, SP9, SP17, SP18, SP21, and SP22 have sediment particles which are extremely fine indicating the possible presence of cohesive materials transported by the rivers.

3.4 Model set-up

For setting up the model, the first step is to establish the domain where the numerical computations will be performed, which involves preparing the model grid and corresponding bathymetry files. Next, the model constraints and boundary conditions are defined to progress to the calibration process and determine the model input parameters accordingly.

As a coupled flow-wave model is adopted in the study, different model grids in Cartesian coordinates have been prepared for the FLOW and WAVE modules. For the WAVE, the model area is selected between 686216 m E - 690176 m E longitudes 4054407 m N - 4061487 m N latitudes in 36S zone, and for the FLOW, it is selected between 686306 m E - 689966 m E longitudes 4054707 m N - 4061427 m N latitudes.

For both of the computational grids, a 3D calculation network is structured over the study area by employing a σ-model type with 11 layers vertically. In order to establish the optimum working method, it is important to determine the optimal time step in the numerical model and the appropriate grid size to avoid instability and accurately model the water flow, precisely representing the underlying terrain and the coastline. On the other hand, the computational cost is a limitation, considering the number of simulations and simulation durations. Hence, a uniform grid size of 30 m has been selected in the model, considering the size of the domain, ability to represent important bathymetric/topographic features, available computational resources and time efficiency. The grid system constructed for the study area is shown in Figure 3.15a. In order to overcome the stability problems in the model, a smaller domain has been specified in the FLOW (blue grid system) than in the WAVE (red grid system).

A digital elevation model to be used in the numerical modeling of water circulation and sediment transportation in Fethiye Bay was developed by integrating the current topography and bathymetry data via QUICKIN tool in Delft3D. Similarly, two

different computational files have been prepared for FLOW and WAVE, where the corresponding depth file for FLOW is given in Figure 3.15b.

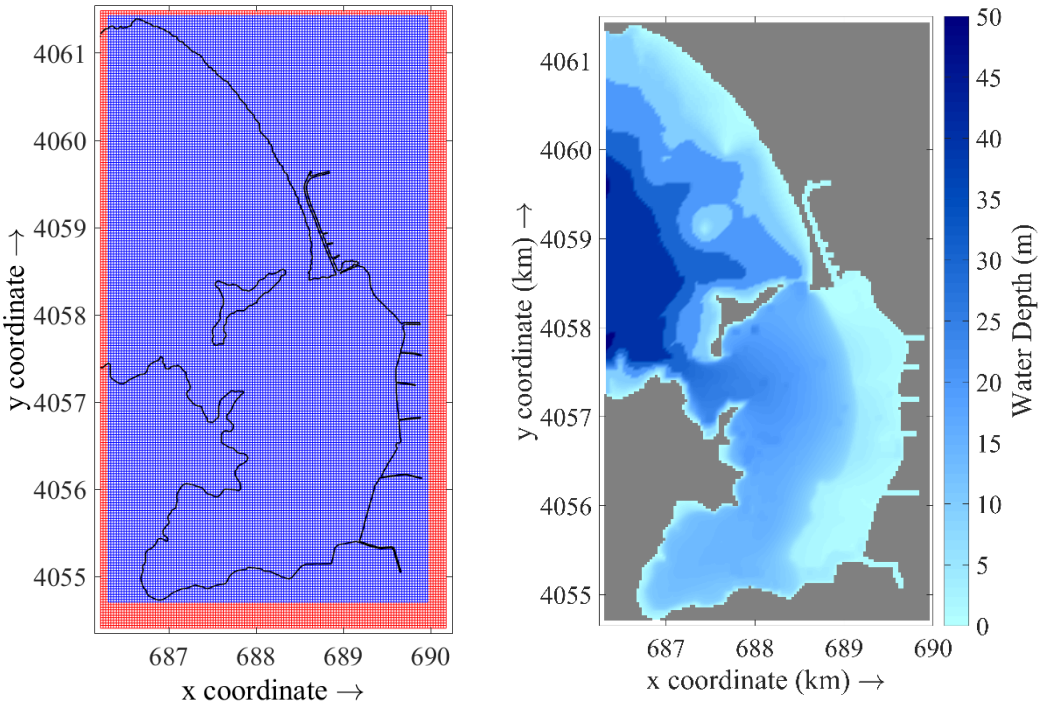

Figure 3.15. a. Horizontal grid system of FLOW (blue grid) and WAVE (blue and red grids) modules b. Model bathymetry used in Delft3D

The entrances of bays and rivers at the determined grid size are also reflected in the model, thus, over the previous models, the topography of the region is represented more accurately.

3.5 Model calibration

Selecting the appropriate parameters is an important step for reflecting real-life hydrodynamic conditions in a numerical model. Therefore, calibrating the model to match real life conditions is a priority to get more accurate results. The water circulation models typically provide outputs such as the spatial distribution of

velocity fields, water level fluctuations, salinity and temperature. Among these outputs, measurements taken from the region indicate that current velocity will be the primary focus during the calibration phase. It is also important to note that a morphological calibration should have been considered, but it could not be implemented due to model limitations. Since the bathymetric variations of the region are identified through two separate measurements taken in 2007 and 2022, the model set-up containing data for a 15-year period for the input conditions was not feasible in terms of computational time.

Before the calibration process, a quality control process was followed for the field measurements of current velocities to identify the potential outliers and observe a better relation. This control methodology is conducted by following the approach described in Williams et al. (2019). The values that deviate by 3 standard deviations from a spline fitted using a least squares method have been identified as spikes and subsequently removed for each calibration layer in RDCP01 (Figure 3.16) and in RDCP02 (Figure 3.17).

For this study, a manual calibration methodology is followed. In the first stage of calibration, hydrodynamic parameters that are unknown or not measured in the field are taken as default in the model. Then, for each calibration parameter, a new range of values was selected, and the extent to which this parameter affects the results was evaluated. Various statistical methods are employed to measure the agreement of the results with the observed data. This process continued until the parameters specified in the model produced results that closely matched real-life observations.

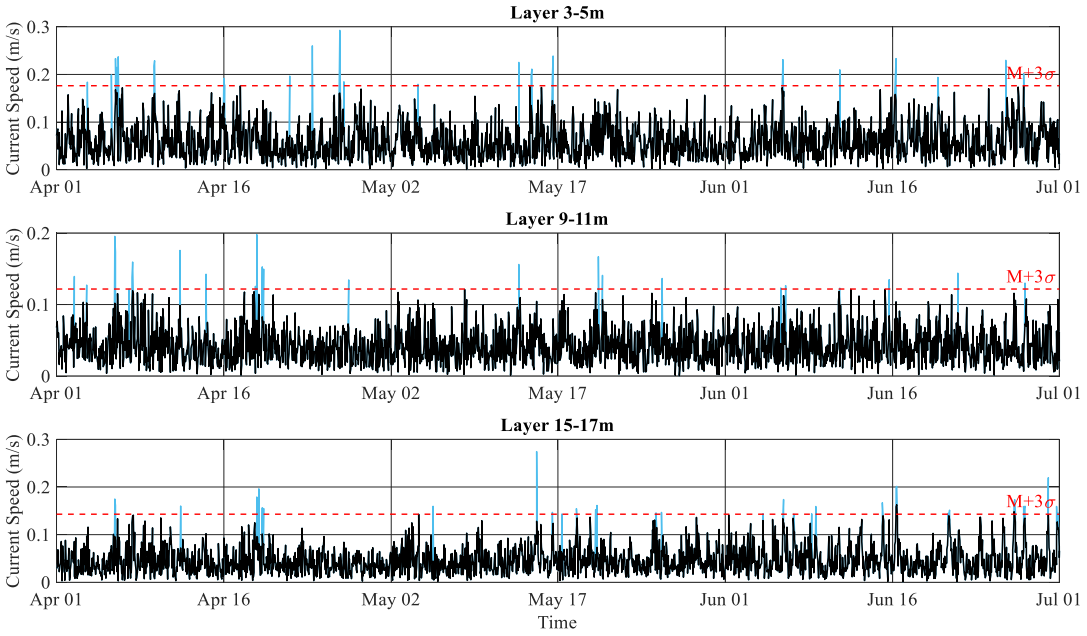

Figure 3.16. Time series of horizontal current velocity measured in RDCP01 and identified spikes after quality check for three different vertical layers

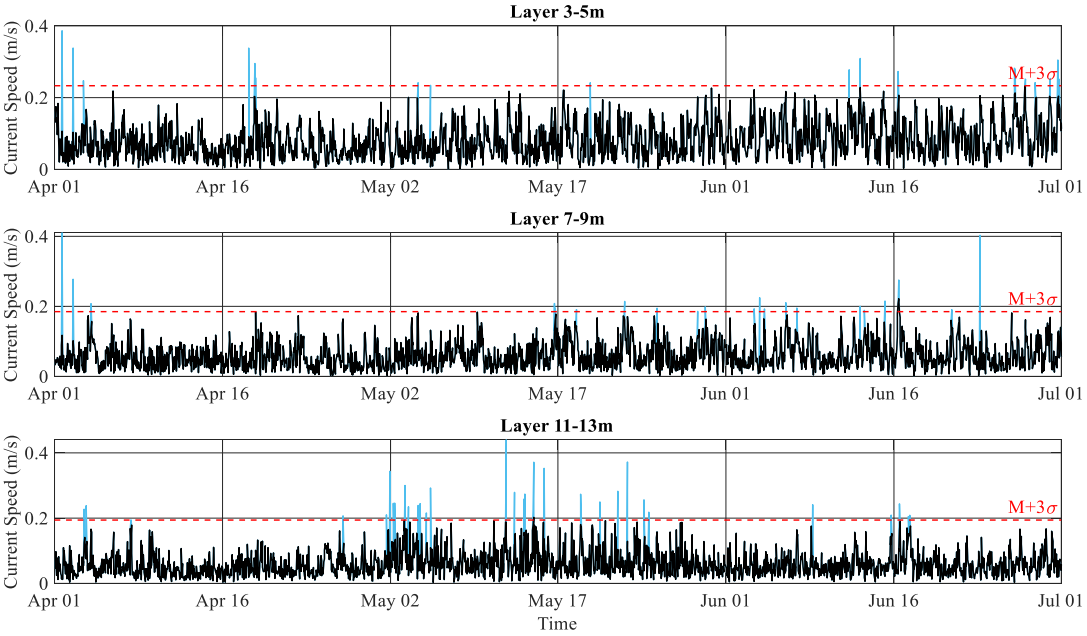

Figure 3.17. Time series of horizontal current velocity measured in RDCP02 and identified spikes after quality check for three different vertical layers

3.5.1 Input parameter selection

In the literature, water circulation and sediment transport models are generally considered driven by the tide and wind. Initially, the model is run using the Delft3D FLOW under only tide and wind forcing. Next, the model is coupled with the WAVE to consider the wave effect. Finally, the model results are obtained by integrating the fluvial component, river discharges, into the coupled model for a complete analysis. The input parameters discussed are given in Table 3.1.

Table 3.1 Input parameters and the different cases considered in the model

Case No	*Delft3D Module*	*Model Inputs*
1	FLOW	Tide, Wind
2	FLOW + WAVE	Tide, Wind, Wave
3	FLOW + WAVE	Tide, Wind, Wave, River Discharge

The simulations are conducted under these input cases while keeping all model parameters consistent. The resulting outputs are then evaluated for the three pre-determined layers in RDCP01 (Figure 3.18) and in RDCP02 (Figure 3.19). The results show that considering wind and tidal effects in the model, while using only the FLOW is insufficient. The inclusion of wave effects significantly increases horizontal current velocity and changes the current velocity behavior. Furthermore, when river discharge is added to the model, it results in a relatively greater increase in current velocity than wave effects alone, leading to more accurate reflections of the actual conditions in the model results at various points. This shows the importance of each parameter planned to be addressed within the scope of this study. Accurately capturing the region's characteristics in the combined analysis enhances the model's precision and, consequently, the reliability of predictions for future developments in real life. Thus, all relevant input parameters are included in the model calibration and then a sensitivity analysis is performed accordingly.

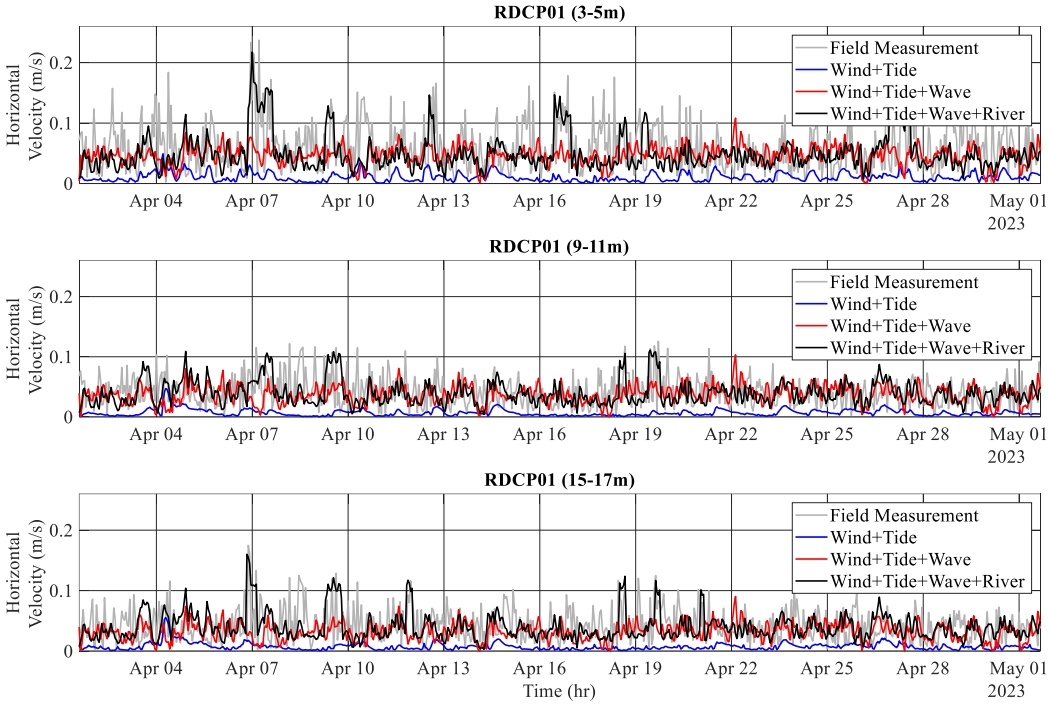

Figure 3.18. Comparison of the outputs from the three run cases with different inputs in RDCP01 for three different vertical layers

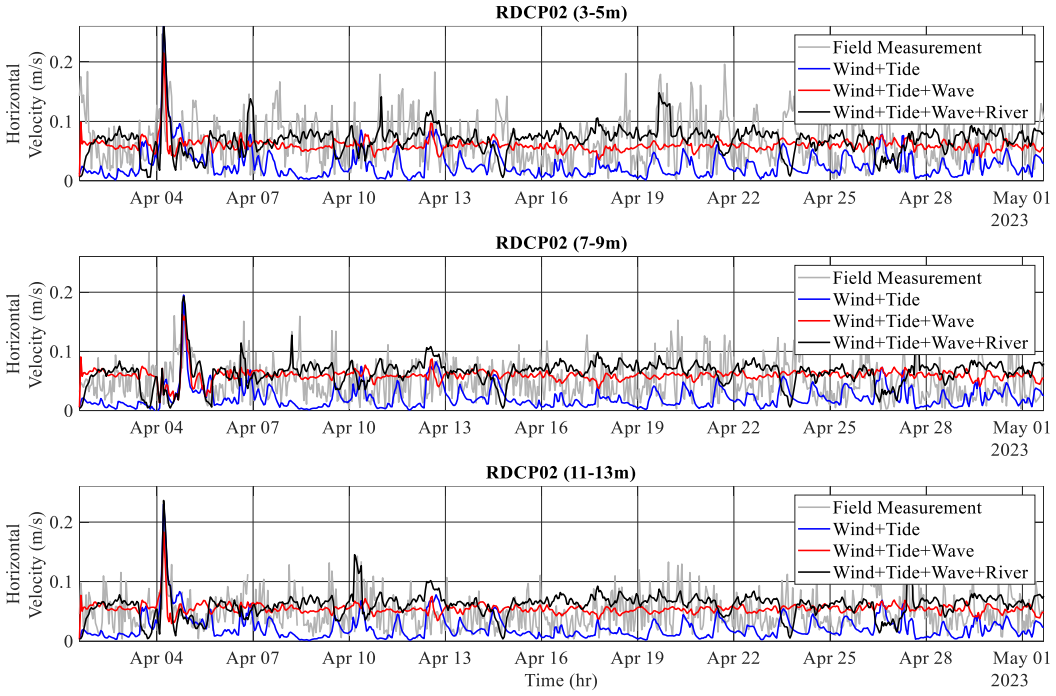

Figure 3.19. Comparison of the outputs from the three run cases with different inputs in RDCP02 for three different vertical layers

3.5.2 Sensitivity analysis

A detailed sensitivity analysis against the input parameters used in the model is conducted to assess their effect on the flow regime, and to select the best calibration parameters. For this analysis, only the water circulation behavior is examined and evaluations are made on current speeds and patterns. In the model, the hydrodynamic parameters, which are considered to affect the model results, are initially determined as candidates for calibration parameters and those are tested with the values given in Table 3.2.

Table 3.2 Parameters used in the calibration process

Parameter	*Tested Value*	*Final Values*
Horizontal viscosity and diffusivity (m^2/s)	1, 10, 50, 100, 200, 300	1
Vertical viscosity and diffusivity (m^2/s)	0.00005, 0.0001, 0.0005, 0.001	0.00005
Manning coefficient	0.010, 0.015, 0.018, 0.020, 0.040	0.020
Wind-drag coefficient breakpoints (coefficients)	0.0 – 0.1	
Wind-drag coefficient breakpoints (wind speeds)	0.0 – 100.0	
Air density (kg/m^3)	1.000, 1.225, 1.500	1.000
Turbulence model	*k–e*, algebraic	*k–e*

The sensitivity of the selected parameters was assessed by comparing the horizontal current velocity values obtained from the model results and field measurement values using the Root Mean Square Error (RMSE) function (James et al., 2013) (Equation 3.17).

$$RMSE = \sqrt{\frac{\sum_{i=1}^{N}\left(v_{measured} - v_{predicted}\right)^2}{N}} \tag{3.17}$$

Where N is the total number of the data points, here corresponding to the time step array, $v_{predicted}$ is the model result of horizontal velocity, and $v_{measured}$ is the measured velocity data. The final values used in the model are chosen based on the results with lower RMSE values for two stations of RDCP01 (Figure 3.20) and RDCP02 (Figure 3.21) for three selected velocity layers. where a detailed table containing each RMSE value calculated is given in Appendix A.

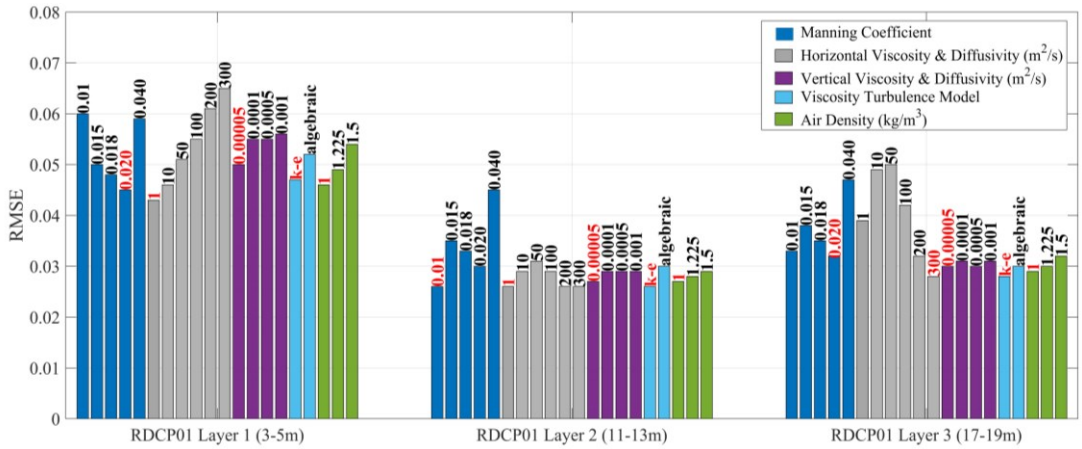

Figure 3.20. Calculated RMSE values for the comparison of horizontal current velocities in RDCP01 layers

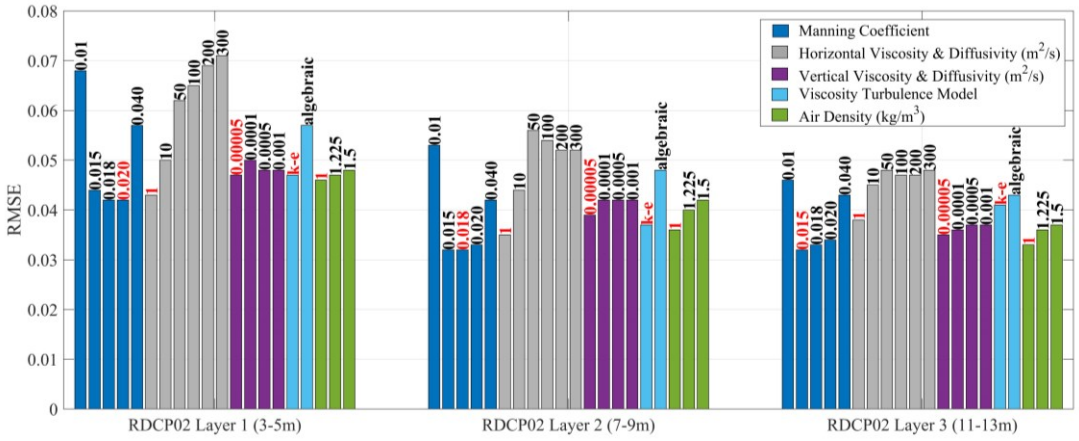

Figure 3.21. Calculated RMSE values for the comparison of horizontal current velocities in RDCP02 layers

During the sensitivity analysis, manning coefficient, horizontal viscosity and the selected viscosity turbulence model were found to alter the calculated RMSE values with more rapid changes, while vertical viscosity and air density showed less change. This indicates that the manning coefficient, horizontal viscosity and diffusivity and turbulence model selection have high sensitivity, while air density has moderate sensitivity and vertical viscosity and diffusivity have low sensitivity on the results of horizontal velocities as expected.

It should also be noted that, behind the bottom roughness methodology selection, considering the type of the channel or basin, data availability, channel geometry and flow regime, the two most used approaches, Chezy and Manning have been investigated through the literature for the bottom roughness. The Manning's approach has been selected since it is used for natural channels, rivers and basins with irregular shapes, and it is applicable for both subcritical and supercritical flows, making it versatile for a variety of flow conditions. For the coefficient selection, Imamura et al. (2006), Linsley & Franzini (1979) and Mays (2010) have been checked, and a Manning coefficient of 0.02 has been selected according to the model results.

Moreover, horizontal viscosity values were also observed to change the results relatively higher than the other parameters since they affect the density in the model, and therefore, their sensitivity level was also observed to be high. In this regard, although relatively smaller values for the horizontal viscosity are selected, they result in an overall good agreement with the observed current velocities. It is noted that these calibration parameters, including the horizontal viscosity, and their corresponding values to be used in the model should be evaluated based on the agreement of model results with the measurements during calibration.

The choice of turbulence model affects how well boundary layers are represented, and the accuracy of modeled currents, eddies and coastal upwelling depends on how well the turbulence model captures the horizontal velocity fields. Hence, the selection of turbulence model becomes critical. Since the algebraic model, also

known as the zero-equation model, is a simpler form of turbulence models, that does not solve any additional transport equations, it is generally used in simple examples due to the low accuracy as it is also observed with the higher RMSE results in the study. On the other hand, a more detailed representation of turbulence is provided by the *k–e* model, accounting for the production and dissipation of turbulence, which resulted in lower RMSE values in the results as expected.

Similarly, in such semi-enclosed basins where the wind effects are strong, it is seen that the sensitivity of wind drag coefficient (C_D) is high, significantly affecting the results by changing the surface currents as expected. C_D values have also been checked through the literature. Delft3D default values and Garrat (1977) and Donelan (2004) methodology, where C_D is specified for any wind speed as $C_D = (\min(0.75 + 0.067U_{10}, C_{Dmax}, \max(4.34 - 0.061U_{10}, 0.5)) * 10^{-3}$. The data obtained from the MEVBIS station is investigated, where the mean wind speed magnitude governed through the region is determined approximately as 5 m/s. Hence the corresponding value of C_D is calculated for 5 m/s as 0.001085, and the determined C_D value for 100 m/s in Delft3D as 0.00723. By specifying the C_D as 0.00076157 for the 0 m/s in the model, a continuous function of C_D, varying under different wind speeds, is tested and used in the numerical model.

Overall, the calibration is completed considering the results of this sensitivity analysis for RDCP01 (Figure 3.22) and for RDCP02 (Figure 3.23). While evaluating the RMSE results, it is important to consider the limitations of the model calibration. The calibration was performed on a continuous model over a duration of 1 month, with results generated at every minute, while field measurements were taken at three different depths and 1-hour intervals. In this context, in addition to the statistical values obtained, the calibration process was also evaluated to determine whether the model results reflect the major current value changes observed in the obtained time series to a certain extent. As a result of these evaluations, it was concluded that the calibration was complete, and the model validation was carried out with the selected parameters.

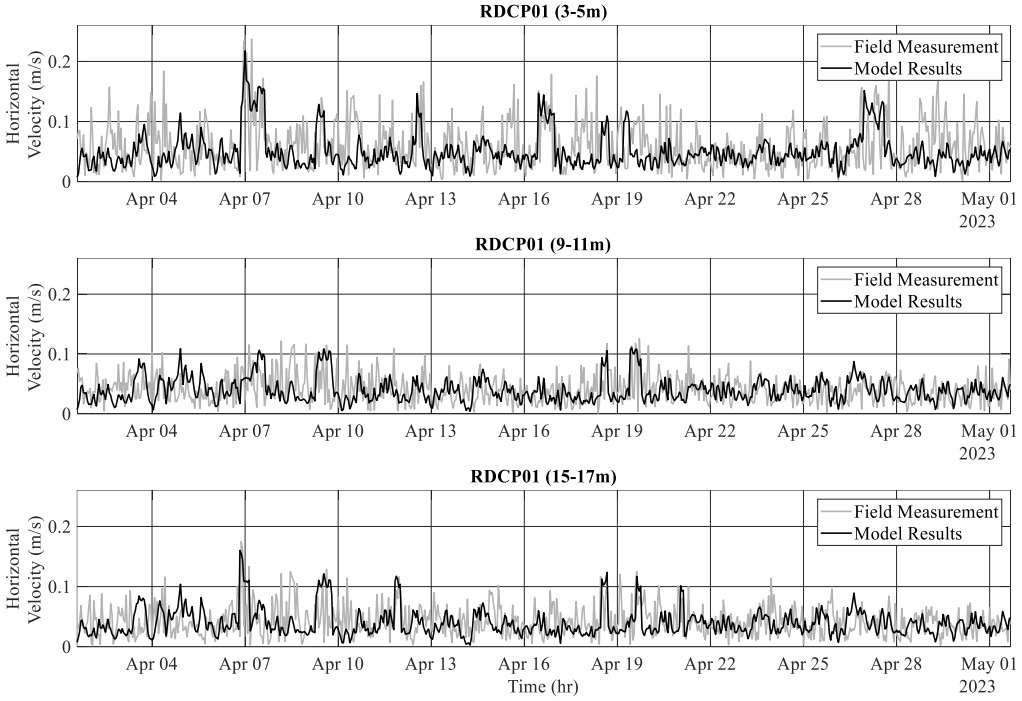

Figure 3.22. Comparison of modeled and measured horizontal current velocities at RDCP01 for three different layers

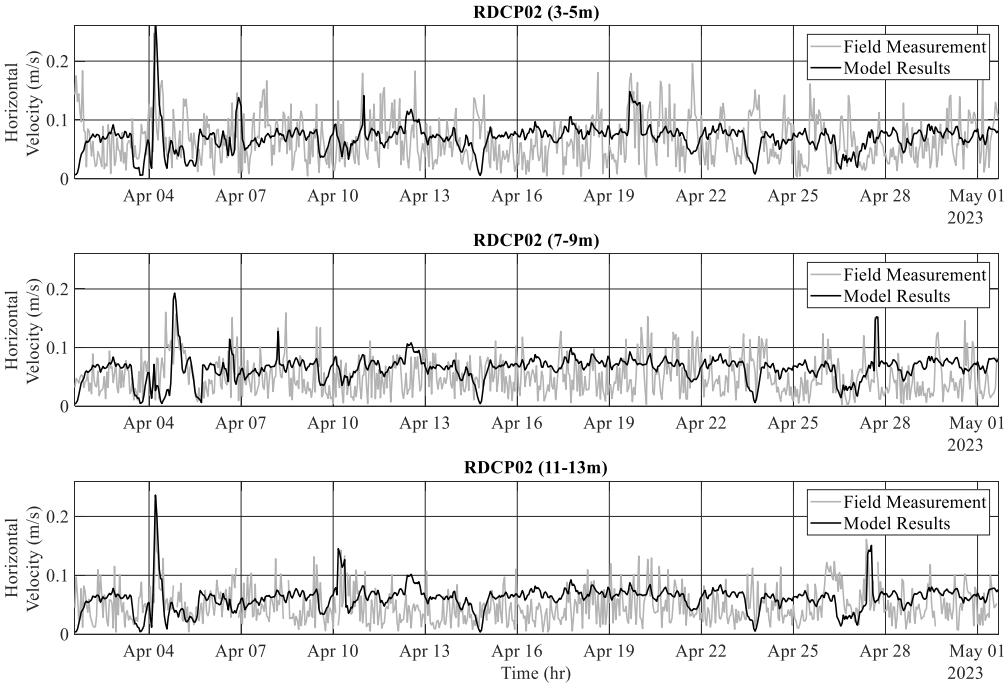

Figure 3.23. Comparison of modeled and measured horizontal current velocities at RDCP02 for three different layers

3.6 Model validation

The field measurement data covering the available horizontal velocity values is divided into two steps, calibration and validation, to compare the results obtained in the model. Due to the computational time constraint caused by the time-consuming manual calibration methodology, the horizontal velocity results of the first month covering the April 2023 data are used for parameter selection in the calibration part of the model.

The remaining two months, covering May and June 2023, were run with the input parameters determined in the calibration step and the results were evaluated within the scope of model validation. As in the calibration step, RMSE values between model results and field measurements were calculated (Table 3.3).

Table 3.3 RMSE values calculated for the validation runs

Parameter	$RMSE_{RDCP01}$	$RMSE_{RDCP02}$
Layer 1	0.037	0.040
Layer 2	0.031	0.036
Layer 3	0.039	0.044

These values are found to be at similar levels to the values calculated in the calibration part. This shows that the parameters selected in both the calibration and validation sections are in similar proximity to the field measurements taken, which implies the adequate fit of the input parameters. In addition, when the RMSE values calculated at two different points are compared, the model results and field measurements obtained for the RDCP01 point are found to be more consistent under the selected parameters.

Overall, the validation is assumed to be adequately completed for both RDCP01 and for RDCP02, and the corresponding time series comparisons are given respectively in Figure 3.24 and Figure 3.25.

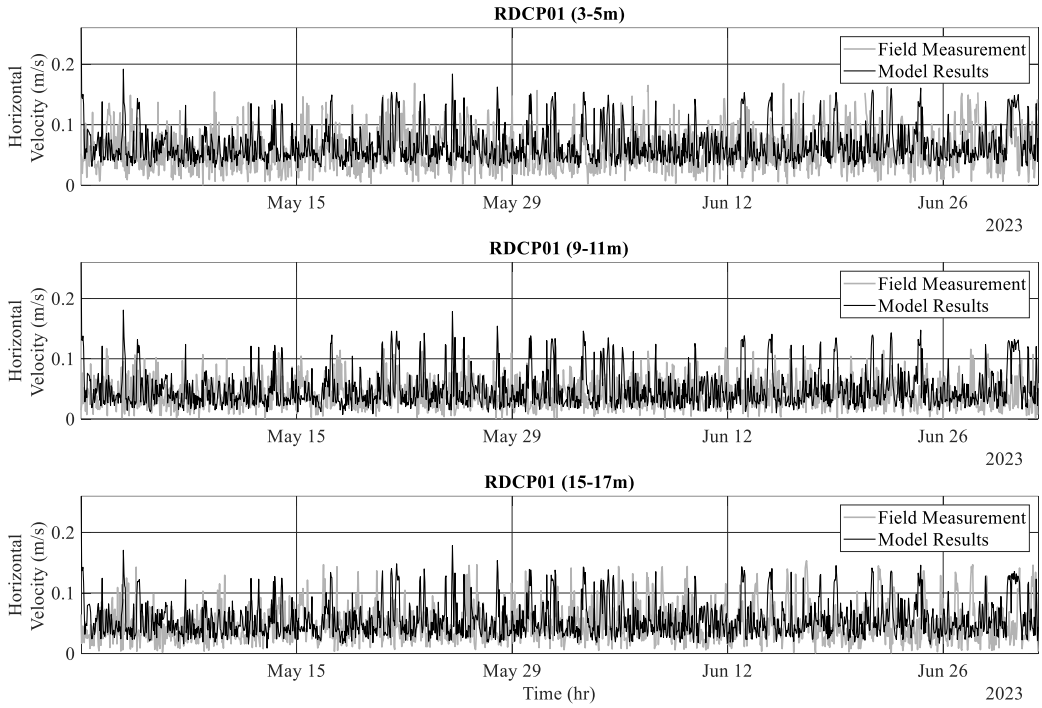

Figure 3.24. Comparison of modeled and measured horizontal current velocities at RDCP01 for three different layers

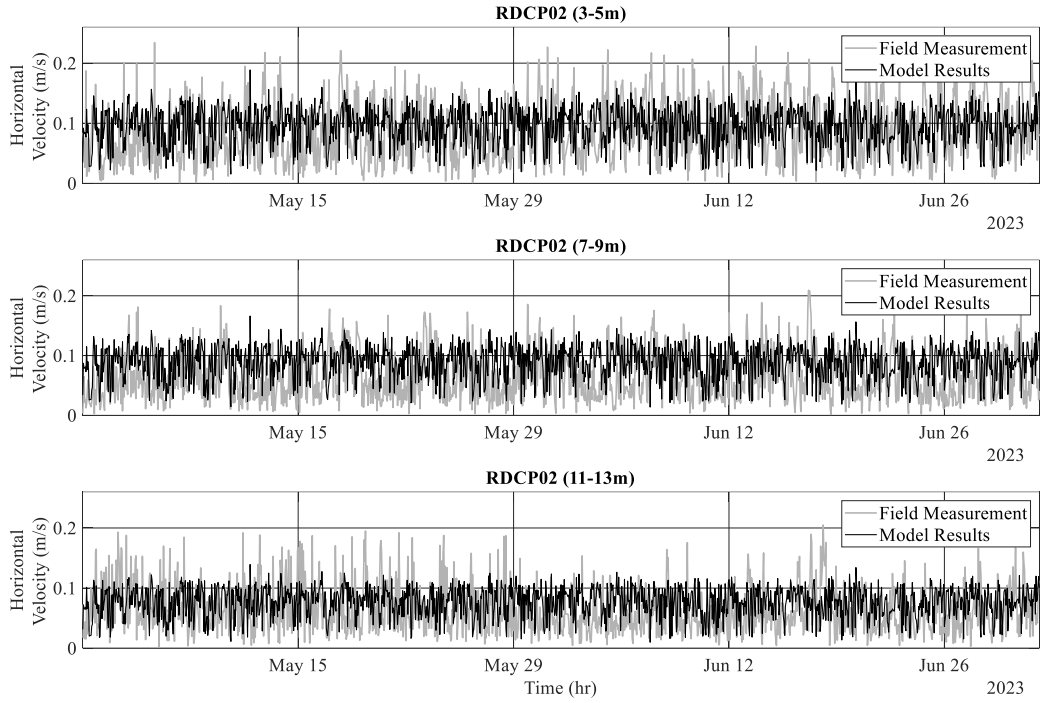

Figure 3.25. Comparison of modeled and measured horizontal current velocities at RDCP02 for three different layers

CHAPTER 4

MODEL INPUTS AND SCENARIO SIMULATIONS

Various simulation scenarios are determined to understand the behavior of the model, which is calibrated and validated with current measurements reflecting the characteristics of the region, under different potential input conditions. These scenarios are developed considering two different perspectives: different model inputs for wind and wave variations obtained from long-term and extreme analyses, and different dredging depths and areas in the inner bay area. This chapter covers the methods and analysis followed to determine these model inputs and the dredging scenarios discussed in this thesis.

4.1 Long-term and extreme wind statistics

To understand the long-term wind climate of Fethiye Bay, the hind casted wind data from the two data sources, ERA5 and CFSR, are compared and evaluated in terms of their distance from the study area and wind variability in the area, and the CFSR data is considered to be more appropriate to reflect the long-term wind characteristics in the region. For this reason, the wind data from CFSR for the closest location to the study area is analyzed using the cumulative exceedance probability of wind speed at 10 m above mean sea level (U_{10}) to determine the wind inputs for the long term (Figure 4.1). Through the long-term wind statistics, the steepness is calculated as 0.039, and the results of U_{10} for different directions calculated based on different exceedance hours are given in Table 4.1 and the detailed long term wind analysis equations are given in Appendix B.

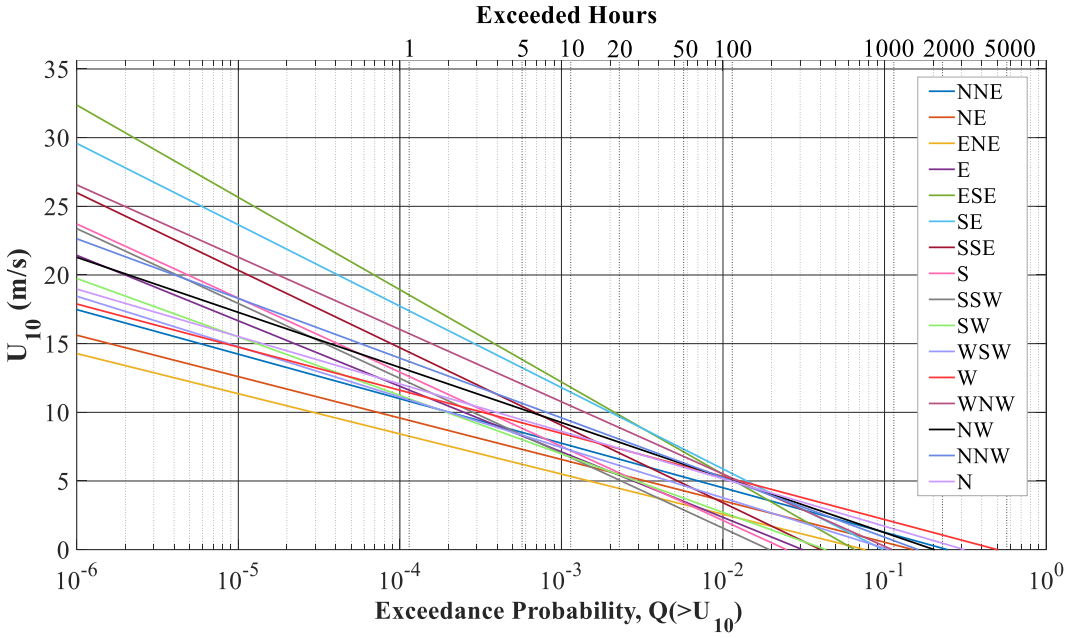

Figure 4.1. Long-term wind statistics results

Table 4.1 Long-term U_{10} results for different wind directions and exceedance hours

Exc.	*Wind Directions*															
Hrs	*NNE*	*NE*	*ENE*	*E*	*ESE*	*SE*	*SSE*	*S*	*SSW*	*SW*	*WSW*	*W*	*WNW*	*NW*	*NNW*	*N*
1	10.81	9.41	8.26	11.62	18.54	17.39	14.38	12.61	12.16	10.99	10.9	11.43	15.73	13.04	13.69	11.87
5	8.54	7.30	6.22	8.28	13.84	13.24	10.43	8.84	8.35	8.01	8.34	9.23	12.05	10.23	10.66	9.45
10	7.56	6.40	5.33	6.85	11.82	11.46	8.73	7.21	6.7	6.73	7.23	8.29	10.47	9.03	9.35	8.41
20	6.59	5.49	4.45	5.41	9.80	9.68	7.04	5.59	5.06	5.45	6.13	7.34	8.88	7.82	8.04	7.37
50	5.3	4.29	3.29	3.51	7.12	7.32	4.79	3.44	2.89	3.75	4.67	6.1	6.79	6.22	6.31	6.00
100	4.32	3.38	2.41	2.08	5.10	5.53	3.09	1.81	1.25	2.47	3.56	5.15	5.2	5.02	5.00	4.96

When the annual wind speeds exceeding 10 hours are obtained as a result of the analysis, the dominant wind directions are found to be ESE, SE and WNW. Considering the dominant wind directions and to observe the effect of different direction selection in the model, the wind directions have been grouped as four different representative directions, and NNE (7.56 m/s), ESE (11.82 m/s), SSW (6.7 m/s), and WNW (10.47 m/s) directions have been selected as the scenario groups

(Figure 4.2). The determined wind speeds and directions are employed in the model in the long-term cases, where the sediment transport movement and water circulation pattern are investigated.

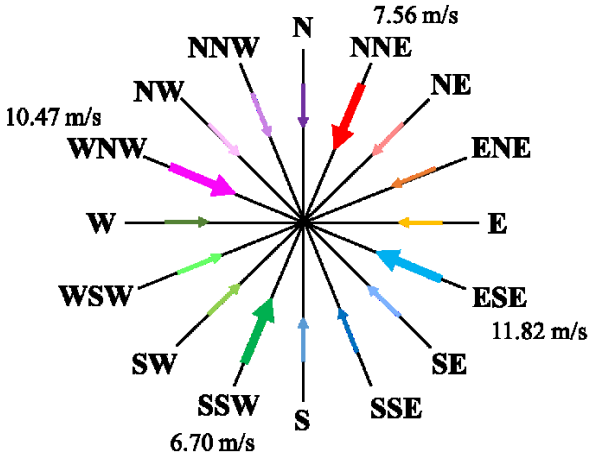

Figure 4.2. Selected different wind directions and corresponding wind speeds

In addition to the long-term analyses reflecting the characteristics of the region, extreme wind statistics is also conducted for the study area to examine the water circulation behavior and sediment distribution pattern under storm conditions. The extreme analysis is performed for the two dominant wind directions (ESE, WNW) obtained in the long-term analysis (Figure 4.3).

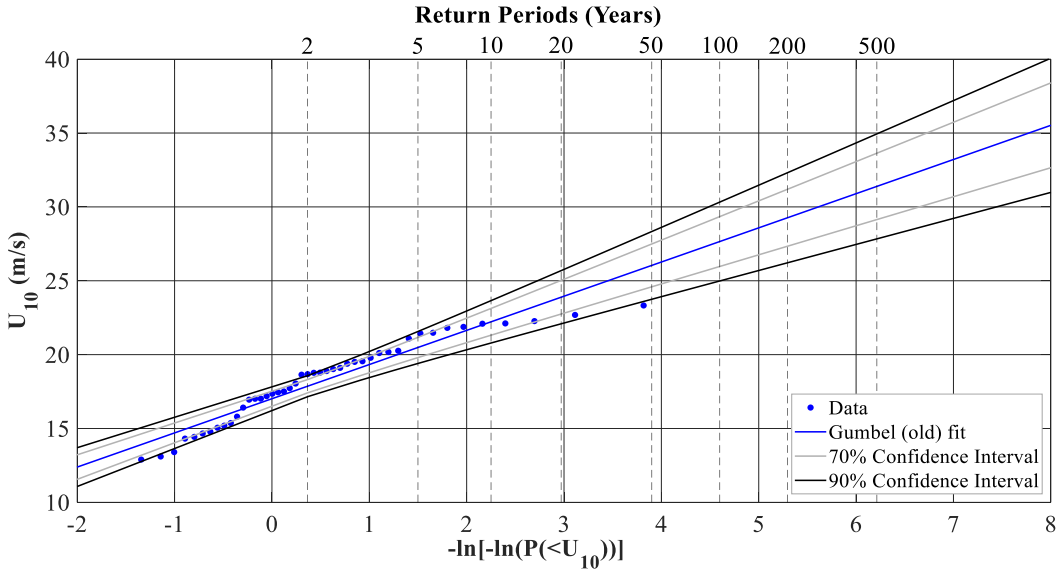

Figure 4.3. Extreme wind statistics results according to Gumbel (old) fit

Using extreme wind statistics, the Gumbel (old) fit ($X = 2.3134\,x[-\ln[-ln(P(< U_{10})]] + 17.0145$) has found to govern among other fitting distributions, projecting a wind speed of 30.32 m/s for a 100-year return period. In order to reflect real-life storm dynamics, a sample storm condition is created with a duration of 12 hours and a peak value of 30 m/s at 6 hours, based on the extreme analysis results (Figure 4.4).

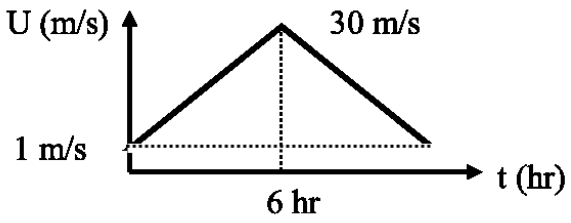

Figure 4.4. Specified sample storm condition

Considering the long-term and extreme analysis results, six different wind-input cases are determined for the model scenarios. For the long-term cases, the specified four directions with their corresponding wind speeds are chosen, and for the extreme cases, two most dominant wind directions are selected, and investigated through the described sample storm condition.

4.2 Long-term and extreme wave statistics

In order to determine the long-term wave climate of the region, the ERA5 wave data obtained for Fethiye Bay is examined. The significant wave height values are found to be relatively lower, even in a data extracted from a point far offshore from the bay. However, in order to examine the significant wave heights and to reflect their effects in the model, long-term and extreme analyses are performed using the dataset. Through the long-term wave statistics, the steepness is calculated as 0.031 and the general wave characteristics of the region are determined for each wave direction (Figure 4.5). The calculated long-term significant wave heights for different directions based on different exceedance hours are given in Table 4.2, and the detailed long-term wave statistics equations are given in Appendix B.

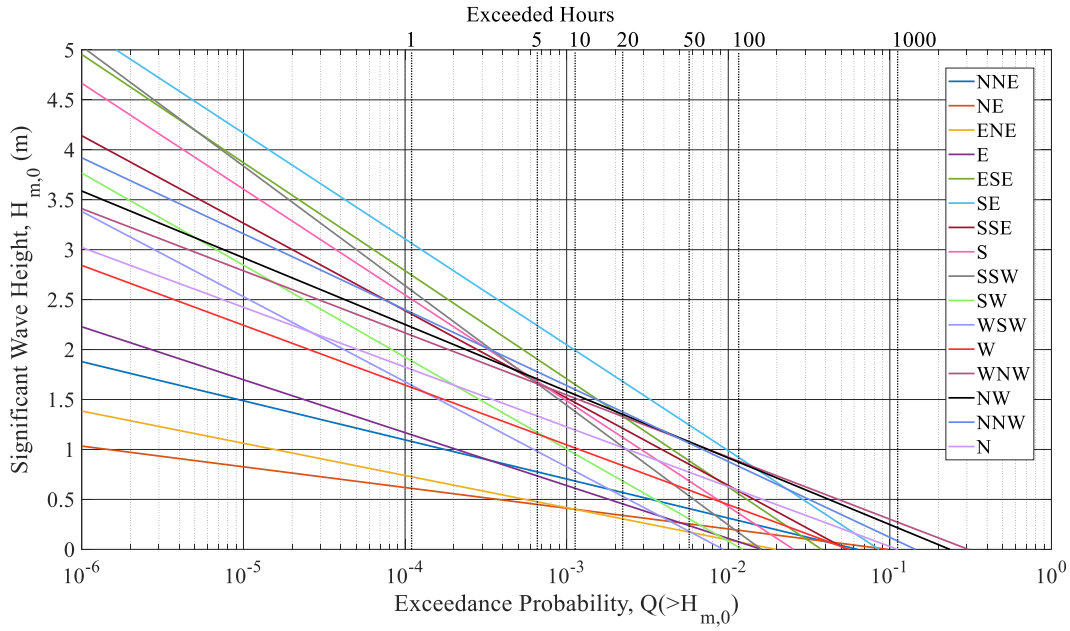

Figure 4.5. Long-term wave statistics results

Table 4.2 Long-term significant wave heights for different wave directions and exceedance hours

Exc.	*Wind Directions*															
Hrs	*NNE*	*NE*	*ENE*	*E*	*ESE*	*SE*	*SSE*	*S*	*SSW*	*SW*	*WSW*	*W*	*WNW*	*NW*	*NNW*	*N*
1	1.09	0.65	0.69	1.13	2.73	3.04	2.34	2.5	2.57	1.87	1.61	1.58	2.12	2.25	2.34	1.76
5	0.81	0.49	0.47	0.76	1.97	2.3	1.73	1.76	1.73	1.23	1.02	1.17	1.69	1.77	1.81	1.35
10	0.7	0.43	0.38	0.6	1.65	1.98	1.47	1.44	1.37	0.95	0.76	0.99	1.5	1.57	1.58	1.17
20	0.58	0.36	0.28	0.44	1.32	1.67	1.21	1.12	1.01	0.67	0.51	0.81	1.32	1.37	1.35	0.99
50	0.42	0.27	0.16	0.23	0.89	1.24	0.86	0.69	0.54	0.31	0.17	0.58	1.07	1.1	1.05	0.76
100	0.3	0.21	0.06	0.08	0.56	0.93	0.59	0.37	0.17	0.03	0	0.4	0.88	0.9	0.82	0.58

Similar to the wind analysis, values of the significant wave height exceeding 10 hours per year are investigated. As the results indicate, the waves coming from the SE and ESE directions were found to be dominant in agreement with the long-term wind analysis results. However, considering the location of the data point outside of

the model boundaries, the wave direction is chosen for the model input as West boundary in the model.

In addition to the long-term analyses reflecting the characteristics of the region, extreme wave statistics are also carried out for considering their effect in the model and to examine the water circulation behavior and sediment distribution pattern under storm conditions. Using the extreme wave statistics, Gumbel (old) fit ($X = 0.3933\ x[-\ln[-ln(P(< Hs)]] + 2.6875$) is found to be governed among fitting distributions, projecting a significant wave height of 5 m for a 100-year return period (Figure 4.6).

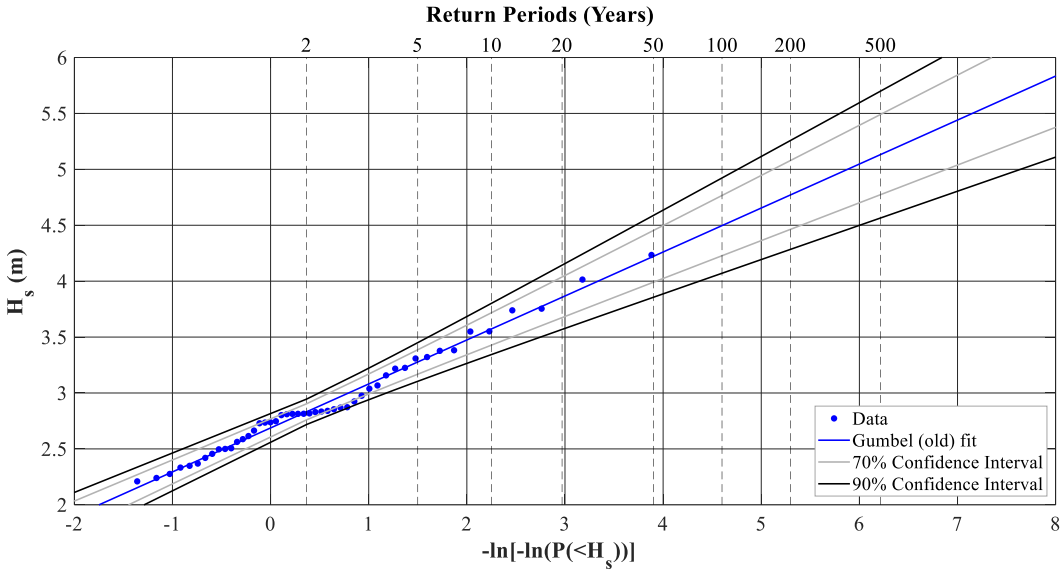

Figure 4.6. Extreme Wave Statistics results according to Gumbel (old) fit

Due to computational time constraints and model fields evaluated in previous studies, the selected model field in the study is not compatible with the wave statistics point obtained, therefore a basic SWAN analysis is carried out using a low resolution model mesh, where the bathymetry obtained by General Bathymetric Chart of the Ocean (GEBCO) (2024), the results of which are given in the Appendix B. When assessing the wave conditions, two scenarios are determined for the long-term and extreme conditions. For the long-term case, a wave condition with a significant wave height of 1.5 m and a corresponding period of 3.5 sec was applied

from the western boundary in the model area. For the extreme case, a wave condition with a significant wave height of 2.5 m and a corresponding period of 4.2 sec was used in the model with the JONSWAP 3.3 spectrum.

4.3 Bathymetric variations between 2007 – 2022

The differences between the two available bathymetry maps are analyzed to identify different dredging depths and areas to develop the dredging scenarios for the numerical simulations. Hence, the changes in water depth are investigated between 2007 and 2022 bathymetry maps, as well as eroded and deposited areas (Figure 4.7). It is important to note that the bathymetry from 2007 and 2022 are obtained under different field conditions and do not meet the same measurement standards and specifications.

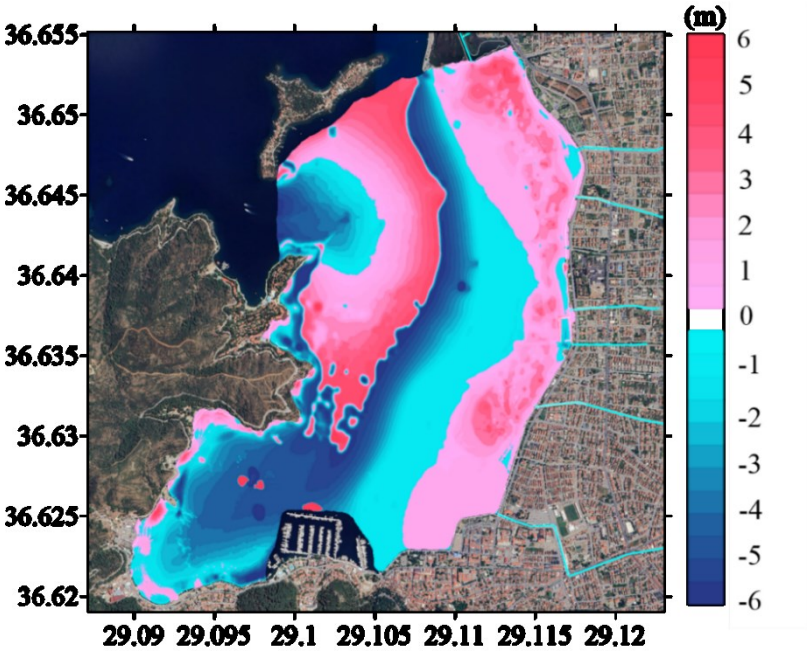

Figure 4.7. Map showing the bathymetric changes in the Fethiye Bay

When analyzing these bathymetric changes, the deposition observed in the area behind the Şövalye Island highlights the diffraction mechanism caused by the presence of the island in the bay. This suggests that the incoming sediment settles

on the seabed due to the low current velocities in this area. In addition, a shallowing zone is in the bay over time, particularly at the river discharge points, taking into account that the pink area indicates the deposition on the seabed. This situation is in alignment with the observations during the site visit and the identified issues in the bay. The accumulation of sediment in front of the rivers and channels within the inner bay supports the initial ideas for dredging depths and areas. Given that the material in this section is a mixture of cohesive material coming from the rivers, dredging and cleaning these areas are likely to improve the water quality in the bay and reduce pollution. Therefore, dredging scenarios are developed for varying depths in this area consisting of -1 m, -2 m, -3 m, -4 m and -5 m (Figure 4.8).

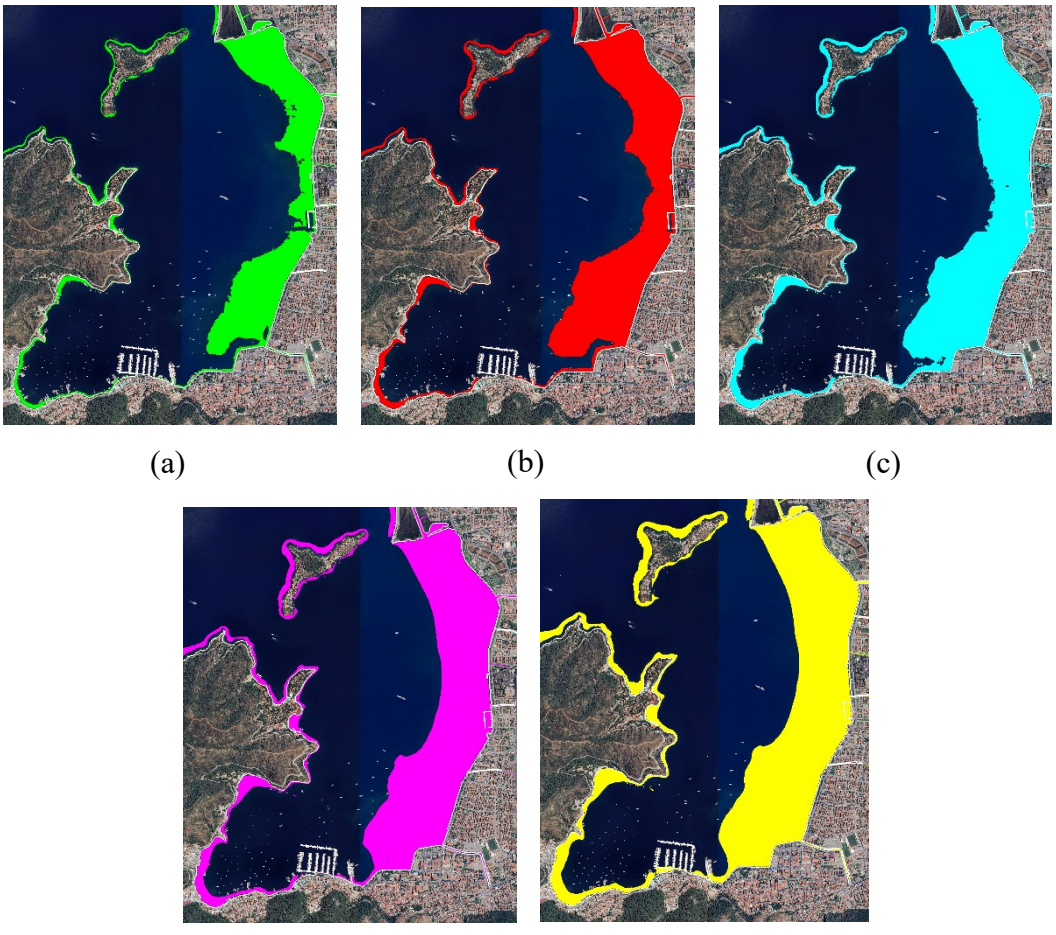

(a) (b) (c)

(d) (e)

Figure 4.8. The dredging depths and areas considered for the scenarios according to the bathymetric changes in the Fethiye Bay a. -1 m, b. -2 m, c. -3 m, d. -4 m, e. -5 m

For each dredging scenario, the dredging volumes are calculated, by using the up-to-date bathymetry data. The total inner bay volume is calculated as 68,594,616.17 m^3 (≈ 68.5 million m^3), where the horizontal area is determined as 6,845,612.78 m^2 (≈ 6.8 million m^2). To understand the physical correspondents of dredging volumes through the inner-bay volume, relative dredging volumes are calculated by dividing each dredging volume to the total inner bay volume. The total volumes planned for dredging at each of these depths and the corresponding ratios of total inner bay volume are given in Table 4.3.

Table 4.3 Dredging depths and total volumes to be dredged

Dredging depth (m)	*Total Volume (m^3)*	*Relative Dredging Volume (%)*
-1	156,547.40	0.228
-2	998,909.81	1.456
-3	2,451,967.44	3.575
-4	4,253,701.73	6.201
-5	6,293,695.30	9.175

Under these selected dredging scenarios, the water circulation and sediment transport patterns are analyzed in the numerical model under different conditions using specified input parameters. The resulting distributions and the relationships between them are then evaluated within the context of each dredging scenario.

4.4 Scenario development

Tidal, wind, wave and river discharge conditions in the region are examined and these conditions are analyzed through two different scenario types: long-term and extreme storm behaviors. Considering the semi-enclosed nature of the basin, the four most effective wind conditions identified in the long-term analysis are selected. These wind conditions are determined for annual 10 hours, to obtain their long-term

behavior and an idealized storm scenario is created to reflect an extreme storm event. The tidal input is defined as a harmonic series with an amplitude of 30 cm in each scenario to reflect the regional characteristics. Wave conditions are also reflected as a spectrum in both long term and extreme wave scenarios to accurately represent regional characteristics. For the river discharge, two alternatives are considered, one with reflecting normal conditions and the other that is evaluating the cases of excessive precipitation. The scenario runs are used to assess water circulation and sediment transport, along with their corresponding details, are given in Table 4.4. The coupled Delft3D FLOW and WAVE models, inputted by the determined parameters are also conducted for different dredging scenarios.

Table 4.4 Input parameters considered in the scenarios

No	Type *	Tide Input	Wind Input		Wave Input			River Input**					
		a (m)	U_{10} (m/s)	Dir	H_s (m)	T_s (s)	Dir	Q_{R1} (m^3/s)	Q_{R2} (m^3/s)	Q_{R3} (m^3/s)	Q_{R4} (m^3/s)	Q_{R5} (m^3/s)	Q_{R6} (m^3/s)
1	LT	± 0.30	11.82	ESE	1.2	3	W	3.43	0.25	3.32	1.58	1.09	12.68
2	LT	± 0.30	10.47	WNW	1.2	3	W	3.43	0.25	3.32	1.58	1.09	12.68
3	LT	± 0.30	7.56	NNE	1.2	3	W	3.43	0.25	3.32	1.58	1.09	12.68
4	LT	± 0.30	6.70	SSW	1.2	3	W	3.43	0.25	3.32	1.58	1.09	12.68
5	EX	± 0.50		ESE	1.2	3	W	10.29	0.75	9.96	4.74	3.27	38.04
6	EX	± 0.50		WNW	1.2	3	W	10.29	0.75	9.96	4.74	3.27	38.04

* LT: Long-term, EX: Extreme

** Q_{R1}, Q_{R2}, Q_{R3}, Q_{R4}, Q_{R5} are river discharges for the corresponding rivers of River-1 (FBD01), River-2 (FBD02), River-3 (FBD03), River-4 (FBD04) and River-5 (FBD05) given previously.

CHAPTER 5

MODEL RESULTS

The model results are discussed by focusing on i) the relation between water circulation dynamics and sediment transport patterns inside the bay considering the current conditions, ii) the effect of dredging on the water circulation and sediment transport behaviors, iii) relationship between the total water volume entering and leaving the bay and the volume of sediment deposited in problematic areas within the bay.

5.1 Water circulation and sediment transport in the bay under current conditions

The spatial distributions of hydrodynamic model outputs are evaluated under different combinations of input parameters given in Chapter 4. For clarification, the inner bay area is divided into four sub-areas of A1, the area in front of the rivers along the bay that is planned to be dredged, A2, the water exchange opening area near Şövalye island, A3, the center area, and A4, the southern area (Figure 5.1).

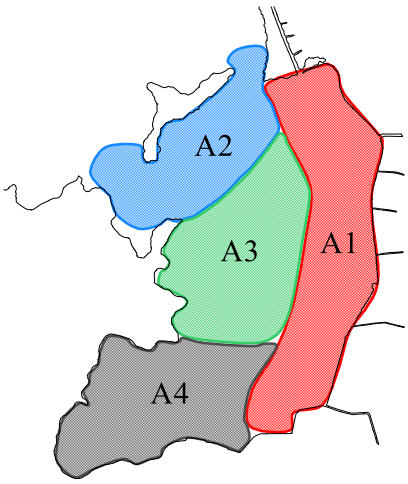

Figure 5.1. The sub-areas of the bay determined for the model results analysis

The spatial distributions of hydrodynamic model outputs in this region are considered in three aspects: areal water circulation patterns within the bay and associated current velocities, areal sediment transport patterns and the associated erosion and deposition distributions and their quantities. The model results for each input scenario through current bathymetric conditions in the study area are given in Figure 5.2 for maximum horizontal velocities at the sea bottom, in Figure 5.3 for total sediment transport, and in Figure 5.4 for cumulative sediment deposition. In addition to the areal distributions for each scenario, the sediment deposition calculated over the area A1 is given in Appendix C.

Comparing the different input scenario conditions, the maximum intra-bay current speed magnitudes at the sea bottom during simulations are observed at similar levels, where the current patterns vary significantly due to the effect of wind (Figure 5.2). Current speed magnitudes of Scenario 1 (Figure 5.2.a), having the wind condition coming from the ESE direction with the highest wind speed magnitude among the long-term scenarios, are relatively lower compared to the results of Scenario 2 in the case of WNW, the second dominant wind direction, where a complete cyclonic circulation movement through A2 is observed (Figure 5.2.b). In Scenario 3, with NNE wind direction, the southern currents over A1 and higher current speeds at the northern entrance in A2 is modeled (Figure 5.2.c). Whereas, in Scenario 4, with SSW wind direction, an opposite water circulation dynamic is observed with northern currents through A1 (Figure 5.2.d). These results reveal the profound effect of wind direction rather than wind strength on water circulation in Fethiye Bay, selected as a sample semi-enclosed basin area in this study. When examining the results for Scenario 5 and 6, extreme cases of ESE and WNW, determined as a 12-hour storm with wind speeds reaching up to 30 m/s, it becomes more clear that the water circulation behavior varies significantly depending on the wind direction, which is partially captured in the long-term scenario results. In Scenario 6, a cyclonic circulation over the areas of A2 and A3 with higher current speeds are observed (Figure 5.2.f), while, in Scenario 5, two different cyclonic circulations moving in reverse directions through A2 and A3 (Figure 5.2.e).

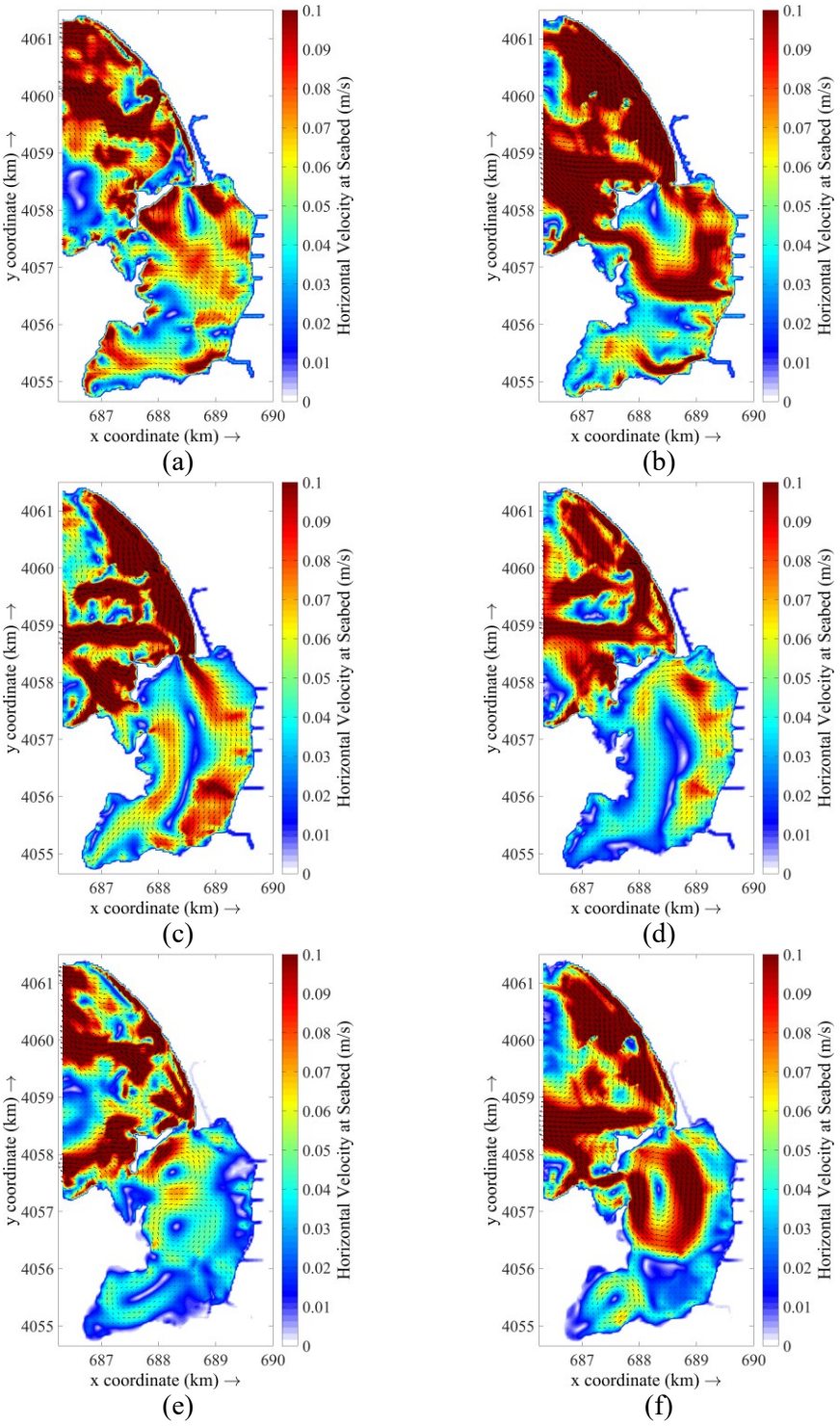

Figure 5.2. The areal distribution of maximum horizontal velocity profiles at the sea bottom for different inputs of a. Scenario 1, b. Scenario 2, c. Scenario 3, d. Scenario 4, e. Scenario 5, f. Scenario 6

Winds blowing from ESE direction drives currents mostly in northwest direction in the outer bay, depresses the current speeds at the openings near the island, resulting decrease in the water exchange and current speeds. Whereas, the winds from the WNW direction drives southeast currents, supplying the water movement in the direction of water inflow from the outer bay to the inner bay, and resulting in higher current speeds with a significant water exchange between the inside and outside of the bay. In addition, as observed in the results of all modeled scenarios, the computed current speeds inside the bay are considerably lower than the velocities outside the bay. These results confirm the low intra-bay circulation, as in the current condition of Fethiye Bay.

To understand the sediment transport behavior in the inner bay area of Fethiye Bay under given input conditions, first, the total sediment transport computed during the simulation have been analyzed (Figure 5.3). For the long-term cases (Scenario 1, 2, 3, and 4), the total sediment transport patterns, depending on the current velocity levels and water circulation results, vary with the wind direction and the bay characteristics. In each scenario, sediment transport is observed over the area A1, in parallel with the river discharges. The maximum sediment transport at final time step of the simulation in the inner bay for Scenario 2 (Figure 5.3.b) and Scenario 3 (Figure 5.3.c) are higher than in Scenario 1 (Figure 5.3.a) and Scenario 4 (Figure 5.3.d). As expected, total sediment transport distribution and ratios in the extreme scenarios (Scenario 5 and 6) are more dominant than in the long-term scenarios. In Scenario 6, a cyclonic sediment transport pattern observed over the area A2 (Figure 5.3.f)., while a not-uniform transport pattern is observed in Scenario 5 (Figure 5.3.e). This difference also highlights the effect of the wind direction change on the sediment transport behavior.

The total sediment transport results show that, across all wind conditions tested in different scenarios, sediment transport is higher over the area of A1, shallower areas of the inner bay initially considered for dredging, which is an important finding for understanding the current shallowing trend in the bay before considering the cumulative erosion and deposition amounts and their areal distributions (Figure 5.4).

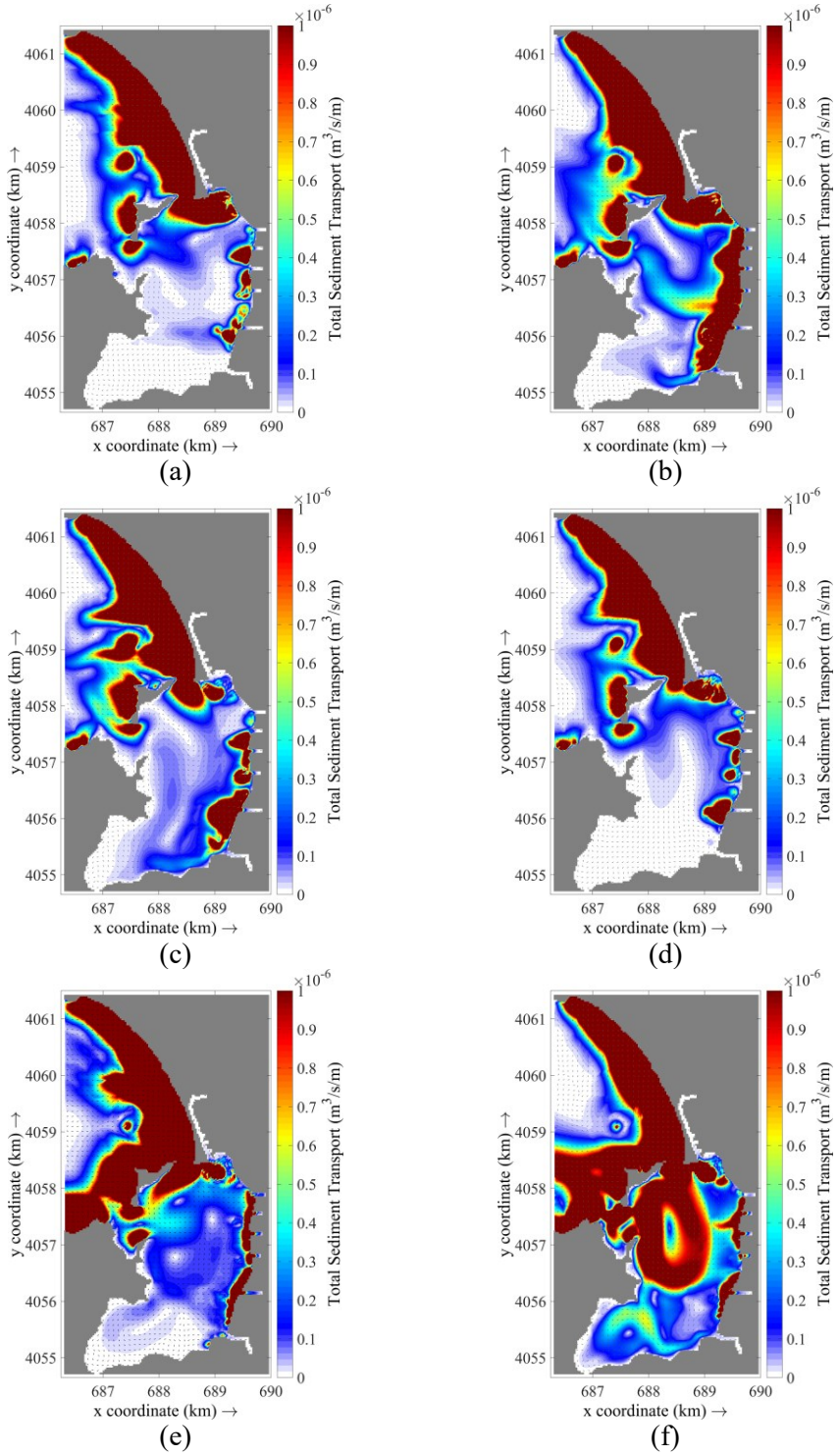

Figure 5.3. The areal distribution of total transport patterns at the sea bottom for different inputs of a. Scenario 1, b. Scenario 2, c. Scenario 3, d. Scenario 4, e. Scenario 5, f. Scenario 6

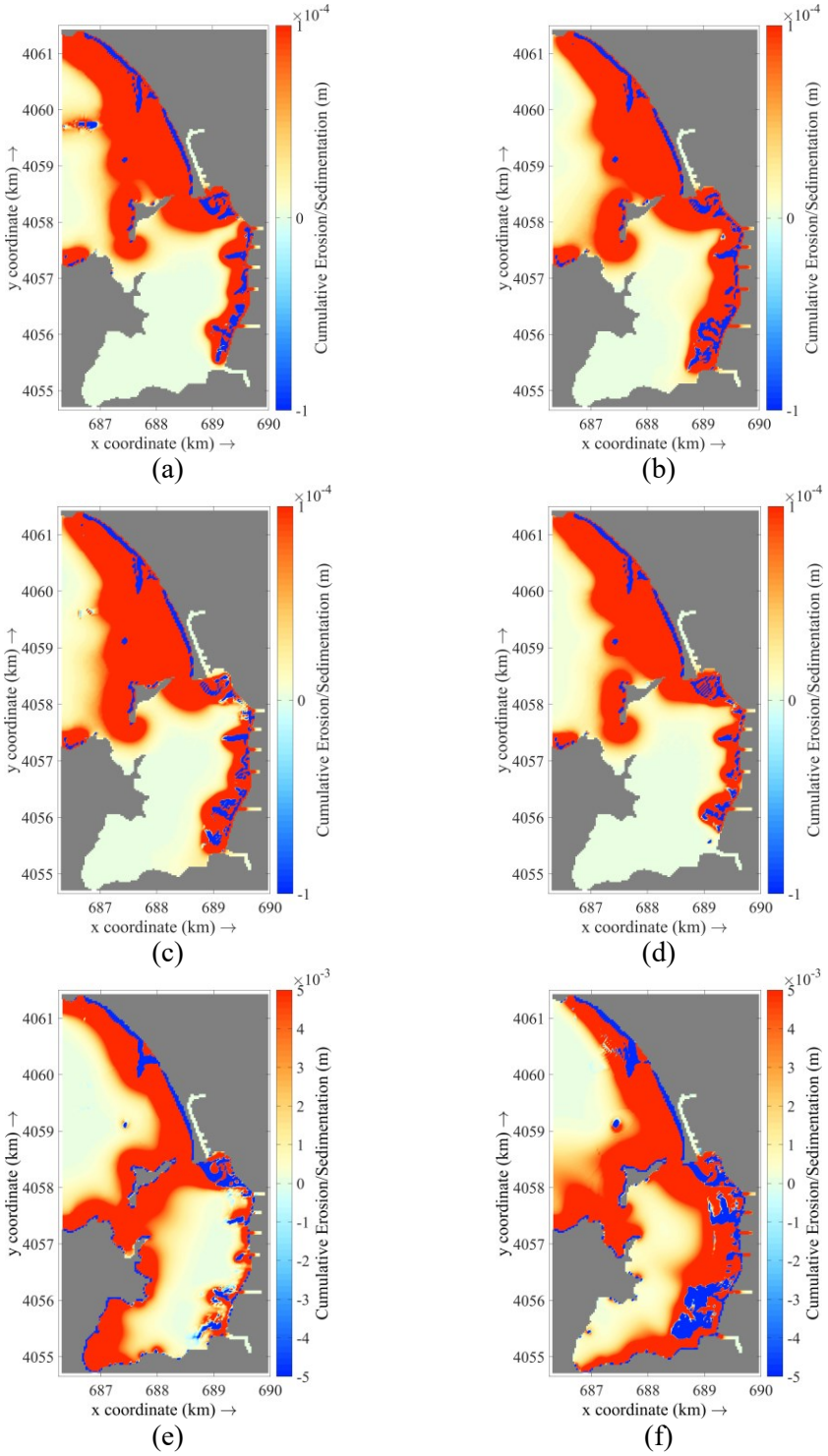

Figure 5.4. The areal distribution of cumulative erosion and deposition patterns for different inputs of a. Scenario 1, b. Scenario 2, c. Scenario 3, d. Scenario 4, e. Scenario 5, f. Scenario 6

Under all wind conditions, similar sediment depositions are observed over the area of A1, implying that the model, which has been calibrated and validated in previous stages, has a good agreement with real life observations. Furthermore, the inputs determined through the results of the long-term wind and wave analysis, along with the tidal conditions and the river discharge data collected in the study area, accurately reflect the real life conditions in the numerical model. These findings reveal the current problematic state of the bay and the amount of deposition in the bay to occur if no dredging will be operated.

Both the river discharge inputs determined in the model and the corresponding low current speeds over the area A1, leads a similar pattern of sediment deposition in each scenario (Figure 5.4). For the long-term scenarios, the maximum sediment deposition area is observed in Scenario 2, and decreases over Scenario 1, 3 and 4. Since the WNW wind direction defined in Scenario 2, leads a cyclonic circulation at higher current speeds, the amount of cumulative sediment deposition is influenced in the bay accordingly (Figure 5.4.b). From the extreme case comparison between Scenario 5 and 6, an aligned statement can be made, where significantly larger area of deposition is occurred in Scenario 6 (Figure 5.4.f), rather than in Scenario 5 (Figure 5.4.e).

When the areal distribution of water circulation and sediment transport are examined the observed dynamics are found to be similar for the same wind directions and corresponding cases. The wind speed and direction have a greater impact on both the circulation and sediment transport patterns than other input parameters. This similarity indicates that changes in current velocity and water circulation behavior within the bay directly influence the pattern of sediment accumulation in the region. These findings show that potential dredging operations, which are expected to alter the water circulation behavior, will significantly impact the sediment deposition patterns.

5.2 Water circulation and sediment transport under dredging operations

One of the key questions addressed in the thesis is the effect of dredging operations on water circulation and sediment transport dynamics. The model is run for five different dredging operations, with depths ranging from -1 m to -5 m, decreasing by 1 m for each case. All of the input scenarios given earlier in Table 4.4, is applied separately in every dredging case, and the results are obtained. Similar to the analysis given in the previous section, the changes of these dynamics within the inner bay area are primarily analyzed based on areal model outputs.

The variations within the bay for different dredging scenarios are evaluated through horizontal velocities and current directions computed on the seafloor to form a basis for understanding the circulation and consequent sediment movement, at the end of the 10-hour simulation. These assessments have been conducted for all scenarios, particularly for different wind directions. As an example, the model results for the Scenario 1, with the dominant direction of ESE are given in Figure 5.5 for maximum horizontal velocities at the sea bottom, in Figure 5.6 for total sediment transport, and in Figure 5.7 for cumulative sediment deposition. The areal distributions of those parameters for each dredging condition under each input scenario (Scenario 2, 3, 4, 5 and 6) are given in Appendix C.

Through the water circulation results, a localized current speed increase at the seabed has been observed over the area A1, addressing the positive effect of the dredging over the sediment deposition (Figure 5.5). This change can be attributed to the gradual increase in the dredging depth considered in each scenario. The current velocities in the areas A2 and A3 are relatively higher when dredged to -1 m compared (Figure 5.5.b) to the non-dredged scenario (Figure 5.5.a). The velocities in the area A1 also increase when the corresponding area is dredged to -2 m (Figure 5.5.c). This trend becomes relatively more significant with higher current speeds when dredged to -3 m (Figure 5.5.d), compared to the other dredging depths. In addition, the current speeds influencing the outflow to the outer bay over the area A2, strengthens slightly near the Murt River, as the dredging depths increased.

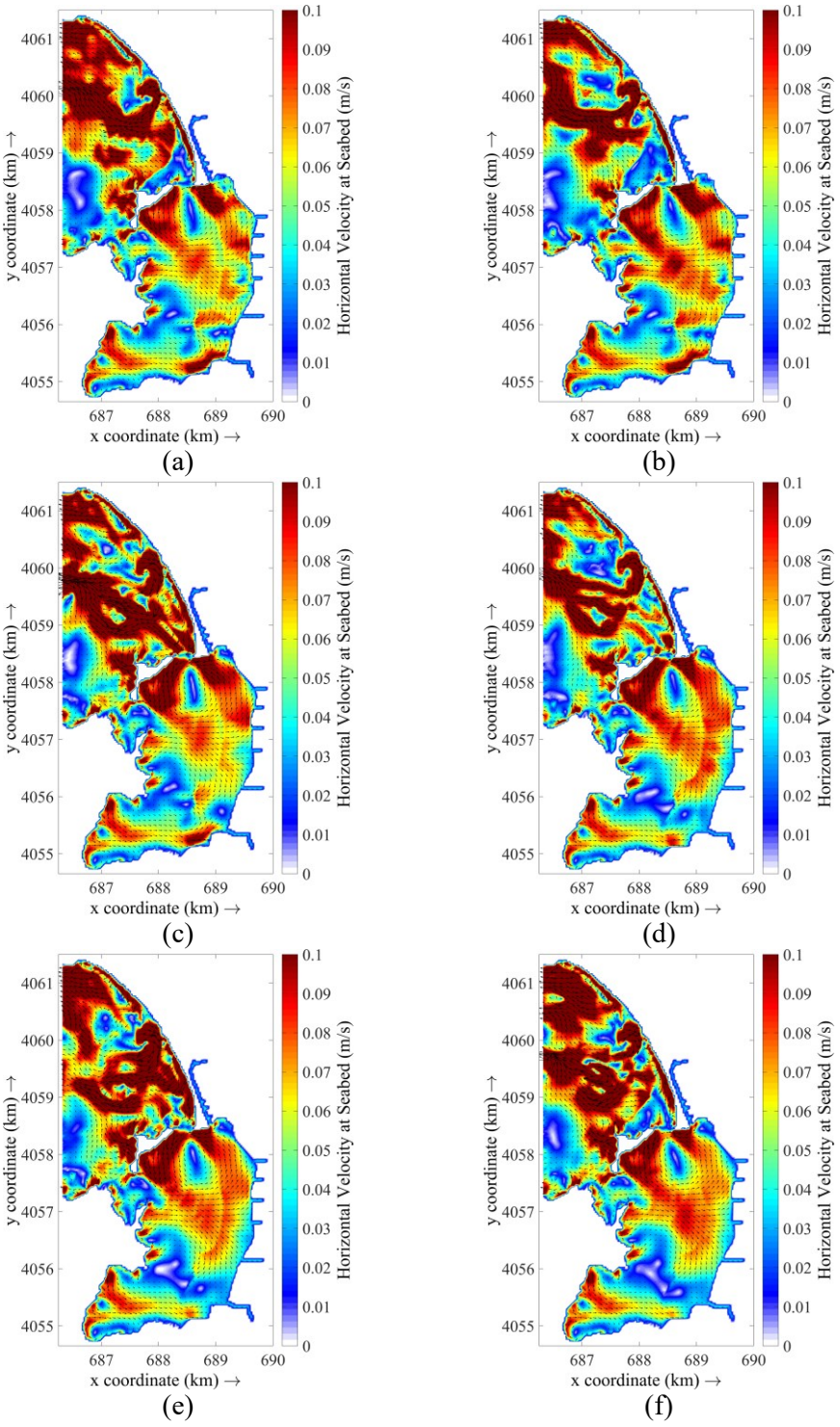

Figure 5.5. The areal distribution of maximum horizontal velocity profiles at the sea bottom under Scenario 1 for a. not-dredged, b. dredged to -1 m, c. dredged to -2 m, d. dredged to -3 m, e. dredged to -4 m, f. dredged to -5 m

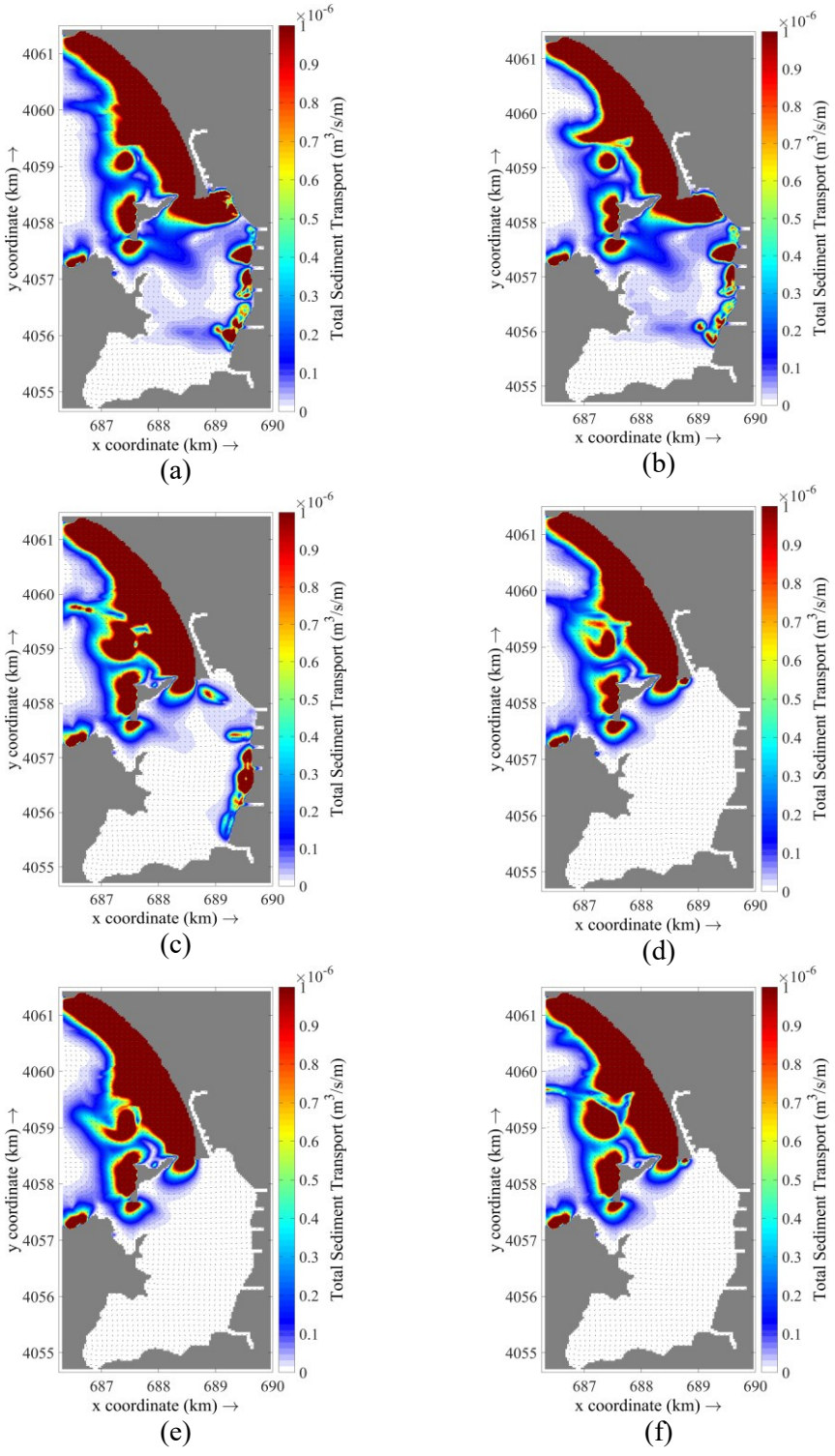

Figure 5.6. The areal distribution of total sediment transport under the effect of Scenario 1 for a. not-dredged, b. dredged to -1 m, c. dredged to -2 m, d. dredged to -3 m, e. dredged to -4 m, f. dredged to -5 m

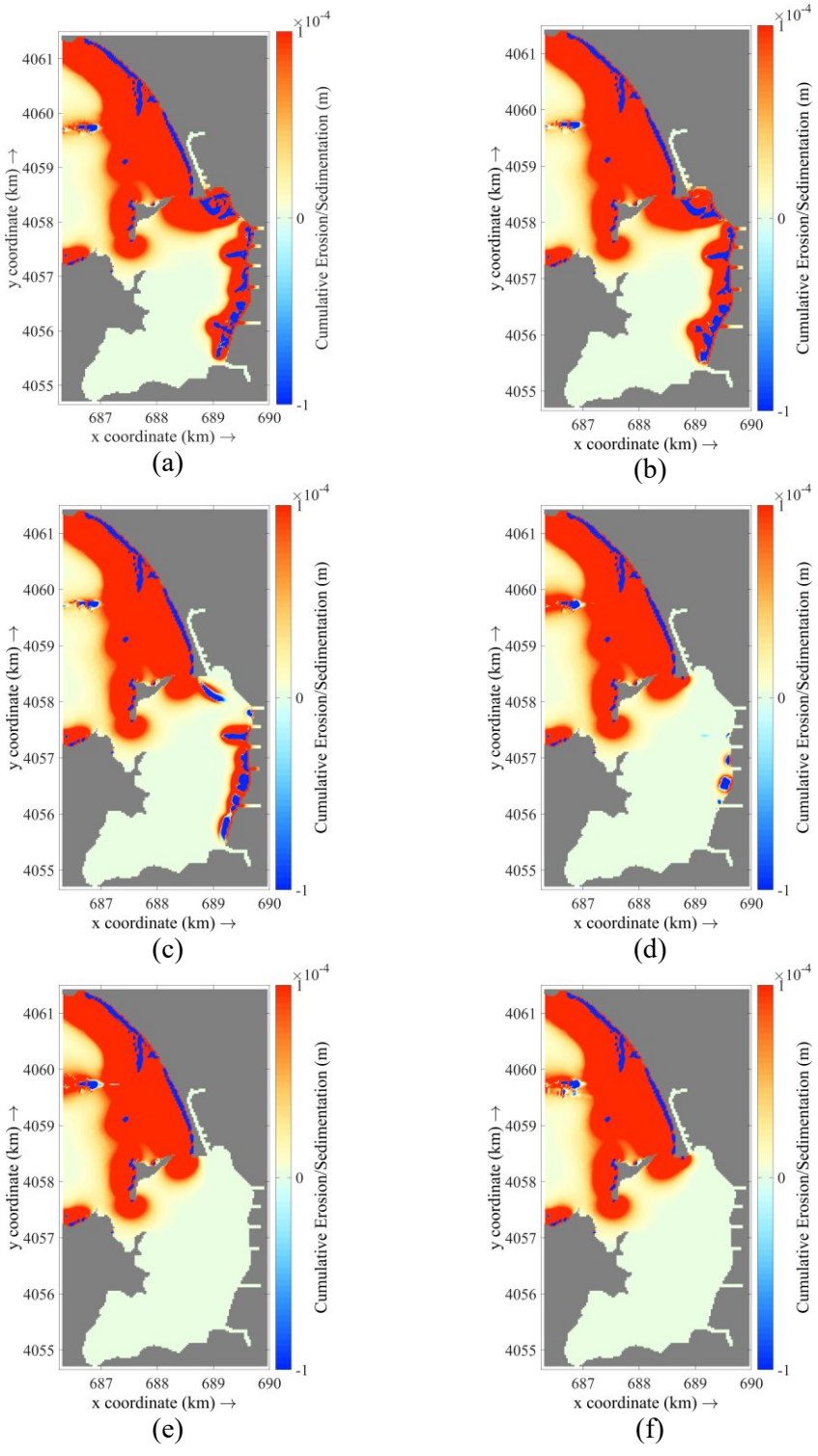

Figure 5.7. The areal distribution of cumulative erosion and deposition under the effect of Scenario 1 for a. not-dredged, b. dredged to -1 m, c. dredged to -2 m, d. dredged to -3 m, e. dredged to -4 m, f. dredged to -5 m

The sediment transport and cumulative deposition in area A1, in the current (non-dredged) condition decreases as the dredging depth and area increases in general (Figure 5.6, Figure 5.7). In addition, the total sediment transport is slightly decreased in the -1 m dredging condition (Figure 5.6.b) compared to the non-dredged condition (Figure 5.6.a), where this situation is further reduced in the -2 m dredging condition (Figure 5.6.c), and starting from the -3 m dredging depth (Figure 5.6.d) and at subsequent depths, the sediment transport in the bay is minimized under long-term scenario input conditions. Accordingly, partial sedimentation is observed in the non-dredged (Figure 5.7.a), dredged to -1 m (Figure 5.7.b) and dredged to -2 m scenarios (Figure 5.7.c), where it is also minimized from the condition of dredging to -3 m (Figure 5.7.d). With the decrease in sedimentation in the bay starting from the dredging to -3 m depth, an optimum dredging depth and area is indicated.

Although the sediment deposition values obtained in extreme cases (Scenario 5, and 6) are higher compared to long-term (Scenario 1, 2, 3, and 4), and it may lead to an overestimation for the deposition, while it is necessary to check the post-dredging effects in the area A1 under storm conditions. Hence, the changes in water circulation and sediment transport dynamics within the bay are similarly analyzed as areal outputs of corresponding parameters (Figure 5.8, Figure 5.9, and Figure 5.10).

The water circulation behavior appears to be higher in terms of current velocity magnitudes compared to the results obtained in the long-term analysis (Scenario 1, Figure 5.8). In all scenarios, the winds coming from the ESE direction for 12 hours creates two cyclonic circulation pattern in the areas of A2 and A3. The northern cyclonic feature located at the south of Şövalye Island has a direct impact on the water inflow into and outflow from the bay. While, the southern one has a slightly positive effect on the increasing current speeds over the area A1. The current velocities in the area A1, gradually increase with deeper dredging, becoming particularly significant in the scenario of dredging to -5 m (Figure 5.8.d).

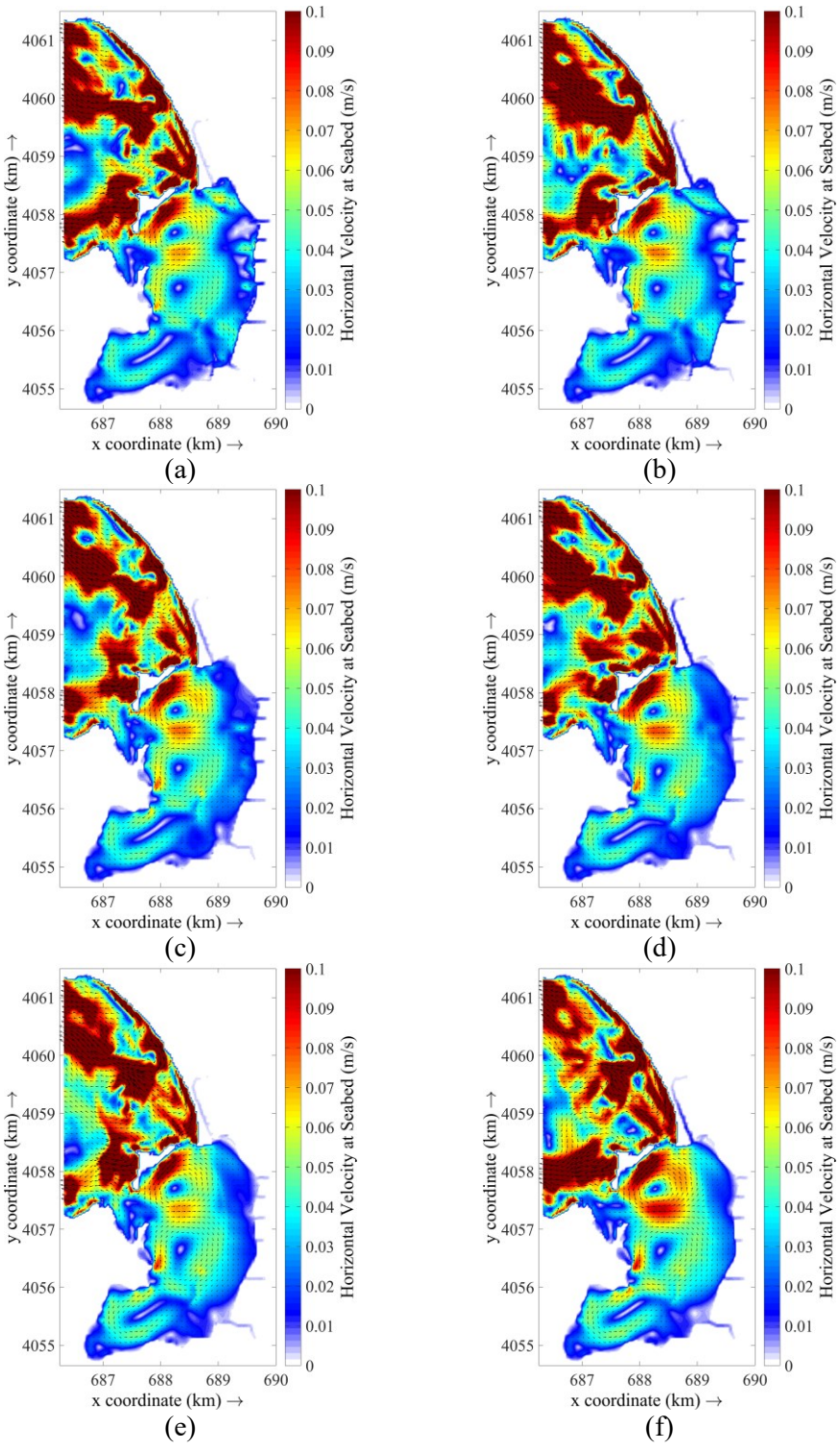

Figure 5.8. The areal distribution of maximum horizontal velocity profiles at the sea bottom under the effect of Scenario 5 for a. not-dredged, b. dredged to -1 m, c. dredged to -2 m, d. dredged to -3 m, e. dredged to -4 m, f. dredged to -5 m

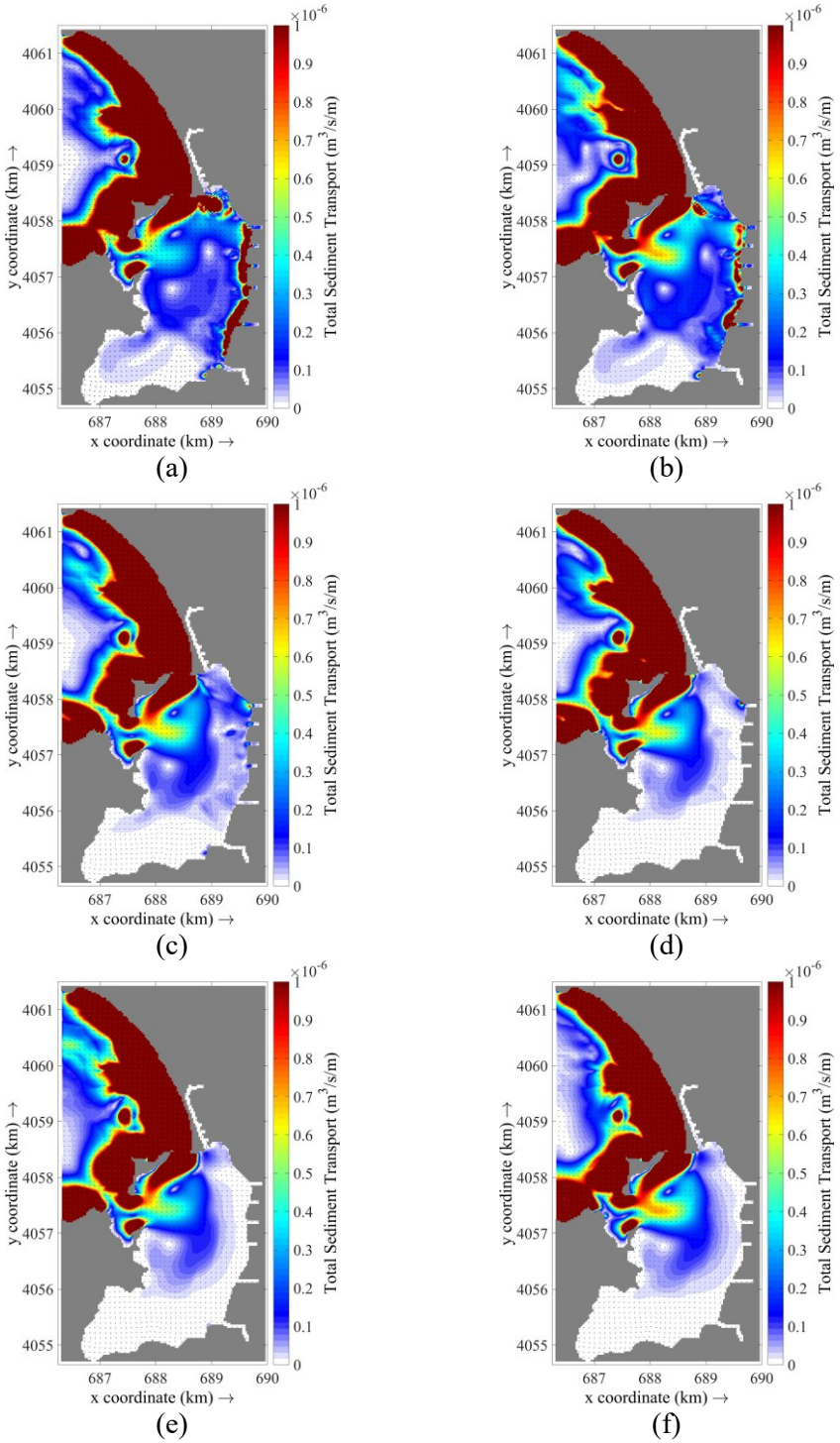

Figure 5.9. The areal distribution of total sediment transport under the effect of Scenario 5 for a. not-dredged, b. dredged to -1 m, c. dredged to -2 m, d. dredged to -3 m, e. dredged to -4 m, f. dredged to -5 m

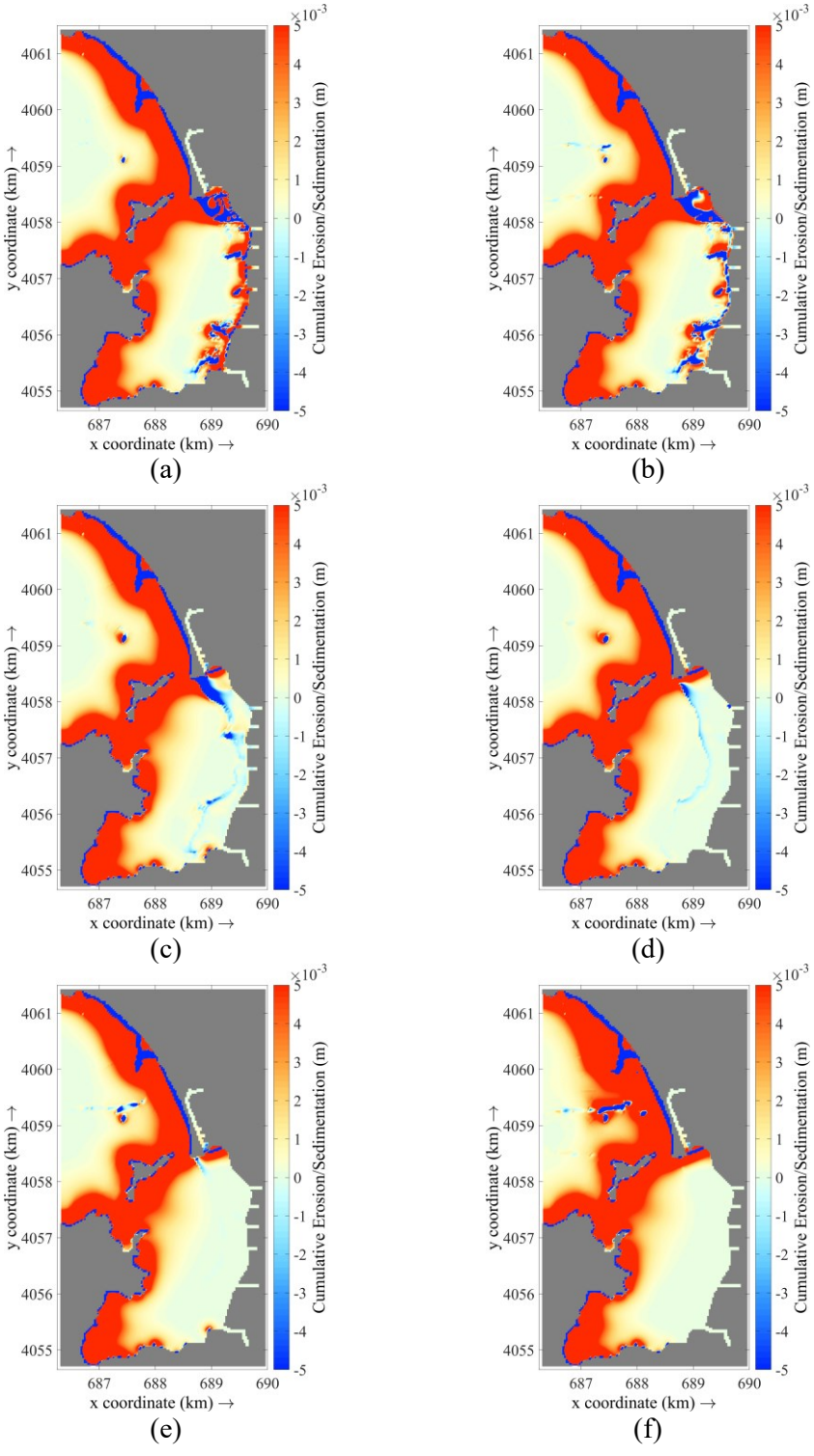

Figure 5.10. The areal distribution of cumulative erosion and deposition under the effect of Scenario 5 for a. not-dredged, b. dredged to -1 m, c. dredged to -2 m, d. dredged to -3 m, e. dredged to -4 m, f. dredged to -5 m

The cyclonic circulation behavior around the island, resulting from the current pattern, also dominates the sediment transport (Figure 5.9). This supports the increase in deposition also at the area A4 in the bay, which is not observed in the long-term scenarios. In addition, the amount of sediment transport in the problematic area correspondingly decreases in the case of dredging (Figure 5.9.b). Similarly, starting from the -3 m dredging depth (Figure 5.9.d) and at subsequent depths, the sediment transport over the dredged area in the bay is minimized and becomes more uniform compared to the non-dredged case (Figure 5.9.a). In line with these findings, the amount of sediment deposition in the area A1, decreases under dredging scenarios (Figure 5.10) also for the extreme conditions. The distribution in this area becomes more uniform, particularly at dredging depths of -2 m (Figure 5.10.c) and -3 m (Figure 5.10.d). In these scenarios, the observed erosion in the dredging zone which is assumed to be not-realistic, is likely due to the intense wind conditions in the simulation.

A significant positive effect on water circulation and sedimentation within the inner bay area has been observed under dredging operations for both long-term and extreme cases through the analysis of areal distributions of water circulation and sediment transport. For the sediment transport results, the low magnitudes of cumulative deposition results should be evaluated considering the short simulation duration of 10 hours. Through these results, the importance of the areal distribution of the sediment deposition is emphasized, rather than the quantity. For a better understanding of the cumulative sedimentation magnitudes, the simulation durations should be increased. The results of these two sub-chapters indicate that wind direction and dredging depths are two major parameters influencing the water circulation and sediment transport results, where the relation between them is also investigated through water exchange and cumulative deposition volumes and presented in the next chapter.

5.3 Relationship between water exchange and cumulative deposition in the bay under dredging scenarios

In addition to the areal distributions of water circulation and sediment transport in Fethiye Bay, the changes in those parameters under the dredging scenarios are analyzed by calculating the total volume of water entering and leaving the bay and the volume of sediment deposition. The total volume of water entering and leaving the bay is determined based on the model results through the two openings located in the A2 area for two-cross sections (CS01 and CS02) specified in Figure 3.5. The calculated volumes from the simulation results of all scenarios are given in Appendix C in detail.

Dimensionless volume ratios for the water exchange and the sediment deposition are calculated to better understand the physical aspects behind the observed variations. For water exchange ratio, the volume of water entering and leaving the bay obtained at the end of the simulation is divided by the total inner-bay volume (Equation 5.1).

$$V_{Water\ Exchange}(\%) = \frac{V_{model\ results}}{V_{inner\ bay}} x\ 100 \tag{5.1}$$

For cumulative deposition ratio, the volume of deposition in the problematic area obtained after 10 hours of simulation is divided by the total sediment volume in this problematic area (Equation 5.2).

$$V_{Cumulative\ deposition}(\%) = \frac{V_{deposition\ in\ A1}}{V_{sediment\ in\ A1}} x\ 100 \tag{5.2}$$

In this way, the effect of the dredging operation on these two processes is examined via a multiple parameter analysis based on the model results to reveal their relationship under several different scenarios (Figure 5.11).

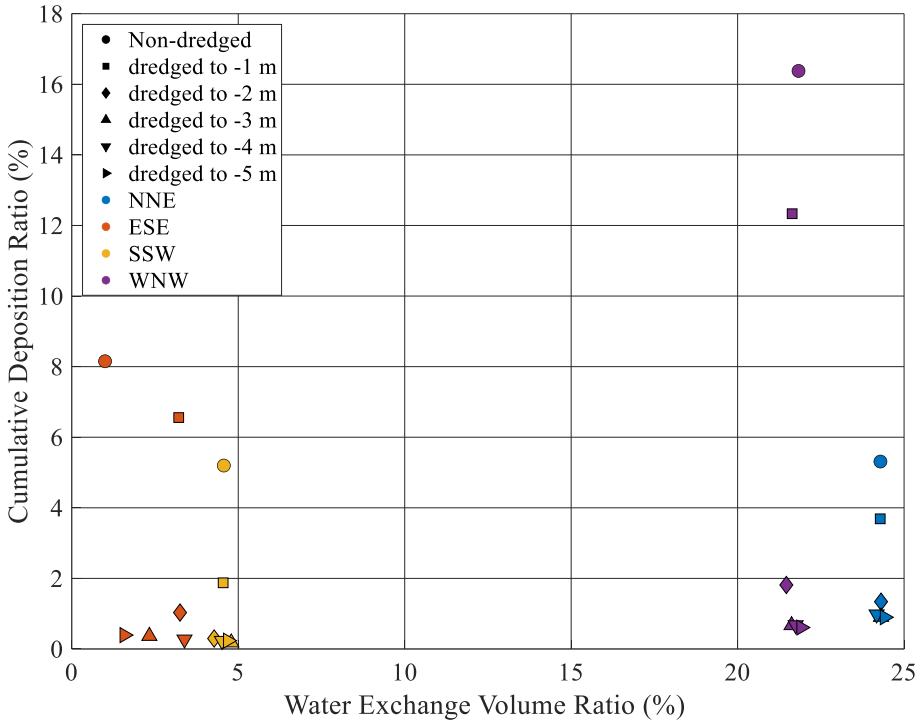

Figure 5.11. The relationship between water exchange volume ratio and cumulative deposition ratio under the dredging scenarios

Figure 5.11 illustrates that the relationship between these two processes does not follow a simple linear trend. Consequently, it is difficult to conclude whether the amount of water entering and leaving the bay correlates with an increase or decrease in cumulative sediment deposited in Fethiye Bay. However, when this relationship is grouped by wind direction and different dredging scenarios, a consistent pattern is observed at different dredging depths for each wind direction. Therefore, the dynamics of water exchange (Figure 5.12) and cumulative sediment deposition (Figure 5.13) are analyzed for different dredging depths and different wind directions, which are also determined as the two affecting major parameters through the areal distribution results.

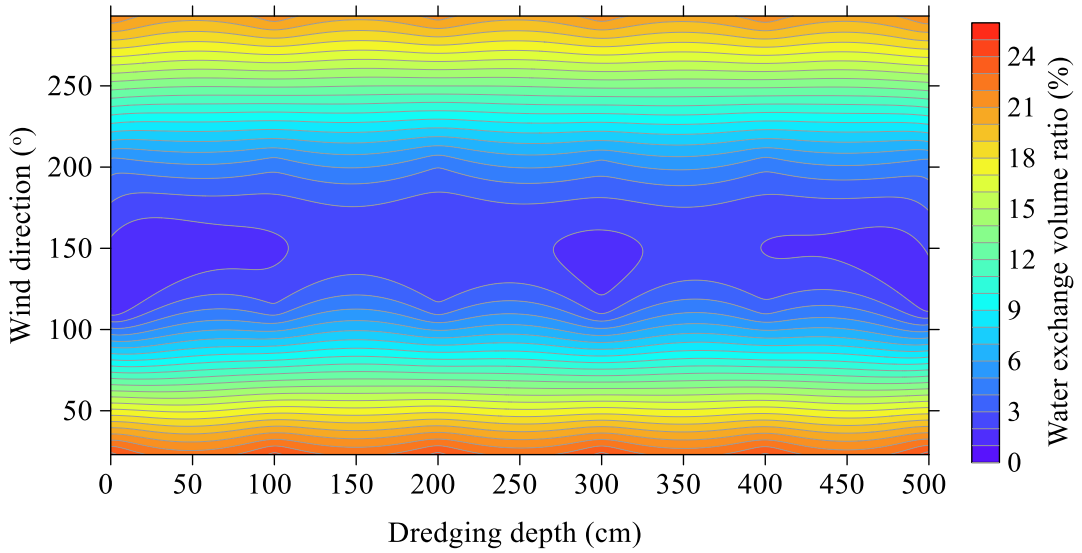

Figure 5.12. The relation of water exchange volume through the dredging depth and wind direction

The amount of water entering and leaving the bay varies more with wind direction than with dredging depth, highlighting the effect of regional characteristics and bathymetry. The model results of water exchange indicate the water inflow and outflow decrease through the ESE (112.5° from North in the clockwise direction) and SSW (202.5° from North in the clockwise direction) directions, whereas they increase in the WNW (292.5° from North in the clockwise direction) and NNE (22.5° from North in the clockwise direction) directions (Figure 5.12). Hence, a similar relationship between water exchange and high inner-bay current velocities observed in the areal distributions can be identified in Fethiye Bay. The significant impact of the WNW wind direction, observed in the spatial distribution results, is also reflected in the water exchange map in Figure 5.11. On the other hand, no significant relationship was found between increased dredging depth and the volume of water entering and leaving the bay; the amount of water inflow and outflow remained similar across all dredging scenarios. Nevertheless, a different dynamic is observed in the cumulative sediment deposition when analyzed under varying wind directions and dredging scenarios (Figure 5.13).

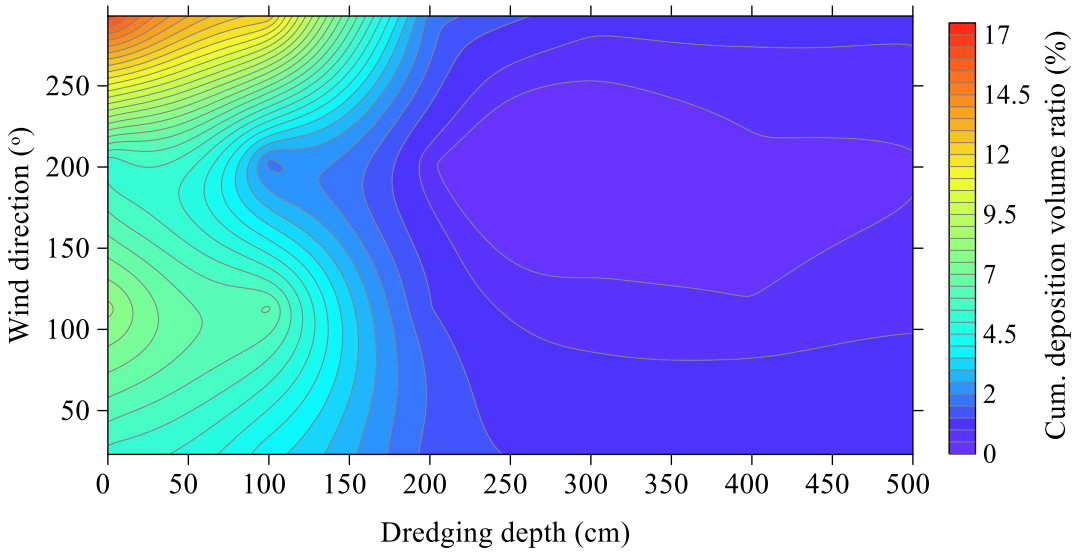

Figure 5.13. The relation of cumulative deposition volume in the problematic area through the dredging depth and wind direction

Cumulative sediment deposition is affected by both wind direction and variations in dredging depth and area to be dredged. In scenarios with shallower dredging depths and consequently smaller areas, the effect of wind direction is particularly noticeable (Figure 5.13). Specifically, winds from WNW and ESE directions significantly affect sediment deposition in the areas planned for dredging within the bay. This effect is less reflected in the model results of NNE and SSW directions. Additionally, the varying 10-hour wind speeds associated with different directions, as obtained in the long-term analysis, may also play a role.

Under different dredging depths, a decrease in the deposition rate is observed across all wind conditions, as reflected in the areal distributions. In addition, sediment transport and consequent cumulative sediment deposition decreases considerably, especially when dredging to -3 m and beyond. This suggests that excessive dredging does not offer additional solutions, likely depending on the characteristics of the region. These findings highlight the complex relationship between water circulation and sediment transport in Fethiye Bay, a semi-enclosed basin.

CHAPTER 6

CONCLUSIONS AND FURTHER STUDIES

6.1 Conclusions

Within the scope of this study, a detailed analysis for water circulation and sediment transport in Fethiye Bay, which is a semi-enclosed basin example addressed with heavy pollution, sedimentation, and low circulation, is carried out taking into account tidal, wind, wave and river conditions. The hydrodynamics of water circulation driven by oceanographic and fluvial sources, as well as sediment transport dynamics are explored via numerical modeling, where the analyzed bathymetric variations over a fifteen-year period indicate potential areas and depths for dredging.

Several scenarios for model input conditions and dredging operations, as mentioned in Chapter 4, are tested for a compound analysis and the model results are evaluated comparing their effects on the water circulation and sediment transport patterns in Fethiye Bay. For the model inputs, tide, wind, wave and river discharge data are collected to best represent the characteristics of the region. The compound approach is found more suitable in the model, effectively incorporating all the current effects into the model.

Firstly, water circulation and sediment transport dynamics are evaluated through areal distributions of the model results. In the long-term scenarios, similar current velocity levels are obtained within the bay, but the water circulation behavior is found to be dependent on the wind direction. Moreover, the computed current velocity magnitudes in the extreme scenarios are found to be higher than the ones computed in the long-term scenarios. For both long-term and extreme cases, the deposition is observed in the area A1, which is considered to be problematic in real life and necessitates to dredging in at the locations of the river mouths. This result

proved that the model, which is primarily calibrated and validated over current velocities at three different depths, provides the results similar to natural processes.

The relation between water circulation and sediment transport in Fethiye Bay also investigated at the different dredging depths and dredging areas. It is observed that, in all scenarios and under all input cases the water circulation behavior is changed under dredging. Due to the rapid changes in the seabed, the currents moving in different orientations in the A1 area have become homogeneous after dredging, and current speeds have relatively increased over the areas of A1 and A2. Hence, the sediment spreading and corresponding cumulative sediment deposition is decreased over the dredged area with the increasing dredging depth.

The model results are also evaluated by focusing on two other related problems: the volume of water entering and leaving the bay and the volume of sediment deposition in problematic areas within the bay. Primarily, it is determined that the volume of water exchange varies considerably depending on the wind direction due to the nature of the basin. Whereas, the volume of cumulative sediment deposition is dependent both on the wind direction and dredging depth and area. According to the results of simulations the optimum dredging depth is found as -3 m, with a total dredging volume of at least 3 million m^3. The increasing trend in the volume of water entering and leaving the bay and the decreasing trend in the sediment deposition at the dredged areas show that dredging operations may be helpful in the pollution measures.

These results show that in Fethiye Bay, as a semi-closed basin example, regional geographical features take important role in the circulation and sediment transport. The dynamics of water circulation within the bay and the associated quantities of water entering and leaving the bay, and the patterns of sediment transport and cumulative erosion and deposition areas are investigated. However, a clear linear correlation is not found.

Dredging operations are among the measures that can be addressed for pollution in terms of reducing the possible sediment deposition and increasing the amount of

water entering and leaving Fethiye Bay. However, it should be taken into consideration that these operations are not only costly, but also have the potential to increase the transport of suspended sediment during the process, which may cause a breakdown in the submarine environment in the region. During the site visit, it has been observed that the predominant sources of pollution in the area are solids, primarily coming from the rivers flowing into the bay, and improper rehabilitation works have increased the severity of the situation. Therefore, in order to develop proper, site-specific pollution control measures, the hydrodynamic characteristics of Fethiye Bay, considering the existing tidal, wind, wave and river discharge characteristics, their interactions and effects on the water circulation and consequent sediment transport should be investigated within a compound analysis, as performed in this study. In addition, parallel to the measures that can be taken through dredging operations, it is also important to assess and address the problem sources in the area.

6.2 Limitations

In addition to previous studies performed in Fethiye Bay, the effects of dredging on the hydrodynamics and sediment transport in the bay are investigated through this study. The model is calibrated using the tidal, wind, wave and river discharge parameters as inputs and a comparison is conducted between the computed current velocities with the measured ones for validation of the model performance.

The fact that the current velocity measurements could be conducted for 3-month duration between April, May and June 2023, which posed a limitation in the calibration process in terms of revealing the behavior of the region under all seasons. In addition, due to time constraints, the calibration of 3 months of current velocities obtained from field measurements using 1 month of data made this situation even more limited. Under these constraints, the computational results are in quite good agreement with the measurement data.

Although bathymetry data from 2007 and 2022 are available, the differences in measurement standards between the two datasets may lead to inaccuracies in the determination of depth changes over the 15-year period. Furthermore, the model is not calibrated morphologically due to the time limitation and the lack of current velocity measurements in the relevant time interval.

The input scenarios used in the model also have certain limitations. Due to the lack of sea level measurement data in Fethiye, the tidal data is retrieved from the Marmaris sea level station, assuming similar tidal conditions in Fethiye and Marmaris. In addition, river discharges inputted to the model are selected based on available field measurements, with the assumption that these instantaneous measurements represent the overall temporal behavior of the rivers. Time series wind data used in the calibration process is obtained from a measurement station for a single point observation, meaning that the spatial variability of wind input is not considered. Additionally, the wave input is applied in the form of a spectrum, rather than a time series. Consequently, each parameter has its margin of errors, that are assumed to be negligible to understand the cumulative dynamics in the region.

Close examination of real-life changes in the numerical model reveals limitations related to both computational time and model resolution due to the use of small grid sizes and short time steps. Therefore, in the numerical model, which utilizes a grid size of 30m, the results are presented as averages over a horizontal area of 900 square meters at the determined gauge points. This situation limits the degree of similarity that can be achieved between the field measurements obtained in real life and the model results. In addition, the selection of model area and the choice of boundary conditions, also have an impact on the variation of the results in the model and lead to constraints on the results obtained.

6.3 Further studies

In the later stages of this study, taking a 1-year field measurement in this selected study area in order to reflect the characteristics of the region under all conditions and adapting the model over daily average current velocity values, rather than calibrating it in detail as a time series, will increase the accuracy of the study results. This 1-year model run will provide more insightful information on sediment deposition and erosion zones within the bay.

In addition to the 2022 bathymetry, taking a bathymetry measurement in 2024, examining the change in bathymetry between these two years, and calibrating and validating the model in terms of current speed and morphological aspects will increase the reliability of the results obtained in the study. Following the updated bathymetry measurements, expanding the model domain and performing a sensitivity analysis on turbulence parameters will further reflect the circulation behavior in the model in real life.

Considering that the sea water temperature changes in Fethiye Bay will have a high impact on the water circulation characteristics in the region, it would be useful to include temperature-dependent circulation behavior in the model but requires continuous field measurements of the parameter.

In addition to the more accurate and longer field measurements of tide, wind, wave and river discharge or the bathymetric data that can be obtained, the identification of other semi-enclosed basin study areas in addition to Fethiye Bay, will be more effective in making a general inference in these areas to examine the changes in water circulation and sediment transport behavior.

The addition of dredging operations to the study of these changes will provide diversity in examining the relationship between water exchange and cumulative sediment deposition volumes.

The dredging scenarios selected in the region focused on the current sediment deposition points. In the further studies, diversifying the dredging scenarios in the entrance and exit areas of the bay will reveal the effect of dredging through different dredging locations, not only in terms of depth and the associated area expansion.

REFERENCES

Akbaşoğlu, S. (2011). Wind-induced circulation and sediment transport in semi-enclosed basins: case study for Fethiye bay. (PhD Thesis, METU Graduate School of Natural and Applied Sciences). Ankara.

Akdeniz, İ. (2018). 3-dimensional numerical circulation modeling: a case study on the coastal processes in Göcek and Fethiye Bays, Turkey. (Master's Thesis, METU Graduate School of Natural and Applied Sciences). Ankara.

Alemán, N., Certain, R., Barusseau, J. P., Courp, T., & Dia, A. (2014). Post-glacial filling of a semi-enclosed basin: the Arguin Basin (Mauritania). *Marine Geology,* 349, 126-135.

Álvarez, M., Carballo, R., Ramos, V., & Iglesias, G. (2017). An integrated approach for the planning of dredging operations in estuaries. *Ocean Engineering*, 140, 73-83.

Advanced Spaceborne Thermal Emission and Reflection Radiometer (ASTER). (2023). ASTER Global DEM. Retrieved April 20, 2023, from https://asterweb.jpl.nasa.gov/

Bai, Y., Wang, Z., & Shen, H. (2003). Three-dimensional modelling of sediment transport and the effects of dredging in the Haihe Estuary. *Estuarine, Coastal and Shelf Science, 56*(1), 175-186.

Beecroft, R., Grinham, A., Albert, S., Perez, L., & Cossu, R. (2019). Suspended sediment transport in context of dredge placement operations in Moreton Bay, Australia. *Journal of Waterway, Port, Coastal, and Ocean Engineering, 145*(2), 05019001.

Brakenhoff, L., Schrijvershof, R., van der Werf, J., Grasmeijer, B., Ruessink, G., & van der Vegt, M. (2020). From Ripples to Large-Scale Sand Transport: The Effects of Bedform-Related Roughness on Hydrodynamics and Sediment Transport Patterns in Delft3D. *Journal of Marine Science and Engineering, 8*(11), 892, https://doi.org/10.3390/jmse8110892

Brown, J. M., & Davies, A. G. (2009). Methods for medium-term prediction of the net sediment transport by waves and currents in complex coastal regions. *Continental Shelf Research, 29*(11-12), 1502-1514.

Campmans, G. H. P., Roos, P. C., Van der Sleen, N. R., & Hulscher, S. J. M. H. (2021). Modeling tidal sand wave recovery after dredging: effect of different types of dredging strategies. *Coastal Engineering,* 165, 103862.

Chen, C. S., Liu, H., Beardsley, R. C. (2003). An Unstructured Grid, Finite-Volume, Three-Dimensional, Primitive Equations Ocean Model: Application to

Coastal Ocean and Estuaries. *Journal of Atmospheric and Oceanic Technology*, 20, 159–186.

Chen, C., Zhong, J. C., Yu, J. H., Shen, Q. S., Fan, C. X., & Kong, F. X. (2016). Optimum dredging time for inhibition and prevention of algae-induced black blooms in Lake Taihu, China. *Environmental Science and Pollution Research*, 23, 14636-14645.

Cheng, G., Gong, W., Wang, Y., & Xia, Z. (2017). Modeling the circulation and sediment transport in the Beibu Gulf. *Acta Oceanologica Sinica, 36*(4), 21-30.

Clark, J. R. (1997). Coastal zone management for the new century. *Ocean & Coastal Management, 37*(2), 191-216.

Copernicus Climate Change Service (C3S). (2023). ERA5: Fifth generation of ECMWF atmospheric reanalyses of the global climate. ERA5 hourly data on single levels from 1940 to present. Retrieved from https://cds.climate.copernicus.eu/cdsapp#!/home

Danish Hydraulic Institute (DHI). (2012). MIKE 21 & MIKE 3 flow model FM. Hydrodynamic and Transport module scientific documentation.

Deltares (2011). *Delft3D-FLOW User Manual*, Delft, the Netherlands.

Deltares (2011). *Delft3D-WAVE User Manual*, Delft, the Netherlands.

Dzabic, M. (2012). Water circulation and yacht carrying capacity of Fethiye Bay. (Master's Thesis, METU Graduate School of Natural and Applied Sciences). Ankara.

Elias, E. P. L., Walstra, D. J. R., Roelvink, J. A., Stive, M. J. F., & Klein, M. D. (2001). Hydrodynamic validation of Delft3D with field measurements at Egmond. *Coastal engineering* 2000 (pp. 2714-2727).

Erdik, T., Şen, O., & Öztürk, İ. (2019). 3D numerical modeling of exchange flows in golden horn estuary. *Journal of Waterway, Port, Coastal, and Ocean Engineering, 145*(5), 04019018. https://doi.org/10.1061/(ASCE)WW.1943-5460.0000516

Fernández-Fernández, S., Ferreira, C. C., Silva, P. A., Baptista, P., Romão, S., Fontán-Bouzas, Á., ... & Bertin, X. (2019). Assessment of dredging scenarios for a tidal inlet in a high-energy coast. *Journal of Marine Science and Engineering, 7*(11), 395.

General Bathymetric Chart of the Oceans (GEBCO). (2023). GEBCO 2023 Grid. Retrieved June 03, 2023, from https://www.gebco.net/

General Directorate of Meteorology Database - MEVBIS (2023). Fethiye and Kızılada Station Hourly Wind Direction (°) and Speed (m/sec). https://mevbis.mgm.gov.tr/mevbis/ui/index.html#/Workspace

Google Earth. (2023). Imagery of Fethiye Bay, Turkey. Retrieved July 29, 2024, from https://www.google.com/earth/

Imamura, F., Yalciner, A. C., & Ozyurt, G. (2006). Tsunami modelling manual. *UNESCO IOC international training course on Tsunami Numerical Modelling*, 137-209.

James, G., Witten, D., Hastie, T., & Tibshirani, R. (2013). *An introduction to statistical learning* (Vol. 112, p. 18). New York: Springer.

Je, C. H., Hayes, D. F., & Kim, K. S. (2007). Simulation of resuspended sediments resulting from dredging operations by a numerical flocculent transport model. *Chemosphere, 70*(2), 187-195.

Jeong, A., Kim, S., Kim, M., & Jung, K. (2016). Development of optimization model for river dredging management using MCDA. *Procedia Engineering*, 154, 369-373.

Karahan, H. (2002). The impacts of sedimentation caused in Izmir Bay by Gediz River on circulation and water quality. *WIT Transactions on Ecology and the Environment*, 58.

Koşucu, M. M., Demirel, M. C., Kirca, V. O., & Özger, M. (2019). Hydrodynamic and hydrographic modeling of Istanbul strait. *Processes, 7*(10), 710. https://doi.org/10.3390/pr7100710

Lagasse, P. F. (1986). River response to dredging. *Journal of waterway, port, coastal, and ocean engineering, 112*(1), 1-14.

Lesser, G. R., Roelvink, J. V., van Kester, J. T. M., & Stelling, G. S. (2004). Development and validation of a three-dimensional morphological model. *Coastal engineering, 51*(8-9), 883-915.

Linsley, R. K., & Franzini, J. B. (1979). *Water-resources engineering*, McGraw-Hill, New York.

Lips, U., Zhurbas, V., Skudra, M., & Väli, G. (2016). A numerical study of circulation in the Gulf of Riga, Baltic Sea. Part I: Whole-basin gyres and mean currents. *Continental Shelf Research*, 112, 1-13.

Liu, H., Xu, K., Ou, Y., Bales, R., Zang, Z., & Xue, Z. G. (2020). Sediment transport near ship shoal for coastal restoration in the Louisiana shelf: A model estimate of the year 2017–2018. *Water, 12*(8), 2212.

Liu, S., Li, G., Liu, S., Xing, L., Pan, Y., & Yu, D. (2024). Impacts of reclamation on hydrodynamic and suspended sediment transport in the Bohai Sea. *Journal of Geophysical Research: Oceans*, 129, e2023JC020570. https://doi.org/10.1029/2023JC020570

Lu, C.Z.; Li, H.; Dai, W.Q.; Tao, J.F.; Xu, F.; Cybele, S.; Zhang, X.Y., and Guo, H.T., (2018). 3-D Simulation of the Suspended Sediment Transport in the

Jiaojiang Estuary: Based on Validating by Remote Sensing Retrieval. In: Shim, J.-S.; Chun, I., and Lim, H.S. (eds.), Proceedings from the International Coastal Symposium (ICS) 2018 (Busan, Republic of Korea). *Journal of Coastal Research, Special Issue*, 85, 116–120.

Mays, L. W. (2010). *Water resources engineering*. John Wiley & Sons.

Maerker, C., Malcherek, A., Riemann, J., & Brudy-Zippelius, T. (2011). Modelling and analyzing dredging and disposal activities using Telemac, Sisyphe and DredgeSim. *XVIIIth Telemac & Mascaret User Club*, 19, 92.

METU OERC (2011). Fethiye Municipality and Fethiye Bay Yacht Carrying Capacity Project, Final Report.

METU TRANSFER, (2007), "Determination of marine vehicles carrying capacity of Fethiye-Göcek special environmental protection area", Middle East Technical University Department of Civil Engineering, Ocean Engineering Research Center

Muğla Metropolitan Municipality. (2022). Fethiye Study Report. Muğla, Turkey.

Mikac, N., Sondi, I., Vdović, N., Pikelj, K., Ivanić, M., Lučić, M., & Krivokapić, S. (2022). Origin and history of trace elements accumulation in recent Mediterranean sediments under heavy human impact. A case study of the Boka Kotorska Bay (Southeast Adriatic Sea). *Marine pollution bulletin*, 179, 113702.

National Centers for Environmental Prediction (NCEP). (2023). Climate Forecast System Reanalysis (CFSR), for 1979 to 2011. Retrieved from https://rda.ucar.edu/datasets/ds093.0/

National Centers for Environmental Prediction (NCEP). (2023). Climate Forecast System Reanalysis (CFSR) v2, for 2011 to present. Retrieved from https://rda.ucar.edu/datasets/ds093.0/

Nishijima, W., Tada, K., Ichimi, K., Asahi, T., Tomiyama, T., Shibata, J., & Sakai, Y. (2019). Nutrient management. In *Integrated Coastal Management in the Japanese Satoumi* (pp. 59-84). Elsevier.

Ozturk, M., & Yuksel, Y. (2023). Tidal and non-tidal sea level analysis in enclosed and inland basins: The Black, Aegean, Marmara, and Eastern Mediterranean (Levantine) Seas. *Regional Studies in Marine Science*, 61, 102848.

Papanicolaou, A. T. N., Elhakeem, M., Krallis, G., Prakash, S., & Edinger, J. (2008). Sediment transport modeling review—current and future developments. *Journal of hydraulic engineering, 134*(1), 1-14.

Raicevich, S., Barausse, A., Canadelli, E., Fortibuoni, T., & Mazzoldi, C. (2018). Historical ecology of semi-enclosed basins and coastal areas: past, present and future of seas at risk. *Regional Studies in Marine Science,* 21, 1-6.

Scovazzi, T. (2024). The Regime of Enclosed or Semi-Enclosed Seas with Special Regard for the Mediterranean Sea. *Portuguese Yearbook of the Law of the Sea, 1*(1), 154-175. https://doi.org/10.1163/29501636-01010009

Shang, J., Sun, J., Tao, L., Li, Y., Nie, Z., Liu, H., ... & Yuan, D. (2019). Combined effect of tides and wind on water exchange in a semi-enclosed shallow sea. *Water, 11*(9), 1762.

Silveira, L., Gomes, G., Taiani, L., Pinheiro, V., Benedet, L., Marques, A., & Loureiro, C. (2017). Integrated method for optimal channel dredging design. *Terra et Aqua*, 146, 5-16.

Song, H., Kuang, C., Wang, X. H., & Ma, Z. (2020). Wave-current interactions during extreme weather conditions in southwest of Bohai Bay, China. *Ocean Engineering*, 216, 108068.

Srše, J., Perkovič, M., & Grm, A. (2023). Sediment Resuspension Distribution Modelling Using a Ship Handling Simulation along with the MIKE 3 Application. *Journal of Marine Science and Engineering, 11*(8), 1619.

Torres, R. J., Abessa, D. M., Santos, F. C., Maranho, L. A., Davanso, M. B., do Nascimento, M. R., & Mozeto, A. A. (2009). Effects of dredging operations on sediment quality: contaminant mobilization in dredged sediments from the Port of Santos, SP, Brazil. *Journal of soils and sediments,* 9, 420-432.

Truong, D. D., Tri, D. Q., & Don, N. C. (2021). The impact of waves and tidal currents on the sediment transport at the sea port. *Civil Engineering Journal, 7*(10), 1634-1649.

Turkish State Meteorological Service. (2023). MEVBİS: Meteorological Data Information System. Hourly wind data for Kızılada Station. Retrieved July 5, 2023, from https://mevbis.mgm.gov.tr/

Qi, J.; Jing, Y.; Chen, C.; Zhang, J. Numerical Simulation of Tidal Current and Sediment Movement in the Sea Area near Weifang Port. *Water 2023*, 15, 2516. https://doi.org/10.3390/w15142516

Wang, YH., Wang, CH., & Tang, LQ. (2014). Long-term morphological response to dredging including cut-across-shoal in a tidal channel-shoal system. *Ocean Dynamics 64*, 1831–1843 https://doi.org/10.1007/s10236-014-0786-6

Wassmann, P., & Tamminen, T. (1999). Pelagic eutrophication and sedimentation in the Gulf of Riga: an introduction. *Journal of marine systems, 23*(1-3), 1-10.

Williams, J., Matthews, A., & Jevrejeva, S. (2019). Development of an automatic tide gauge processing system. National Oceanography Centre Research and Consultancy Report, 64, Southampton, National Oceanography Centre, 26 pp.

Yalciner A. C., Ozer, C., Insel I., & Dilmen D. (2008). Development of Bathymmetry data for Fethiye Bay, Deliverable of EU TRANSFER Project, (METU report).

Yang, J. S. (2012). Development and Application of a Dynamically Coupled Wave-Current Model. (Master's Thesis, Tianjin University), Tianjin, China.

Yu, S., Xu, F., Peng, Z., Guo, L., Wang, X., Xie, W., Zhu, C., Wang, Z., & He, Q. (2024). Dynamic Evolution of Tidal Networks under the Combined Effect of De-reclamation and Decrease of Sediment supply. *Continental Shelf Research*, 105274.

APPENDICES

A. Supplementary Tables and Figures for the Methodology

Table 6.1 Measured instantaneous discharges for the selected discharge points

Date	*Measured Instantaneous Discharges*					
	Q_{FBD01} (m^3/s)	Q_{FBD02} (m^3/s)	Q_{FBD03} (m^3/s)	Q_{FBD04} (m^3/s)	Q_{FBD05} (m^3/s)	Q_{FBD06} (m^3/s)
Dec 22, 2023	2.815	0.296	0.314	1.248	1.525	13.708
Jan 24, 2024	3.312	0.364	0.627	2.106	1.500	14.462
Feb 26, 2024	2.944	0.228	5.643	1.755	0.900	13.559
Mar 28, 2024	5.152	0.182	5.016	1.404	0.750	10.847
Apr 17, 2024	2.944	0.182	5.016	1.404	0.750	10.847
Average	3.433	0.250	3.323	1.583	1.085	12.684

Table 6.2 Measured instantaneous total suspended sediment values for the specified discharge points

Date	*Measured Total Suspended Solids*					
	TSS_{FBD01} (kg/m^3)	TSS_{FBD02} (kg/m^3)	TSS_{FBD03} (kg/m^3)	TSS_{FBD04} (kg/m^3)	TSS_{FBD05} (kg/m^3)	TSS_{FBD06} (kg/m^3)
Dec 22, 2023	0.127	0.037	0.035	0.032	0.134	0.007
Jan 24, 2024	0.100	0.022	0.012	0.025	0.015	0.018
Feb 26, 2024	0.098	0.003	0.013	0.018	0.006	0.004
Mar 28, 2024	0.098	0.003	0.013	0.018	0.006	0.004
Apr 17, 2024	0.188	0.024	0.017	0.010	0.004	0.004
Average	0.122	0.018	0.018	0.021	0.033	0.008

Table 6.3 The calculated RMSE values for each calibration parameter through the comparison between the horizontal velocity of model results and field measurements

Coefficient	*Value*	*RDCP01*			*RDCP02*		
		Layer 1 (3-5m)	*Layer 2 (11-13m)*	*Layer 3 (17-19m)*	*Layer 1 (3-5m)*	*Layer 2 (7-9m)*	*Layer 3 (11-13m)*
Manning	0.010	0.060	0.026	0.033	0.068	0.053	0.046
	0.015	0.050	0.035	0.038	0.044	0.032	0.032
	0.018	0.048	0.033	0.035	0.042	0.032	0.033
	0.020	0.045	0.030	0.032	0.042	0.033	0.034
	0.040	0.059	0.045	0.047	0.057	0.042	0.043
Horizontal viscosity and diffusivity (m^2/s)	1	0.043	0.026	0.039	0.043	0.035	0.038
	10	0.046	0.029	0.049	0.050	0.044	0.045
	50	0.051	0.031	0.050	0.062	0.056	0.048
	100	0.055	0.029	0.042	0.065	0.054	0.047
	200	0.061	0.026	0.032	0.069	0.052	0.047
	300	0.065	0.026	0.028	0.071	0.052	0.048
Vertical viscosity and diffusivity (m^2/s)	0.00005	0.050	0.027	0.030	0.047	0.039	0.035
	0.00010	0.055	0.029	0.031	0.050	0.042	0.036
	0.00050	0.055	0.029	0.030	0.048	0.042	0.037
	0.00100	0.056	0.029	0.031	0.048	0.042	0.037
Viscosity turbulance model	*k-e*	0.047	0.026	0.028	0.047	0.037	0.041
	algebraic	0.052	0.030	0.030	0.057	0.048	0.043
Air density (kg/m^3)	1.000	0.046	0.027	0.029	0.046	0.036	0.033
	1.225	0.049	0.028	0.030	0.047	0.040	0.036
	1.500	0.054	0.029	0.032	0.048	0.042	0.037

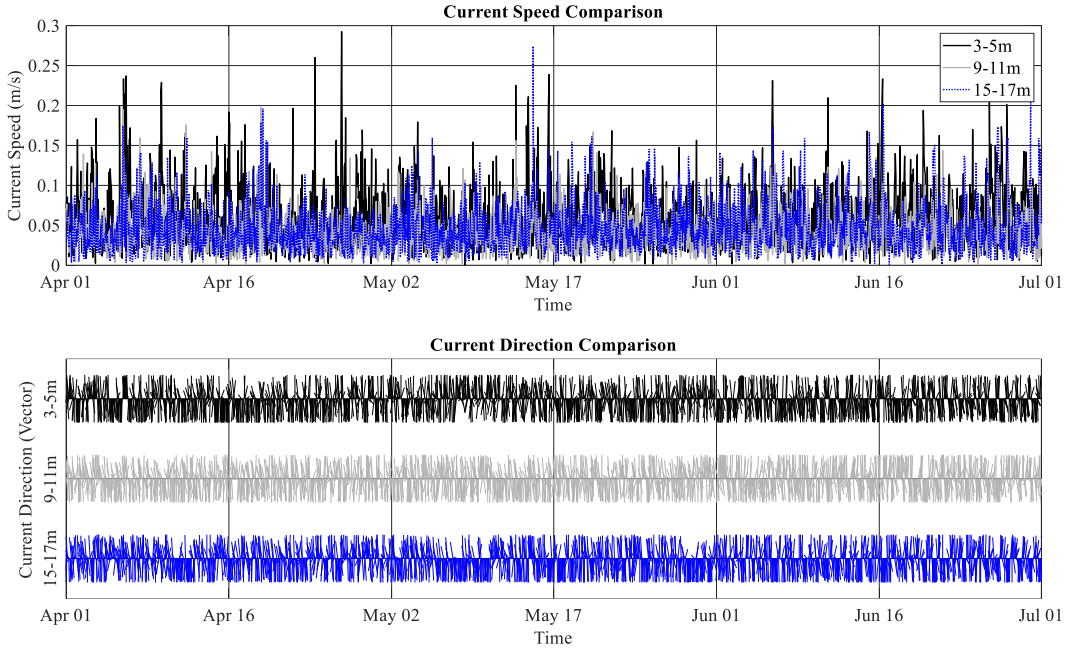

Figure 6.1. Comparison of current speeds and directions in three different measurement levels for RDCP01

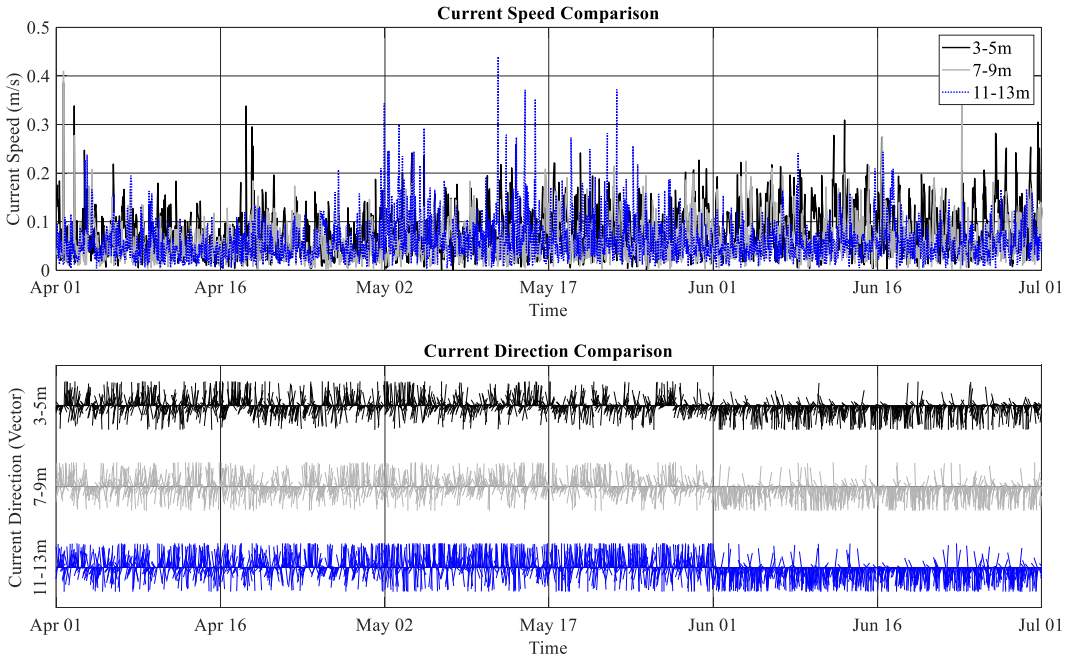

Figure 6.2. Comparison of current speeds and directions in three different measurement levels for RDCP02

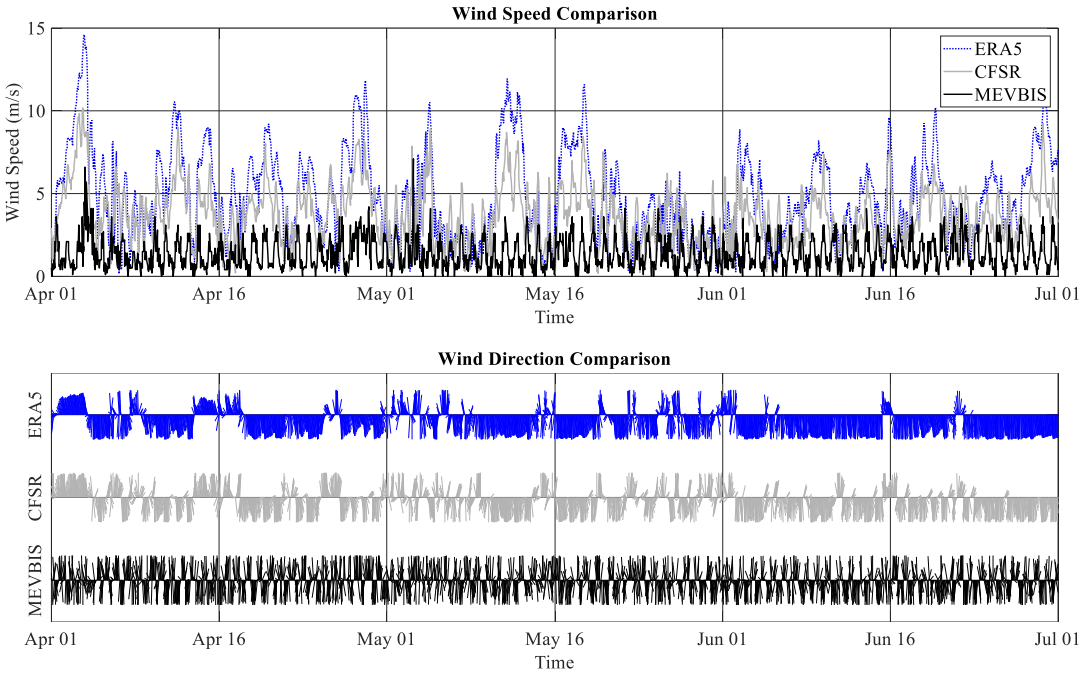

Figure 6.3. Wind speed and direction comparison for April, May and June 2023

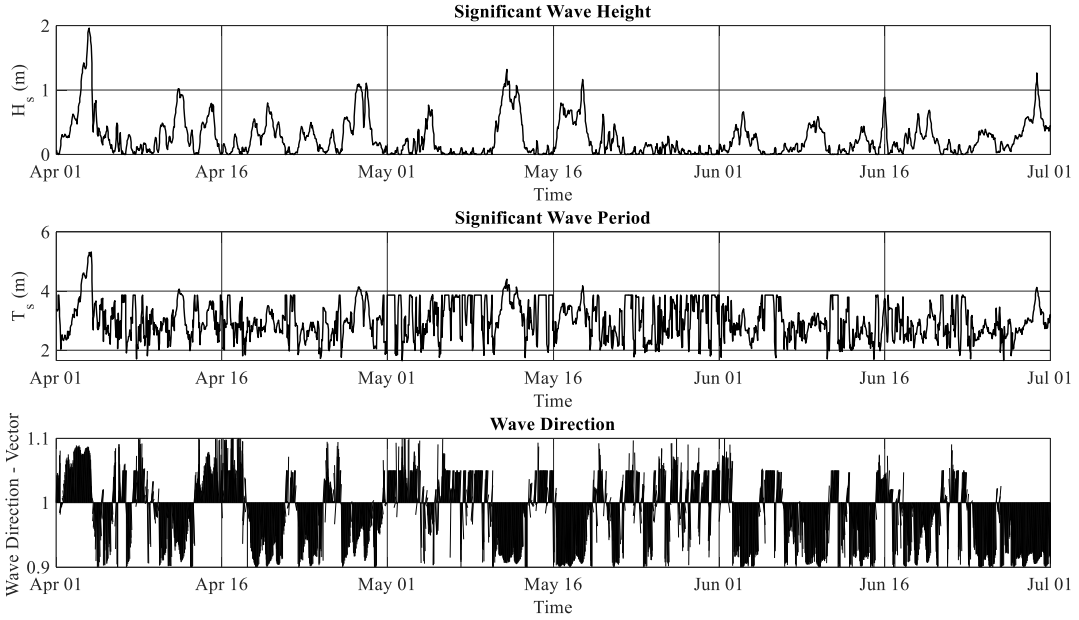

Figure 6.4. Time series obtained for the significant wave height, period and direction for the three-month duration

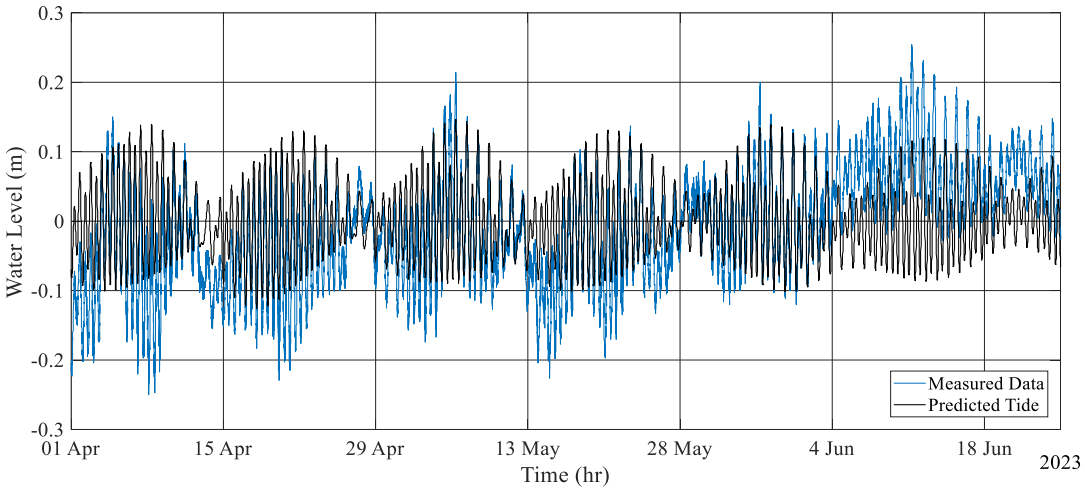

Figure 6.5. Sea level elevation measurements at Marmaris station and predicted tidal time series for the three-month duration

B. Supplementary Tables and Figures for the Model Inputs

Table 6.4 Long term analysis equations specified for the wind and analysis

Directions	*LT Equations for wind analysis*	*LT Equations for wave analysis*
NNE	-1.41 * ln[Q(>U10)] - 1.98	-0.17 * ln[Q(>$H_{m,0}$)] - 0.47
NE	-1.31 * ln[Q(>U10)] - 2.48	-0.09 * ln[Q(>$H_{m,0}$)] - 0.21
ENE	-1.27 * ln[Q(>U10)] - 3.27	-0.14 * ln[Q(>$H_{m,0}$)] - 0.55
E	-2.07 * ln[Q(>U10)] - 7.19	-0.23 * ln[Q(>$H_{m,0}$)] - 0.95
ESE	-2.92 * ln[Q(>U10)] - 7.96	-0.47 * ln[Q(>$H_{m,0}$)] - 1.54
SE	-2.57 * ln[Q(>U10)] - 5.98	-0.46 * ln[Q(>$H_{m,0}$)] - 1.13
SSE	-2.45 * ln[Q(>U10)] - 7.87	-0.38 * ln[Q(>$H_{m,0}$)] - 1.11
S	-2.34 * ln[Q(>U10)] - 8.67	-0.46 * ln[Q(>$H_{m,0}$)] - 1.69
SSW	-2.37 * ln[Q(>U10)] - 9.34	-0.52 * ln[Q(>$H_{m,0}$)] - 2.15
SW	-1.85 * ln[Q(>U10)] - 5.79	-0.40 * ln[Q(>$H_{m,0}$)] - 1.76
WSW	-1.59 * ln[Q(>U10)] - 3.56	-0.37 * ln[Q(>$H_{m,0}$)] - 1.73
W	-1.36 * ln[Q(>U10)] - 0.94	-0.26 * ln[Q(>$H_{m,0}$)] - 0.75
WNW	-2.29 * ln[Q(>U10)] - 5.02	-0.27 * ln[Q(>$H_{m,0}$)] - 0.32
NW	-1.74 * ln[Q(>U10)] - 2.77	-0.29 * ln[Q(>$H_{m,0}$)] - 0.42
NNW	-1.89 * ln[Q(>U10)] - 3.44	-0.33 * ln[Q(>$H_{m,0}$)] - 0.64
N	-1.49 * ln[Q(>U10)] - 1.75	-0.26 * ln[Q(>$H_{m,0}$)] - 0.57

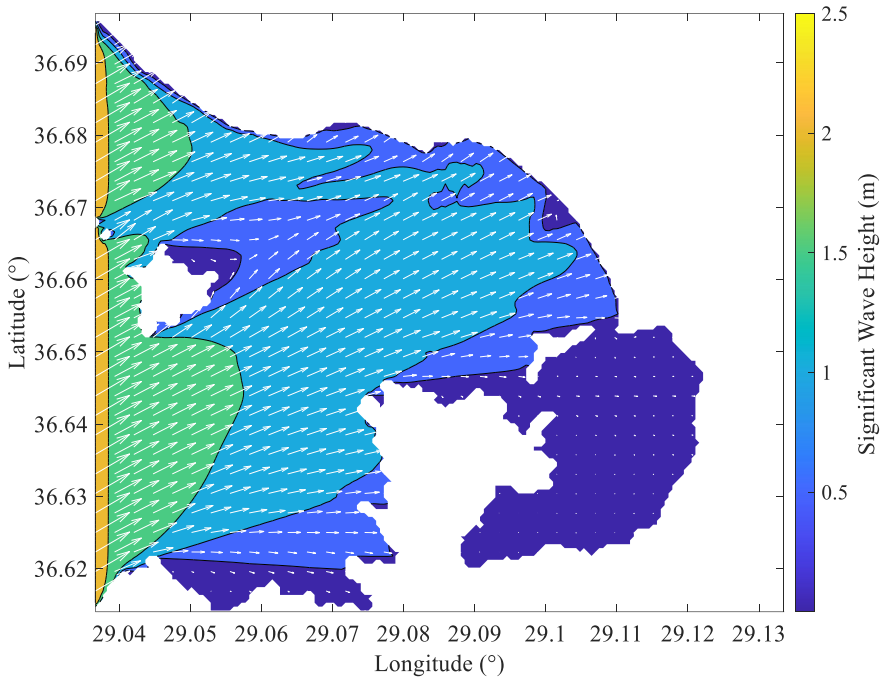

Figure 6.6. SWAN results showing the significant wave height and directions over the Fethiye Bay in larger domain

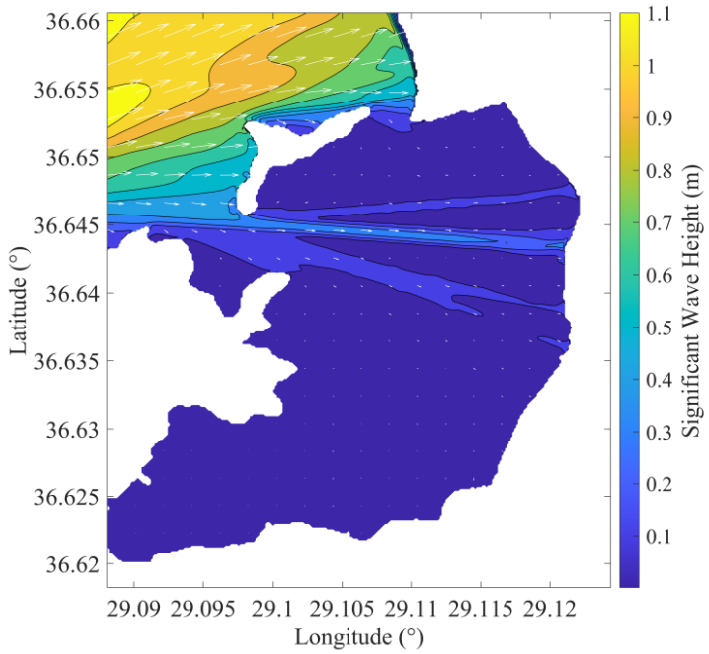

Figure 6.7. SWAN results showing the significant wave height and directions over the Fethiye Bay in nested domain

C. Supplementary Tables and Figures for Results

Table 6.5 Results obtained for water exchange volumes under dredging for each scenario

Scn. No.	Wind Dir.	Water Exchange Volumes at Different Dredging Depths					
		$V_{Not\ dredged}$ ($x10^5\ m^3$)	$V_{-1\ m}$ ($x10^5\ m^3$)	$V_{-2\ m}$ ($x10^5\ m^3$)	$V_{-3\ m}$ ($x10^5\ m^3$)	$V_{-4\ m}$ ($x10^5\ m^3$)	$V_{-5\ m}$ ($x10^5\ m^3$)
1	ESE	6.86	22.03	22.30	15.98	23.22	10.84
2	WNW	149.74	148.43	147.23	148.30	149.15	150.29
3	NNE	166.61	166.57	166.74	166.74	165.83	167.48
4	SSW	31.32	31.19	29.33	32.86	30.94	32.16
5	ESE	85.26	74.33	71.35	62.70	81.95	50.29
6	WNW	337.59	337.90	339.52	343.71	343.45	343.47

Table 6.6 Results obtained for cumulative deposition volume under dredging for each scenario

Scn. No.	Wind Dir.	Cumulative Deposition Volume at Different Dredging Depths					
		$V_{Not\ dredged}$ (m^3)	$V_{-1\ m}$ (m^3)	$V_{-2\ m}$ (m^3)	$V_{-3\ m}$ (m^3)	$V_{-4\ m}$ (m^3)	$V_{-5\ m}$ (m^3)
1	ESE	2746.1	2208.9	347.6	123.7	91.4	132.3
2	WNW	5517.3	4154.6	610.9	226.1	227.7	204.9
3	NNE	1788.8	1242.5	451.4	306.0	330.9	302.5
4	SSW	1750.7	631.5	99.8	61.2	78.6	79.3
5	ESE	15043.1	9311.2	3115.2	2999.3	1990.2	3307.2
6	WNW	37800.0	33300.0	28480.5	14210.8	9470.9	8255.0

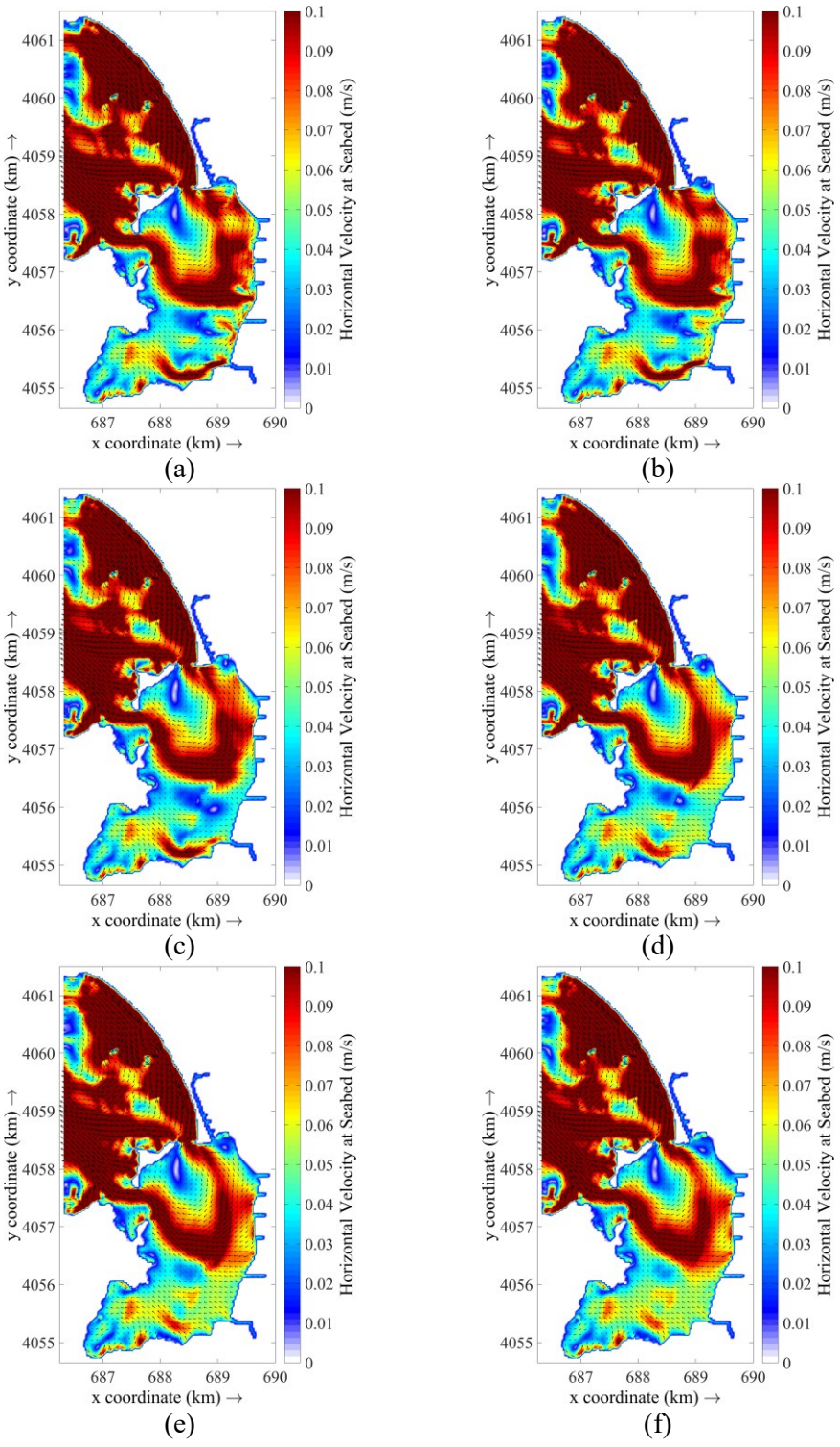

Figure 6.8. The areal distribution of maximum horizontal velocity profiles at the sea bottom under the effect of Scenario 2 for a. not-dredged, b. dredged to -1 m, c. dredged to -2 m, d. dredged to -3 m, e. dredged to -4 m, f. dredged to -5 m

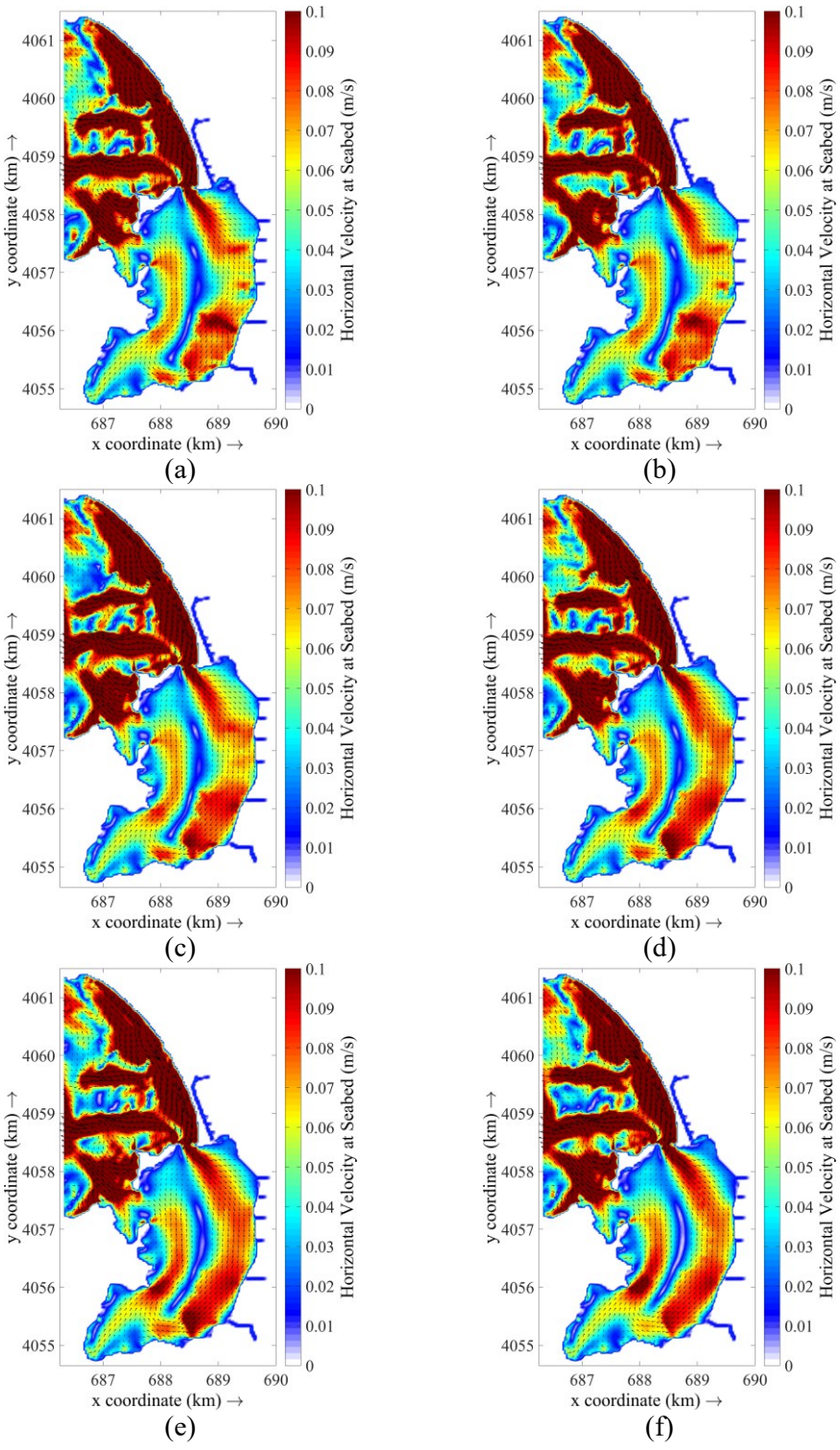

Figure 6.9. The areal distribution of maximum horizontal velocity profiles at the sea bottom under the effect of Scenario 3 for a. not-dredged, b. dredged to -1 m, c. dredged to -2 m, d. dredged to -3 m, e. dredged to -4 m, f. dredged to -5 m

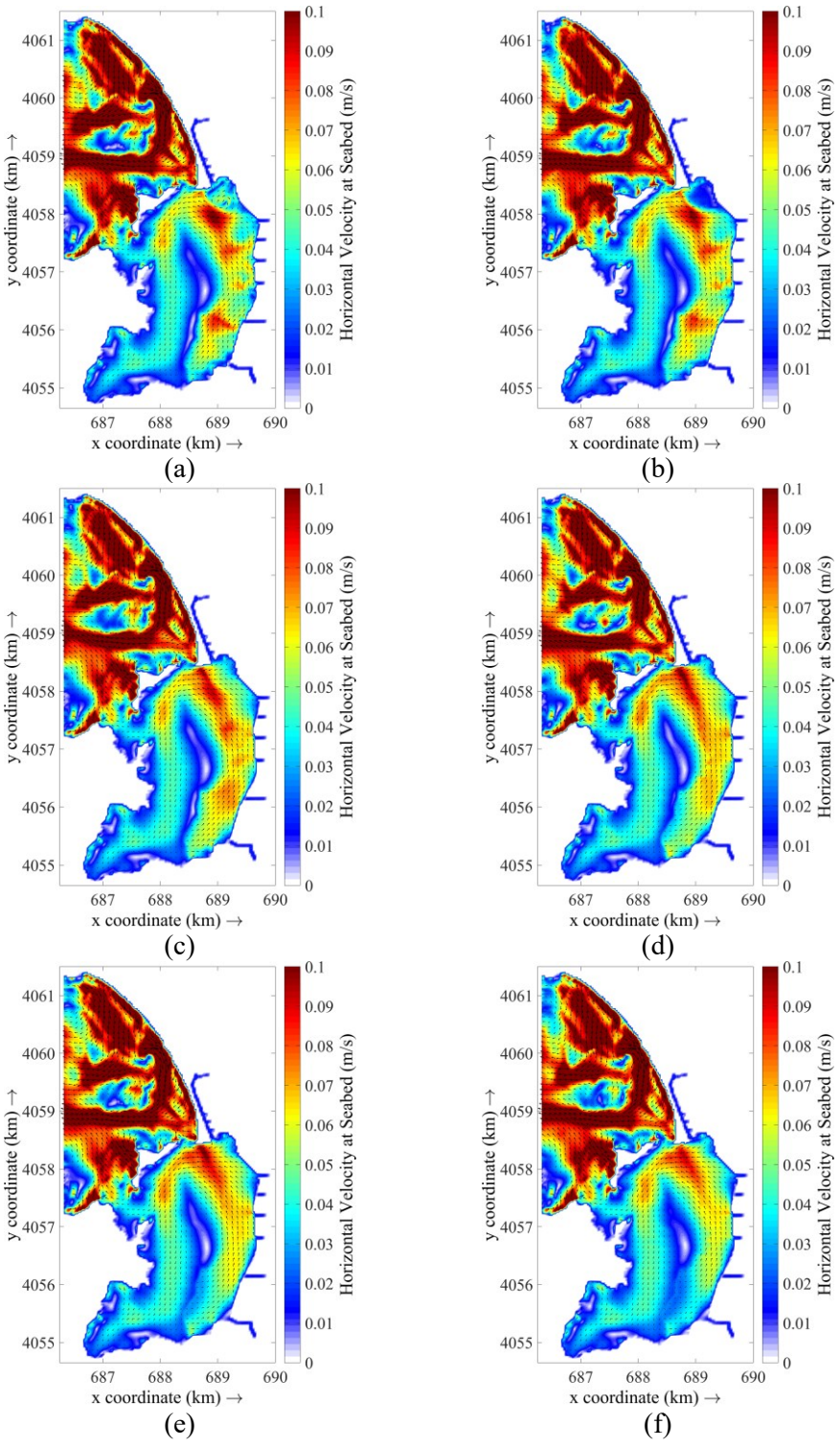

Figure 6.10. The areal distribution of horizontal velocity profiles at the sea bottom under the effect of Scenario 4 for a. not-dredged, b. dredged to -1 m, c. dredged to -2 m, d. dredged to -3 m, e. dredged to -4 m, f. dredged to -5 m

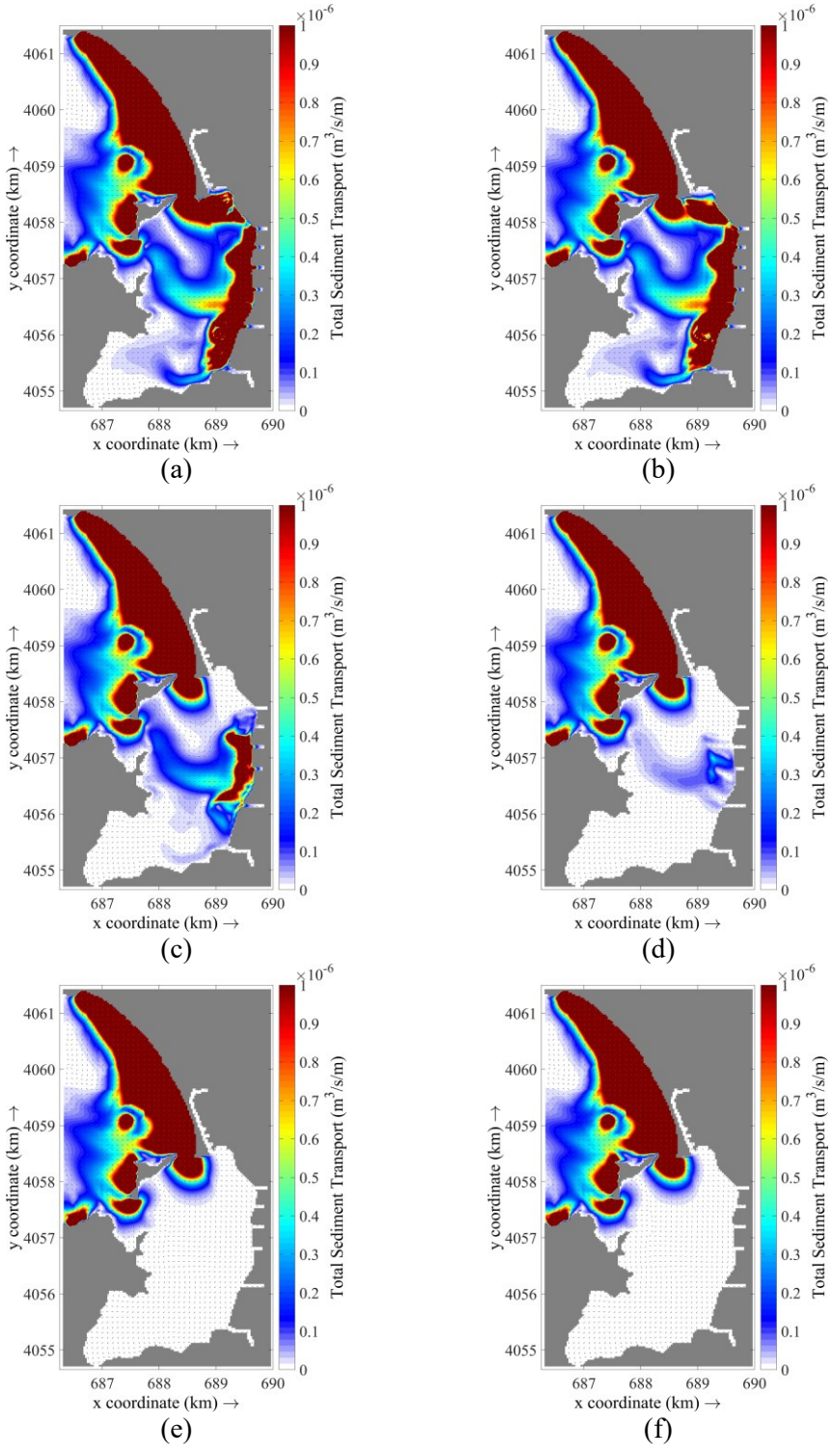

Figure 6.11. The areal distribution of total sediment transport under the effect of Scenario 2 for a. not-dredged, b. dredged to -1 m, c. dredged to -2 m, d. dredged to -3 m, e. dredged to -4 m, f. dredged to -5 m

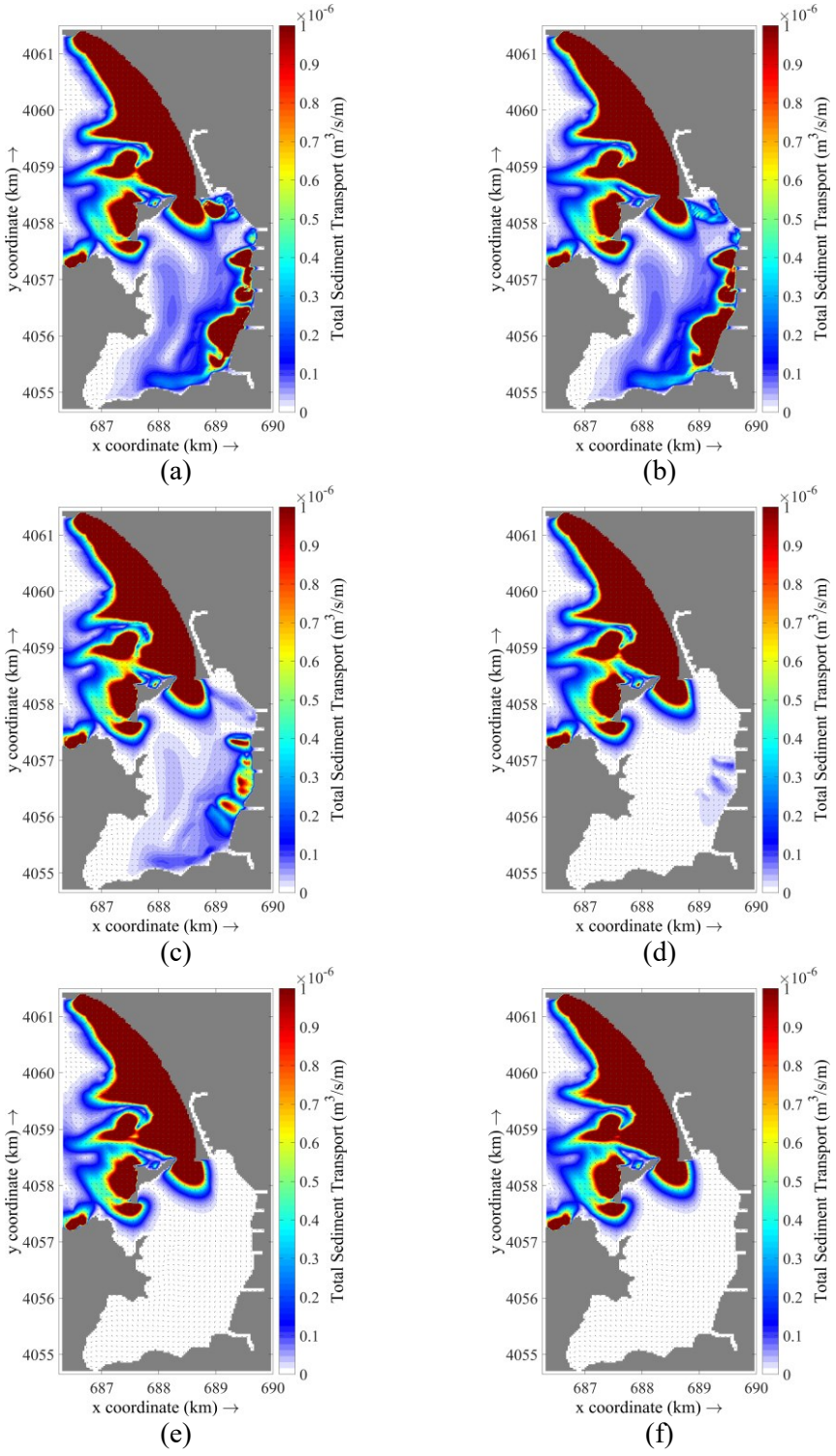

Figure 6.12. The areal distribution of total sediment transport under the effect of Scenario 3 for a. not-dredged, b. dredged to -1 m, c. dredged to -2 m, d. dredged to -3 m, e. dredged to -4 m, f. dredged to -5 m

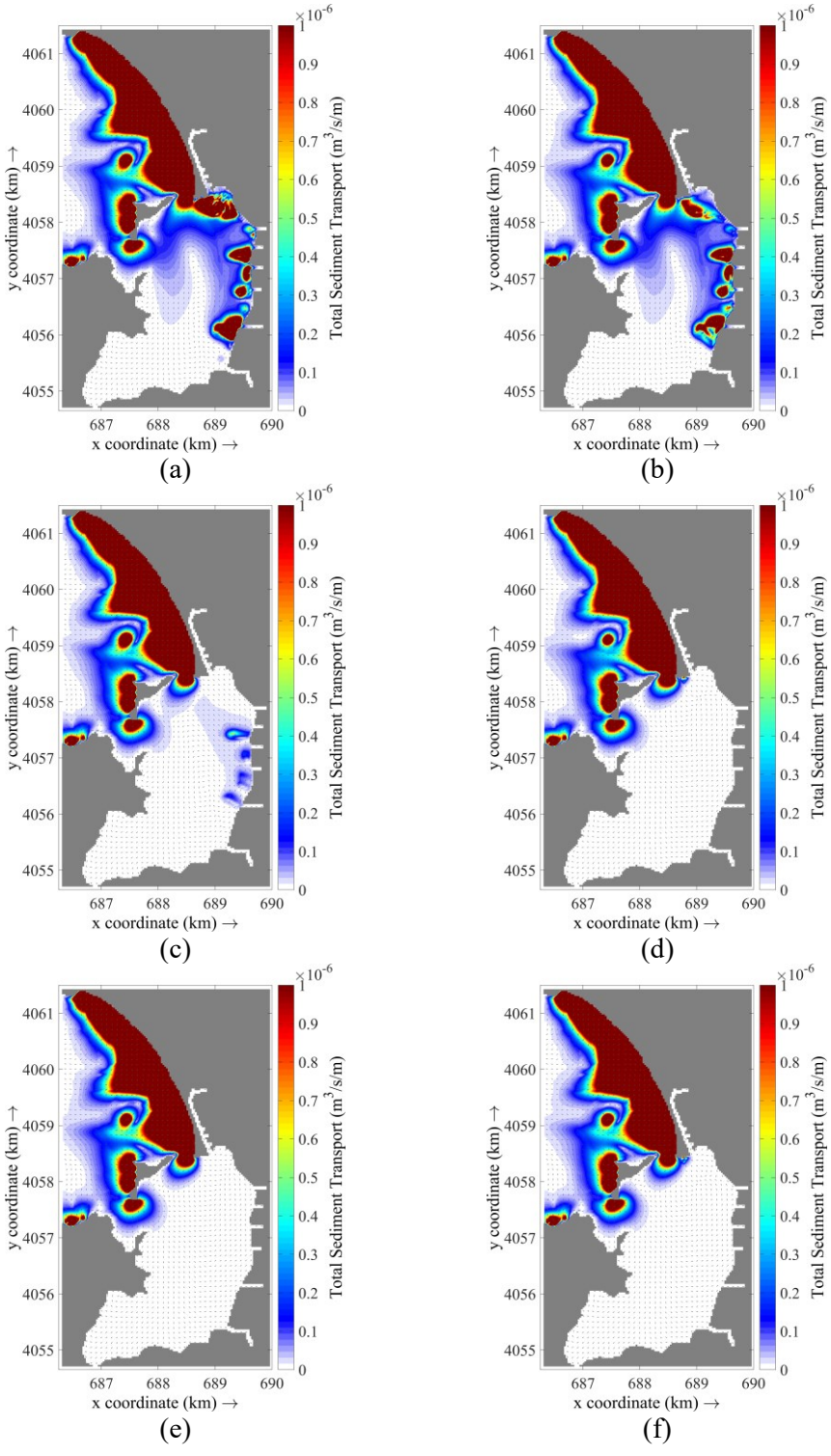

Figure 6.13. The areal distribution of total sediment transport under the effect of Scenario 4 for a. not-dredged, b. dredged to -1 m, c. dredged to -2 m, d. dredged to -3 m, e. dredged to -4 m, f. dredged to -5 m

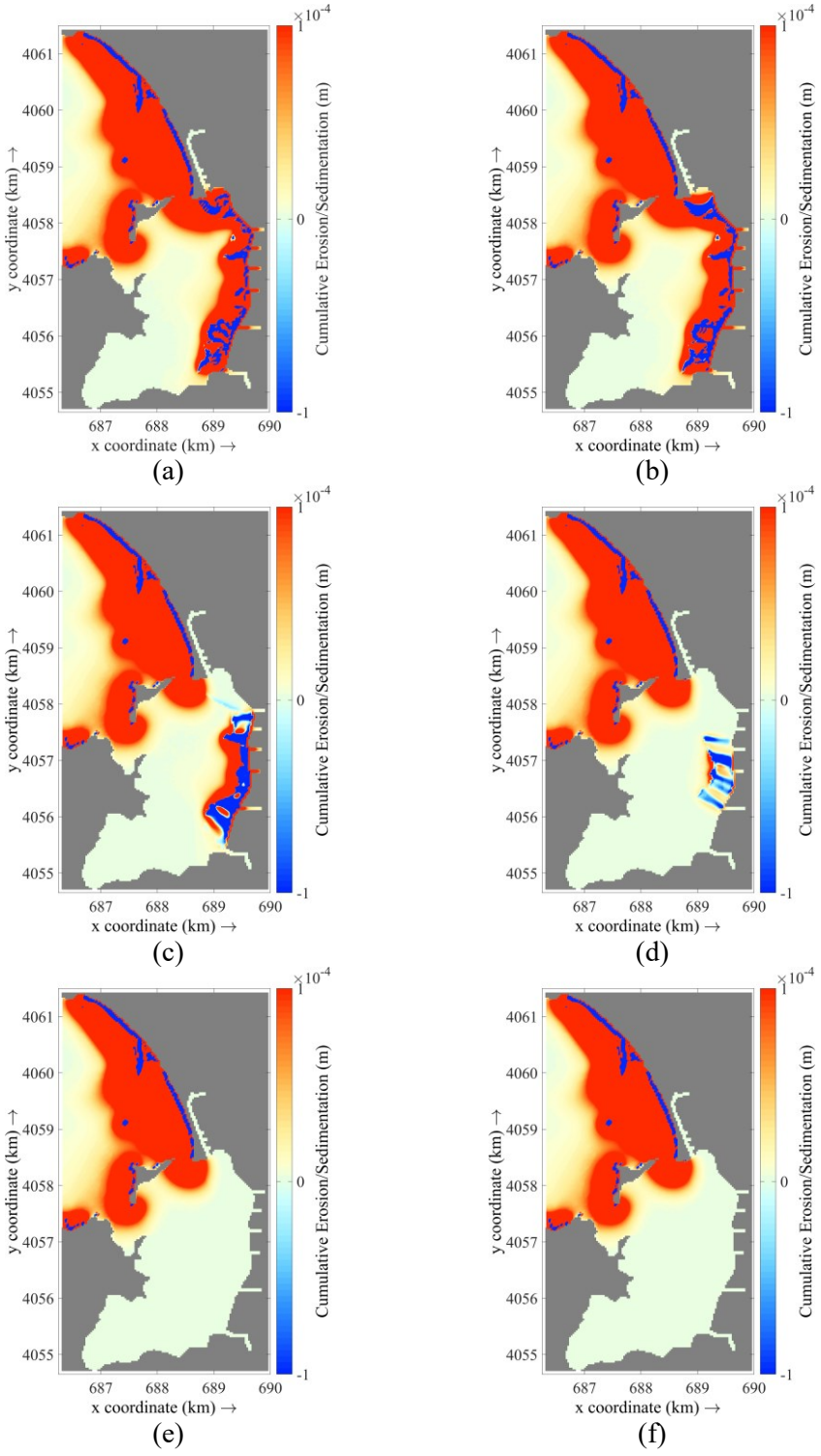

Figure 6.14. The areal distribution of cumulative erosion and deposition under the effect of Scenario 2 for a. not-dredged, b. dredged to -1 m, c. dredged to -2 m, d. dredged to -3 m, e. dredged to -4 m, f. dredged to -5 m

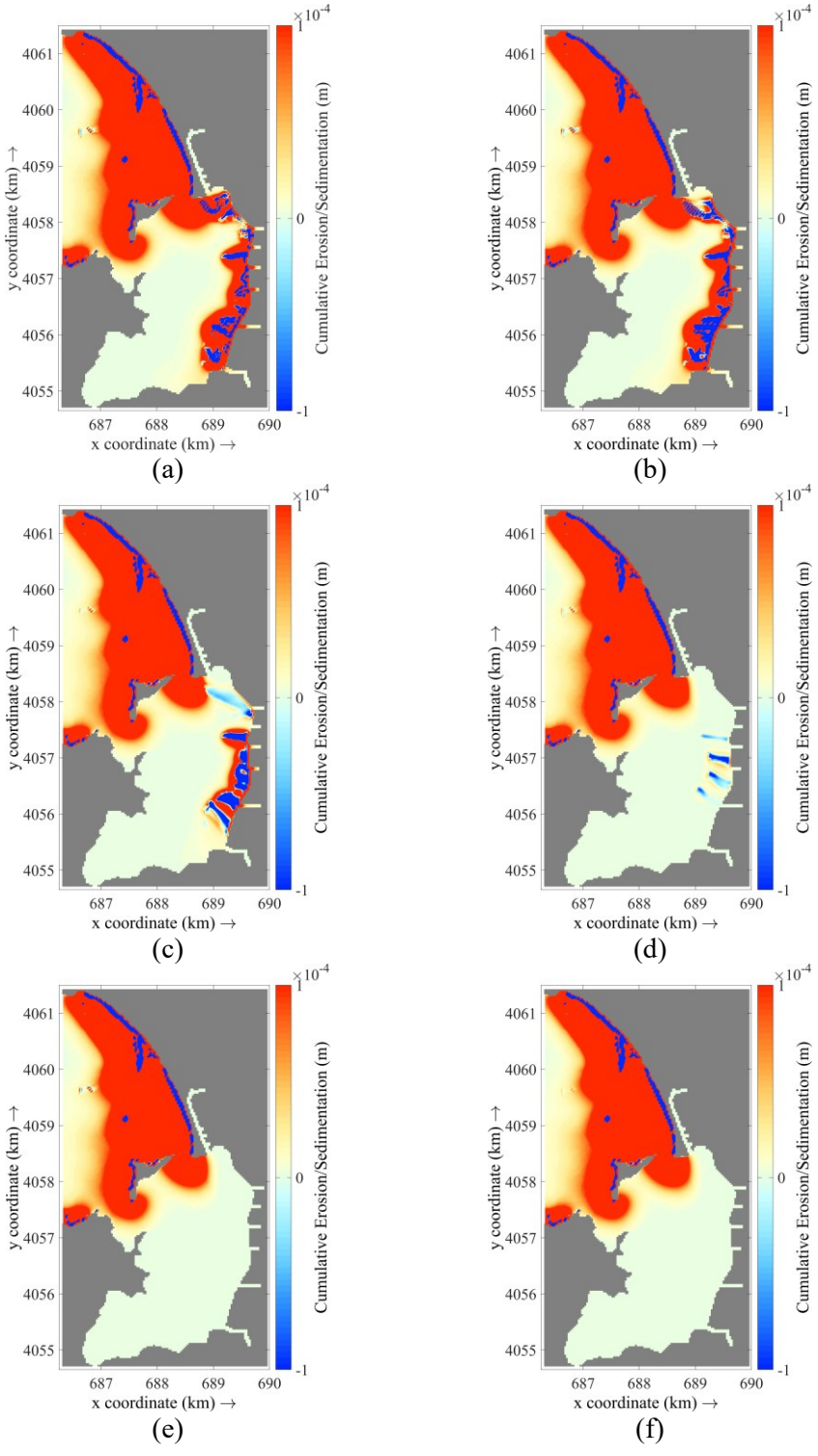

Figure 6.15. The areal distribution of cumulative erosion and deposition under the effect of Scenario 3 for a. not-dredged, b. dredged to -1 m, c. dredged to -2 m, d. dredged to -3 m, e. dredged to -4 m, f. dredged to -5 m

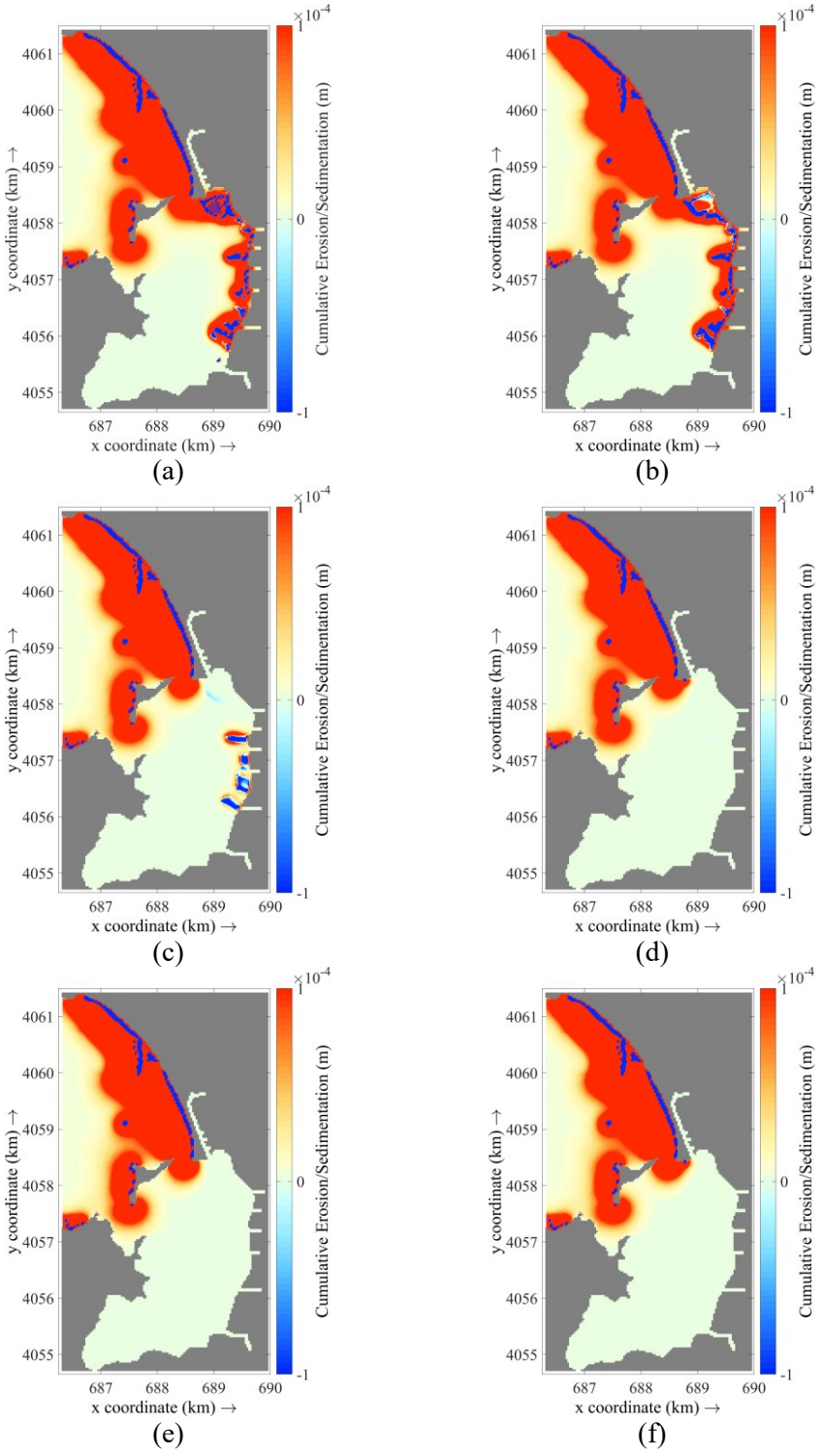

Figure 6.16. The areal distribution of cumulative erosion and deposition under the effect of Scenario 4 for a. not-dredged, b. dredged to -1 m, c. dredged to -2 m, d. dredged to -3 m, e. dredged to -4 m, f. dredged to -5 m

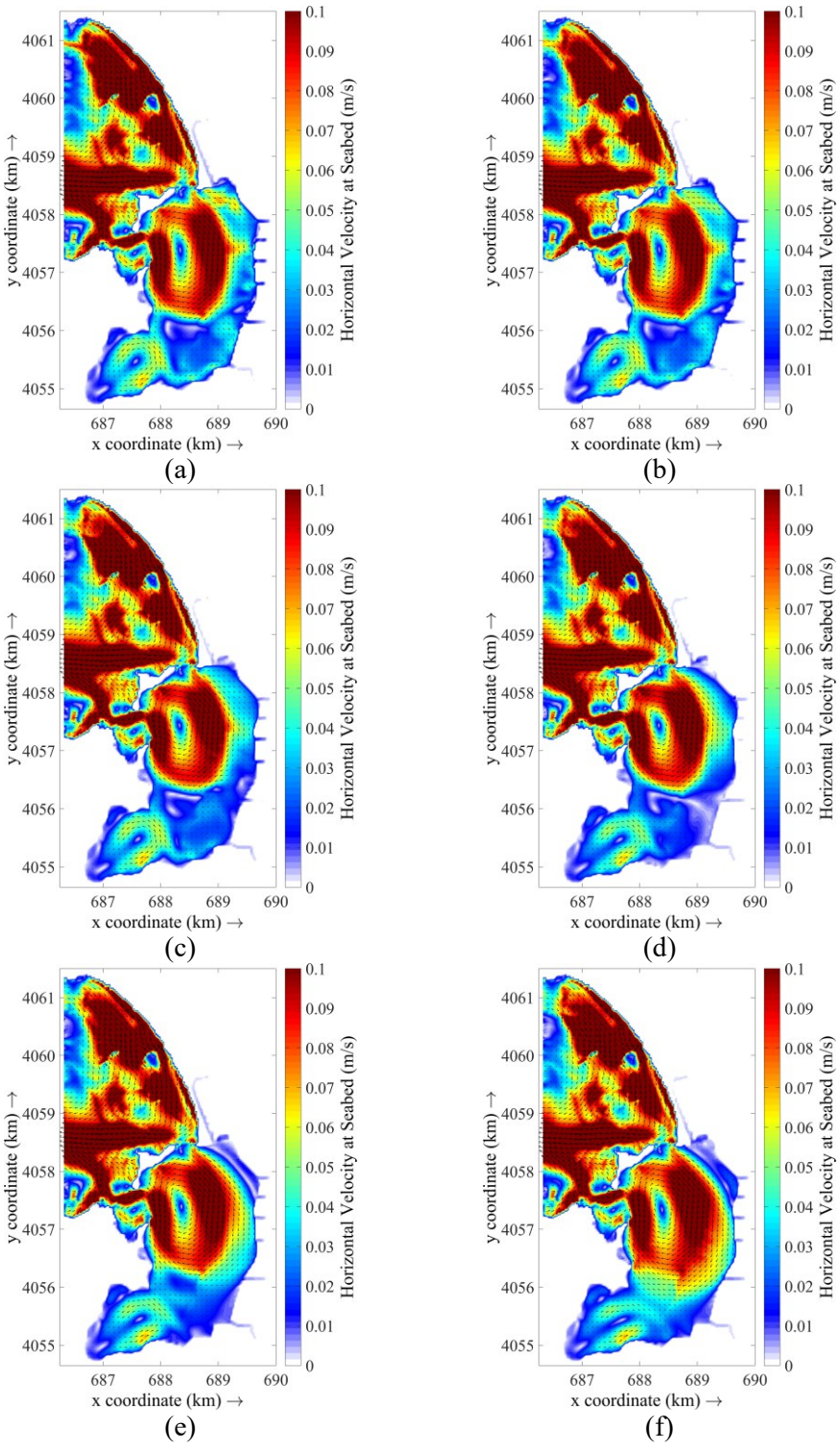

Figure 6.17. The areal distribution of horizontal velocity profiles under the effect of Scenario 6 for a. not-dredged, b. dredged to -1 m, c. dredged to -2 m, d. dredged to -3 m, e. dredged to -4 m, f. dredged to -5 m

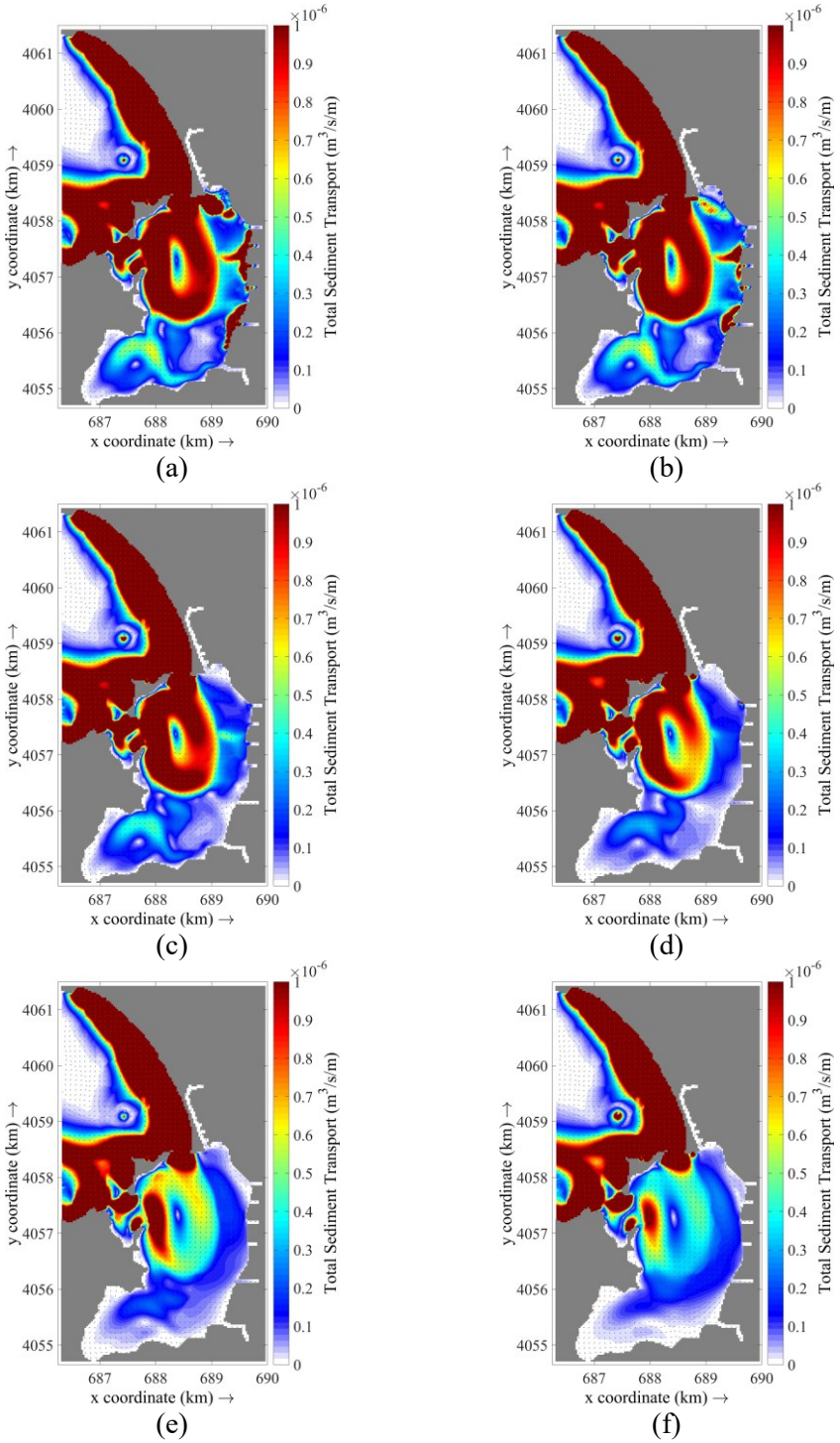

Figure 6.18. The areal distribution of total sediment transport under the effect of Scenario 6 for a. not-dredged, b. dredged to -1 m, c. dredged to -2 m, d. dredged to -3 m, e. dredged to -4 m, f. dredged to -5 m

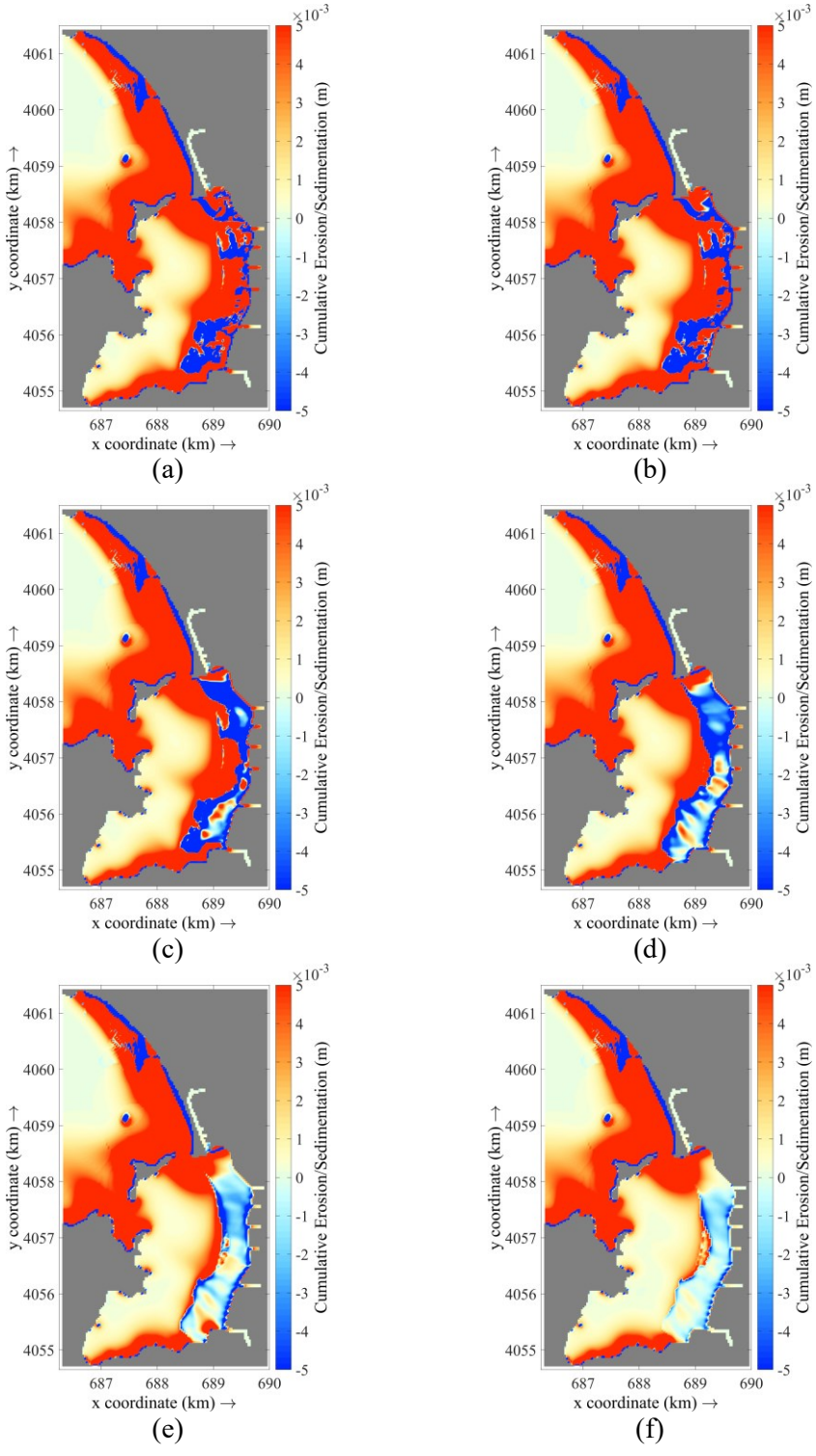

Figure 6.19. The areal distribution of cumulative erosion and deposition under the effect of Scenario 6 for a. not-dredged, b. dredged to -1 m, c. dredged to -2 m, d. dredged to -3 m, e. dredged to -4 m, f. dredged to -5 m

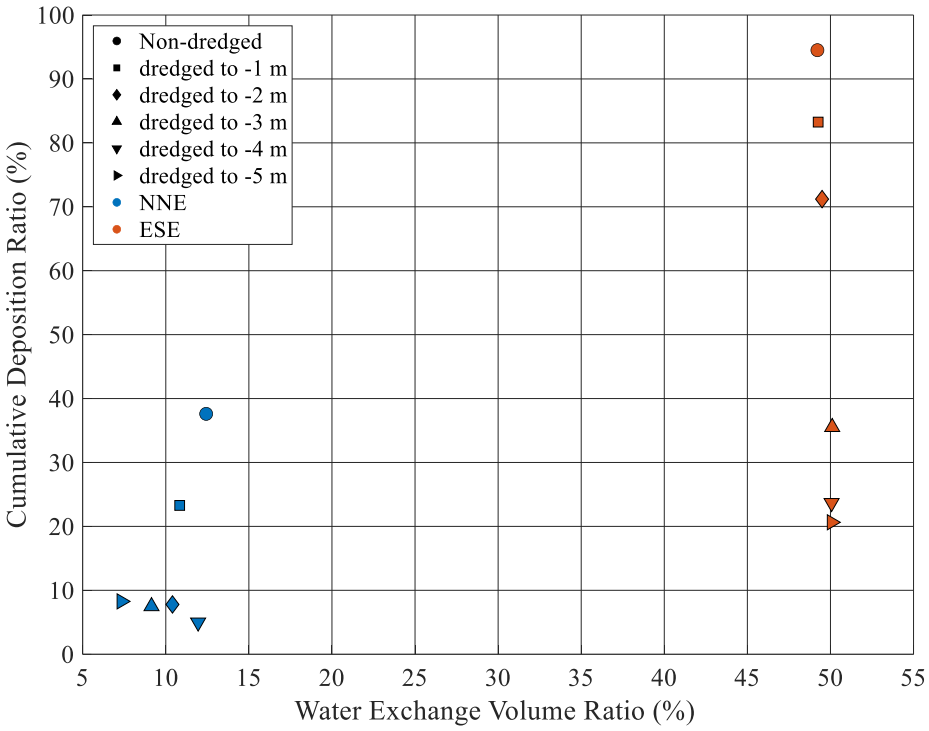

Figure 6.20. The relationship between water exchange volume ratio and cumulative deposition ratio under the dredging scenarios through results of Scenario 5 and Scenario 6